ТЕХНІКА ТА ЕНЕРГЕТИКА

Засновник:
Національний університет біоресурсів і природокористування України

Рік заснування: 2010

*Рекомендовано до друку та поширення
через мережу Інтернет Вченою радою
Національного університету біоресурсів і природокористування України
(протокол № 4 від 23 листопада 2022 р.)*

**Свідоцтво про державну реєстрацію
друкованого засобу масової інформації**
серії КВ № 25126-15066 ПР від 17 лютого 2022

Журнал входить до переліку наукових фахових видань України
Категорія «Б». Галузь наук – Технічні.
Спеціальність: 131 – «Прикладна механіка», 133 – «Галузеве машинобудування»,
141 – «Електроенергетика, електротехніка та електромеханіка»,
151 – «Автоматизація та комп’ютерно-інтегровані технології»
(Наказ Міністерства освіти і науки України від від 17 березня 2020 року № 409)

**Журнал представлено у міжнародних наукометричних базах даних,
репозитаріях та пошукових системах**: Index Copernicus International,
Google Scholar, Фахові видання України,
Національна бібліотека України імені В. І. Вернадського,
AGRIS, BASE, Academic Resource Index ResearchBib

Адреса редакції:
Національний університет біоресурсів і природокористування України
вул. Героїв Оборони, 15, м. Київ, 03041, Україна
E-mail: info@technicalscience.com.ua
www: https://technicalscience.com.ua/uk

MACHINERY & ENERGETICS

Founders:
National University of Life and Environmental Sciences of Ukraine

Year of foundation: 2010

Recommended for printing and distribution
via the Internet by the Academic Council
of National University of Life and Environmental Sciences of Ukraine
(Minutes No. 4 of November 23, 2022)

Certificate of state registration
of the print media
Series KV No. 25126-15066 PR of February 17, 2022

The journal is included in the list of Professional Scientific Publications of Ukraine
Category “B”. Branch of sciences – Technical.
Specialty: 131 – “Applied mechanics”, 133 – “Branch mechanical engineering”,
141 – “Electric power industry, electrical engineering and electromechanics”,
151 – “Automation and computer-integrated technologies”
(Order of the Ministry of Education and Science of Ukraine of March 17, 2020, No. 409)

The journal is presented international scientometric databases, repositories and scientific systems: Index Copernicus International,
Google Scholar, Professional publications of Ukraine,
Vernadsky National Library of Ukraine, AGRIS, BASE,
Academic Resource Index ResearchBib

Editors office address:
National University of Life and Environmental Sciences of Ukraine
03041, 15 Heroiv Oborony, Kyiv, Ukraine
E-mail: info@technicalscience.com.ua
www: https://technicalscience.com.ua/en

Редакційна колегія

ЗМІСТ

CONTENTS

Machinery & Energetics
Vol. 13, No. 4. 2022

Journal homepage:
https://technicalscience.com.ua/en

UDC 631.47
DOI: 10.31548/machenergy.13(4).2022.9-15

Hristo Beloev*
Full Doctor in Technical Sciences, Professor
"Angel Kanchev" University of Ruse
7017, 8 Studentska Str., Ruse, Bulgaria
https://orcid.org/0000-0002-8644-2947

Methodology for experimental study of soil microrelief on ruts in bridge farming

Abstract. The study of issues related to the research of the soil's state on the surface of the most constant technological track is relevant, since the movement of running wheels along narrow tracks determines the traction and coupling properties of the machine-tractor units, their vibrations, the stability of movement and the controllability of movement. The purpose of this study was to increase the efficiency of the process of profiling the microroughnesses of the soil surface located in areas that form a track along which the running wheels of machine-tractor units will move, by substantiating a new scheme of an automated profilograph and developing methods for its use. For this study, modern methods of experimental researches based on IT technologies were used. In particular, an automated complex has been developed for measuring and evaluating the microprofile of soil surface irregularities on the very track of the tramline. The results of experimental studies in this matter have shown that the standard deviation of the soil surface irregularities reaches ±0.84 cm. This gives reason to consider the harmonic components of these functions as damped, having normalized correlation functions. The graphs constructed using PC have showed that most of the dispersions of soil surface irregularities on the ruts are concentrated in the range of 0...0.3 cm^{-1}. It has been established that the generator of the formation of irregularities in the longitudinal profile of traces of a permanent technological track acts as parameters of the treads of the wheels of machines moving along it. The obtained results of the study can be used when selecting the protectors of pneumatic tires of the running wheels of machine-tractor units moving on two tracks

Keywords: track vehicle; irregularities; oscillations; correlation function; spectral density

Article's History: Received: 03.08.2022; Revised: 01.11.2022; Accepted: 23.11.2022.

INTRODUCTION

The traditional farming system has reached the limits of its ability regarding the increase in the crop yields, energy costs of the growing and harvesting process and overall efficiency, as a result of excessive compaction of the topsoil. A wide variety of technical means, their significant weight, the intensive impact of their running systems (propulsion) on the soil, the repeated passes through the fields lead to soil compaction, a decrease in the soil fertility and biodegradation. Restoring the natural state of the soil is very problematic.

Therefore, the so-called bridge farming system is becoming more and more widespread in the world; its main basis lies in the movement of energy resources along two rather narrow tracks, which are used repeatedly and are actually taken out of the usable area on which crops are grown.

For this purpose, new designs of bridge power facilities were developed in researches [1-3], and their theoretical and experimental studies were carried out. According to them, the same transport and technological tracks for the movement of vehicles and energy vehicles are used for tillage, sowing of plants, spraying and harvesting [4-6]. In the works [7-9], it is described the process of formation of compacted and aligned traces of a constant technological track that consists in its laying on the field area with a given step, either as a result of repeated

Suggested Citation:
Beloev, H. (2022). Methodology for experimental study of soil microrelief on ruts in bridge farming. *Machinery & Energetics,* 13(4), 9-15. doi: 10.31548/machenergy.13(4).2022.9-15.

*Corresponding author

passes of agricultural machinery, or with the help of special tools [7-9]. The microrelief (irregularities of the longitudinal profile) of the constant technological track formed in this way is an important characteristic, which has been analized in the articles [10; 11]. Because the intensity of external disturbances acting on the power and transport vehicles moving along it significantly depends on it (microrelief) and largely determines their operational and technological parameters, reliability, smoothness of movement, vibration conditions of the operators' work.

Back in the day [7; 8], it was developed and tested a prototype of an agricultural tool for laying a permanent technological track. The basis of this tool is the middle section of the spring harrow BP-8, which is equipped with additional support wheels, two plow bodies with a width of 0.35 cm each and hydrogenated markers. S-shaped tools of the instrument are turned 180° and are equipped with lancet tines with a working width of 150 mm for better loosening of the soil. After laying the specified tool a constant tramline, the main share of dispersion of its longitudinal profile oscillations was concentrated in the frequency range of 0...2.5 m^{-1}, and the dispersion value of these vibrations was 3.8 cm^2 [8].

It should be noted [12-14] that the methodology of profiling of soil-road backgrounds is well developed based many years of practice. However, in most cases, scientists use either direct discrete measurement of the heights of irregularities of the path micro-profile, or mechanical profilographs with recording the ordinates of irregularities on a paper tape. Thus, traditional methods of measuring track profile irregularities by rails or mechanical self-recording profilographs due to their high labor intensity, as well as due to the lack of automation of measurements are already obsolete.

The modern scientific and technical level of experimental research allows directly and remotely recording the implementation of processes on a PC using analog-to-digital converters with simultaneous automatic processing of results, adjusting the process of experimental research, which significantly increases the accuracy of measurements.

Automated profilographs and profilometers are a promising direction of creation of such devices of new generation, which allow measuring directly the surface micro-profile of the longitudinal profile of the track. These devices can be mounted on a transport or energy vehicle. Such measuring equipment can be equipped with laser, optical, ultrasonic non-contact and other sensors together with the accelerometer and gyroscopes, as well as sensors of angular displacements, etc. However, not enough attention is paid to the issue of creating such devices in the popular science literature.

The purpose of this study is to develop an improved technique for laboratory study of soil irregularities on the tracks along which the running wheels of bridge agricultural vehicles move, which increases the efficiency of profiling through the use of a new design of an automated profilograph.

MATERIALS AND METHODS

Obtaining the reliable information about the unevenness of soil surface is possible in case of using a device-profiler, i.e. a device that is used to assess the irregularities along the length of the distance traversed by any scoring section. Under the guidance of Volodymyr Bulgakov (National University of Bioresources and Nature Management of Ukraine), it has been designed such a profiler, which makes it possible to automate the process of taking information about irregularities, the soil surface, which are present on the traces of track, on which the bridge agricultural vehicle moves. The Figure 1 shows a general view of this profiler, which is a mechanical part in the form of main body 1, which has the ability to freely slide along the guide 2 or fix its location anywhere on the guide 2. The main body 1 contains a mechanism for fixing the unevenness of soil surface on the track in the form of roller 4 freely mounted on the axis, which is located at the end of the arcuate lever 6. The main body 1 moves along the guide 2, while the roller 4 freely rolls along the uneven surface of the soil 5 without crushing the surface soil layer and without deforming it. The arcuate lever 6 is made in the form of a two-arm lever and it is rotatably mounted in a cylindrical hinge. In this case, the second end of the lever 6 is connected to the reohing sensor 3 (the sensor is manufactured industrially and has the brand SP-3A), which rotates when the second (short) part of the arcuate lever 6 is turned as a two-arm lever. When the sensor 3 is rotated, its electrical resistance changes and an alternating electrical signal is transmitted to the electrical part of this device, i.e. to analog-to-digital converter 7 (also produced by the industry and has the PK-9 brand). Converter 7 is connected to a personal computer 9, which (according to the developed program) processes the signal, captures it and transforms the signal in the form of graphs. This measuring system receives electrical power from battery 8. The mechanical and electrical parts of this measuring device were preliminarily configured. The proposed measurements of the unevenness of soil surface were calibrated and the programs of personal computer were adjusted. The measurement and fixation of soil surface irregularities on the tracks of a bridge agricultural vehicle of constant size were carried out when the main body 1 moved at a translational speed of 0.5 $m \cdot s^{-1}$ along the guide 2 from the one end to another.

The signal from the profilograph was processed using Power Graph 2.1, both in analog and digital forms.

The profiler was calibrated (see Fig. 1) on a flat surface, placing plates of different thicknesses under its wheel. Roller 4, freely mounted on the axis and placed at the end of the arcuate lever 6, slid along these plates, turning the SP-3A sensor at fixed angles. In this case, these angles were recorded by a PK-9 transducer and an electrical signal was transmitted to a personal computer. The calibration dependence of the output signal readings (v) in the Power Graph 2.1 environment on the actual ordinates (h, cm) of the profiler irregularities looked like:

$$h=38.8 \cdot v-5.52. \quad (1)$$

Comparing the results of multiple measurements during calibration and similar measurements of fixed heights of soil surface irregularities, their registration and computer processing by this profiler design (see Fig. 1), it has been found that the relative measurement error is no more than 3% (2.5%), which indicates a sufficiently high measurement accuracy.

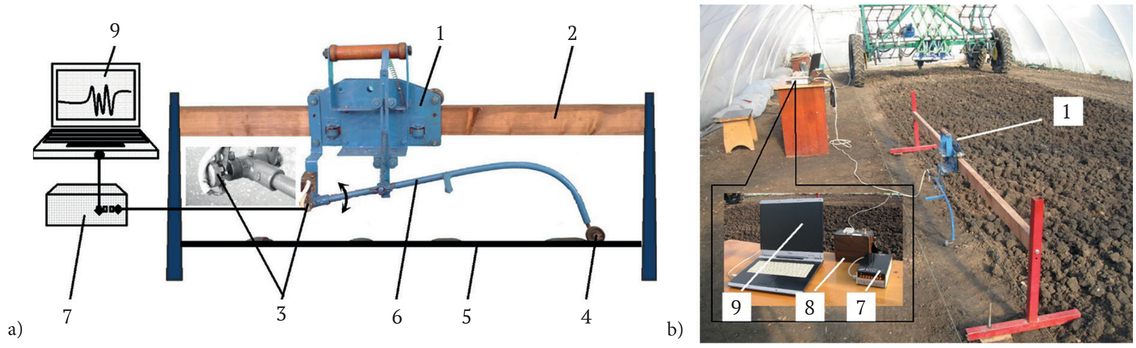

Figure 1. Automated profilograph (a) and hardware-measuring complex (b) for assessing the unevenness of the longitudinal profile of the traces of a permanent technological track and: 1 – profilograph body; 2 – rail; 3 – rheochord sensor; 4 – profiler wheel; 5 – unevenness of the longitudinal profile of the track; 6 – profilograph lever; 7 – analog-digital converter; 8 – battery; 9 – PC

Then, with the help of specially developed program for calculating and constructing the correlation-spectral characteristics of the inequalities of microprofile of soil and road backgrounds in Microsoft Office Excel, it was carried out the mathematical analysis of the data obtained.

The normalized correlation function $\rho(l)$ of the fluctuations of microtrack irregularities of the constant process track was calculated as the ratio of the correlation function to the variance [14]:

$$\rho(l) = \frac{1}{D_h(n-m)} \sum_{i=1}^{n-m} (h_i - m_h)\,(h_{i+m} - m_h), \quad (2)$$

where n – the number of measurements; m – the number of points of correlation function, m=0, 1, 2, ...; h_i – ordinate of inequality, cm, i = 1, 2, ..., m; m_h – mathematical expectation of ordinates of inequalities, cm; D_h – dispersion profile background, cm^2. The normalized spectral density $s(\omega)$ of the oscillations of micro-profile irregularities of the traces of a constant technological track was determined by the ratio of spectral density to the variance of the random function [14]:

$$s(\omega) = \frac{\Delta l}{\pi} \left[1 + 2 \sum_{i=1}^{m} \rho_i(l) \cos(m_i \cdot \Delta\omega)\right], \quad (3)$$

where Δl – profile measurement measurement interval, cm; $\Delta\omega = \frac{\pi}{m \cdot \Delta l}$ – step frequency of profile inequalities, cm^{-1}.

In the theories of probability, the equations (2) and (3) that relate a cross-correlation function to a spectral density function, are called “cosine-Fourier transforms”. Thus, the normalized correlation function and spectral density are expressed one by one via the “Fourier transform”.

Experimental studies were conducted in a greenhouse complex (Fig. 2), on the basis of which the laboratory was specially equipped for testing a bridge agricultural tool, specially designed for its use in the track agriculture. Under the conditions of this laboratory, a permanent technological track was artificially created on the soil. The longitudinal profile of its irregularities was finally formed by means of repeated passes of the engines of the newly constructed axle-driven agricultural machine over it.

Figure 2. Laboratory for testing a new construction bridge agricultural machine with a permanent technological track

Thus, it was reproduced an actual production situation under the laboratory conditions, when a bridge power tool, repeatedly moving its running wheels along the narrow tracks (on both sides) in both directions of movement and performing a real technological process of harrowing the soil, formed the surface layer of soil with the treads of pneumatic tires of its wheels right on the tracks. It was under the influence of real soil resistance during harrowing by this bridge power tool that the pneumatic tire treads of its wheels realized epy real traction properties and thereby formed a structure and corresponding surface irregularities in the surface soil layer.

After 5-6 passes of the bridge power tool, the corresponding surface profile remained on the ruts during the process of harrowing the soil, which was later measured using the developed profiler, and further processed and studied using a personal computer.

It is quite obvious that when performing another technological process (for example, plowing), the bridge power tool, overcoming significant traction resistance, will form irregularities on the surface soil layer in each track with its pneumatic tire treads, which will have different statistical indicators. In this case, the irregularities can be sufficiently smoothed (due to the slipping of the propellers), and their ordinates will be small; the surface layer of the soil can be significantly crushed, and so on.

However, in this experimental study, the statistical characteristics of unevenness of the soil surface were studied precisely during the harrowing of the soil by a bridge power tool.

RESULTS AND DISCUSSION

To study the statistical characteristics of the longitudinal microrelief of soil surface irregularities in the system of track farming, a new method was developed for automated obtaining of the statistical characteristics of these irregularities using the developed profilograph of a new design, consisting of mechanical and electrical parts and a personal computer.

The developed method of experimental study of soil microrelief on tracks in bridge farming makes it possible to obtain reliable values of statistical characteristics with minimal cost and with a high degree of accuracy, which can later be successfully used in studying the dynamics of movement of bridge agricultural machine units equipped with various agricultural machines and implements.

According to the steps of this methodology, i.e. to obtain such results, it is planned to simulate a section of the track technology of tillage in the laboratory and prepare technological tracks along which the running wheels of the bridge power vehicle under study will move. This is a prerequisite: the formation of track by the running wheels when the bridge power tool performs a real technological process, which corresponds to the actual tillage or a particular used agricultural implement. In this case, the studies were carried out during the technological operation of harrowing the soil in the inter-track space. The fulfillment of this condition according to the developed methodology is mandatory, since the running wheels of the bridge power tool are capable of forming the surface layers of track, because the real transmitted torques, real traction forces, real traction properties of the pneumatic tires of the running wheels, as well as the shapes and sizes of the treads of these pneumatic tires will form the external view, geometric dimensions and properties of the longitudinal profile of the unevenness of soil surface on two tracks along which the bridge power vehicle will move.

The repeated movement of running wheels of the bridge power tool makes it possible to form a surface layer of ruts and irregularities as a result of the passage when the technological process is performed in two directions. This is precisely due to the fact that the primary pass will only contribute to the formation of tramline on both sides, and the second pass will form the properties of track. Thus, the passage of bridge power tool in the opposite direction will reflect the real state of unevenness of the soil surface during their subsequent longitudinal measurement. Movements in these directions are carried out under the same external conditions, i.e. the same temperature, air humidity and soil.

Subsequent passes of the experimental bridge energy facility in excess of those indicated will contribute to a strong smoothing of the microrelief precisely on the tramlines. There will be rolling and compaction of the soil surface on the ruts, which will eventually give a distorted picture of unevenness of the soil surface on the ruts. At the same time, it is not mandatory the removal of high-frequency irregularities of the soil surface on the tracks for a bridge power tool for agricultural purposes due to a fairly soft and loose surface layer.

After the passage of this bridge power unit along the tracks, the bridge power tool was stopped according to the specified methodology; using the developed profilometer, it was assessed the state of unevenness of the soil surface located on both sides of the tracks; the measurements were made in the test areas; computer processing of the measurement results was carried out.

Thus, the main results obtained with the help of a new design profiler on the assessment of statistical characteristics of the soil surface irregularities on the tracks along which the running wheels of the bridge agricultural vehicle move, refer only to the data obtained when the bridge power tool performs the technological process of harrowing the soil in the inter-track space. In the case of performing other agricultural work with this bridge power tool, the pattern of unevenness of the soil surface on the tracks will be different.

It should be noted that the running wheels of the bridge power tool during laboratory experimental studies were equipped with pneumatic tires brand 9.5R32 (two wheels on each side), and the harrowing of the field surface in the inter-track space was carried out by three tine harrows brand BZSS-1.0, overlapping the entire width of the inter-track space.

According to the results of experimental studies and their processing on a personal computer, it has been constructed the graphs that should be attributed precisely to this type of agricultural work and this type of wheels and pneumatic tires, which amounted to 2 unites on each side on the studied bridge power facility.

The conducted laboratory experimental studies made it possible to obtain such data. As a result of profiling the irregularities of longitudinal profile of the soil traces of a constant tramline, it has been found that the main statistical indicator (as a standard deviation) in this case reaches ±0.82...0.84 cm. In essence, these are the damped periodic oscillations, as it is shown in the form of a curve of the normalized correlation function (Fig. 3). It should be noted that the form of normalized correlation function shows that the length of correlation connection of the heights of unevenness of the soil surface on the tracks reaches 0.18 m, which is due to the distance between the protrusions of treads of pneumatic tires of the running wheels of the bridge power vehicle. In this case, the bridge power vehicle is equipped with 9.5R32 pneumatic tires, in which the distance between the lugs of tread reaches exactly 0.175 m at normal air pressure inside the tire.

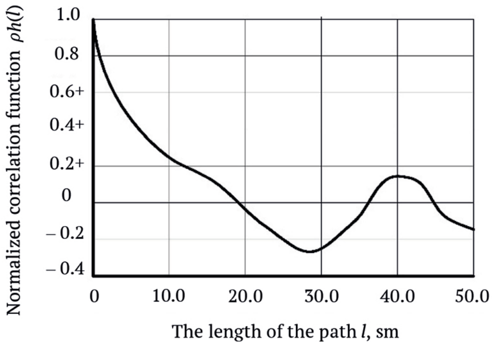

Figure 3. Dependence of the normalized correlation function $\rho_h(l)$ of the roughness of the soil surface of track along which the power tool moves on the length of traveled path

The normalized spectral density of the oscillatory process is the second most important statistical characteristic. After processing the results of experimental study, a new frequency spectrum has been obtained, which characterizes the random function of unevenness of the soil surface in the ruts along which the running wheels of the bridge power vehicle move. The dependence of normalized spectral density of the ordinates of roughness of the soil surface on the oscillation frequency is shown in the Figure 4. As it can be seen on this graph, the cutoff frequency of the oscillatory process under consideration reaches 0.3 cm^{-1}, provided that the main scattering fraction is precisely in the range from 0 to 0.3 cm^{-1}. This is confirmed by the size of depressions in the tread of pneumatic tires of the running wheels of the bridge power tool. It has also been found that the standard deviation of the ordinates of roughness of the soil surface on the tracks is also consistent with the height of tread of the pneumatic tires of the running wheels of the bridge power vehicle. Namely, the dimensions of tread protrusions of a 9.5R32 pneumatic tire are 0.03 m at an average air pressure inside the tires.

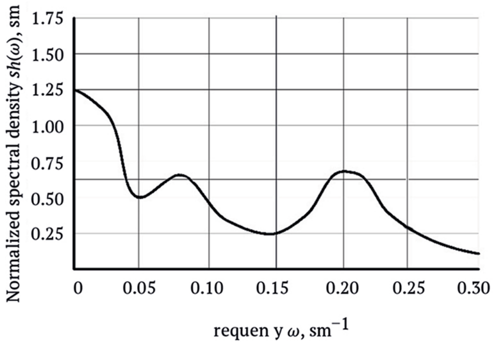

Figure 4. Normalized spectral functions $s_h(\omega)$ of the profiles of bumps in the traces of a constant technological track

The above-mentioned analysis of characteristics of the profile irregularities of traces of the permanent tramlines indicates that the parameters of tire treads of the axle agricultural machine of new construction are the generator of formation of these irregularities.

Thus, the indicated statistical characteristics of the soil surface irregularities on the tracks along which the running wheels of bridge power vehicles move have been obtained and calculated in accordance with the recommendations [14; 15]. The use of such statistical characteristics has been successfully used in the study of movement and the dynamics of other agricultural machines and machine units, which is confirmed in the previously published works [16-18].

It should be emphasized that the formation of unevenness of the soil surface on the tracks along which the running wheels of bridge power vehicles move (due to the passages precisely during the technological process of harrowing the soil) is very important. This is due to the fact that it is the early spring harrowing of the soil (which will form the longitudinal relief of the ruts) that will continue to exist without significant changes until the autumn tillage. This means that the data obtained in the spring on the unevenness of soil surface on the tracks can be successfully used throughout the entire period of growing crops (spring harrowing, sowing, care, harvesting, autumn tillage), which is very important when using a precision farming system.

Thus, the results obtained are confirmed by not only the similar findings from other authors [15; 17; 18]; this fact confirms their reliability and also indicate their significance in the introduction of "High Technologies" into agricultural production. The obtained results of laboratory field studies, in particular, the normalized correlation and spectral functions, their graphical representation, also coincide with similar results presented in the works accompanying this research topic [19; 20]. This also gives grounds to consider the results of the study as reliable.

Obtaining statistical information on the unevenness of soil surface on the tracks along which the running wheels of the bridge power tool move, and the vibrations of agricultural machines, which are used in this case, will make it possible (using the methods of theory of automatic control) to study the dynamics of machine-tractor units more deeply, such as the study of the object behavior in the presence of "input" and "output" signals. This will ultimately make it possible to improve the dynamic characteristics of agricultural machine-tractor units, including bridge units. In general, this will make it possible to significantly improve the quality of products grown in the fields, including the use of bridge farming technologies.

CONCLUSIONS

Devices and methods have been developed for the experimental study of the microrelief of unevenness of the soil surface in the traces of a constant technological track in the bridge farming, which make it possible to immediately obtain its statistical characteristics. This is achieved by the following fact: with the help of a new profiler of the developed design, a statistical calculation program and a personal computer, it is possible to take reliable information, process it and immediately obtain the necessary experimental data to assess the vibrational processes of machines and tools used in such agriculture.

According to the data of multiple experimental studies conducted to determine the statistical characteristics of traces of a constant gauge of a bridge power tool, when reproducing real conditions of the soil harrowing (i.e. after passing along the tracks of the running wheels), the standard deviation of soil surface irregularities is within 0.82...0.84 cm. At the same time, the analysis of obtained graphs has shown that the internal structure of the track surface irregularities, recorded by a profiler and processed on a personal computer, can be characterized as a function containing harmonic damped periodic oscillations, in the presence of random components. The graph of the normalized correlation function has shown that the length of correlation connection of the ordinates of roughness of the soil surface on the traces of a constant technological track, approximately corresponds to the dimensions of height of the treads of the pneumatic tires of the running wheels of the power vehicle.

As a result of profiling the irregularities of the longitudinal profile of the soil surface during laboratory experimental studies according to the program of a multifactorial experiment, it was found that the energy and vehicles of a bridge agricultural machine of a new design moving along it, the running wheels of which move along the traces of the track, the main part of the dispersion is in the range from 0 to 0.3 cm^{-1}. This is confirmed by the size of depressions in the tread of pneumatic tires of the running wheels of the power vehicle.

Further research should be focused on the development of technical means and methods for recording the vibrations of the working bodies of agricultural machines using the similar measuring equipment, which will make it possible to simultaneously evaluate the statistical characteristics of the roughness of soil surface (as an input action) and the characteristics of vibrations of the working bodies, which will act as the reactions to this input. The use of results of the real oscillatory processes at the input in the form of irregularities of the soil surface on narrow tracks along which the bridge vehicle moves, and at the output in the form of vibrations of aggregated agricultural machines, will make it possible to design complex dynamic systems (machine-tractor units) and bridge farming with optimal parameters.

REFERENCES

[1] Beloev, H., Bulgakov, V., Kuvachov, V., Adamchuk, V., Kaminskiy, V., & Ivanovs, S. (2022). Research and justification of running wheels tire parameters of bridge-type transport energy vehicle. *AIP Conference Proceedings*, 2570(1), article number 040009. doi: 10.1063/5.0100122.

[2] Bulgakov, V., Olt, J., Pascuzzi, S., Adamchuk, V., Gadzalo, J., Kuvachov, V., Kaletnik, H., Kaminskiy, V., & Lillerand, T. (2022). Theoretical research of gantry tractor turning. In *Proceedings of the 33rd DAAAM International Symposium on Intelligent Manufacturing and Automation* (pp. 0380-0389). Vienna: DAAAM International. doi: 10.2507/33rd.daaam.proceedings.054.

[3] Beloev, H., Long, N.D., Nhu, D.T., & That, N.D. (2022). Sizes of soil chip cut by a continuously operating planting hole digging machine with an active tillage unit. *Acta Technologica Agriculturae*, 25(2), 79-84.

[4] Bulgakov, V., Olt, J., Pascuzzi, S., Ivanovs, S., Kuvachov, V., Santoro, F., Gadzalo, Ia., Adamchuk V., & Arak M. (2022). Study of the controlled motion process of an agricultural wide span vehicle fitted with an automatic driving device. *Agronomy Research*, 20(3), 508-518.

[5] Kuvachov, V., Bulgakov, V., Adamchuk, V., Kaminskiy, V., Melnik, V., & Olt, J. (2021). Experimental research into new harrowing unit based on gantry agricultural implement carrier. *Agronomy Research*, 19(1), 126-135. doi: 10.15159/AR.20.239.

[6] Nadykto, V.T., & Uleksin, V.O. (2008). *Track and bridge systems of agriculture*. Melitopol: MMD Publishing House LLC.
[7] Bindi, I., Blackwell, P., & Riethmuller, G. (2013). *Controlled traffic farming technical manual*. Narembeen: Department of Agriculture and Food.
[8] Chamen, T. (2015). Controlled traffic farming – from worldwide research to adoption in Europe and its future prospects. *Acta Technologica Agriculturae Nitra*, 3, 64-73.
[9] Gasso, V., Sørensen, C.A.G., & Oudshoorn, F.W. (2013). Controlled traffic farming: A review of the environmental impacts. *European Journal of Agronomy*, 48, 66-73.
[10] Nadykto, V., Findura, P., Kyurchev, V., & Orel, O. (2022). Influence of biodiesel on performance of machine-tractor units. *Acta Technologica Agriculturae*, 25(1), 7-12.
[11] Olt, J., Bulgakov, V., Trokhaniak, O., Klendii, M., Gadzalo, Ia., Ptashnik, M., & Tkachenko, M. (2022). Harrow with screw-type operating tools: Optimisation of design and process parameters. *Agronomy Research*, 20(4), 751-763.
[12] Kuvachev, V., Mitkov, V., & Shulga, O. (2016). Modeling of plane-parallel movement in the vertical plane of a wide-gauge agricultural vehicle for a track farming system. *Motrol*, 18(1), 3-12.
[13] Khlepitko, M.N. (1998). Assessment of the cross-country ability of mobile vehicles. *Tractors and Agricultural Machines*, 5, 20-22.
[14] Dmitrichenko, S.S., & Zavyalov, Yu.A. (1983). On the determination of the statistical characteristics of the microprofiles of unpaved roads and fields. *Tractors and Agricultural Machines*, 5, 9-11.
[15] Patent of Ukraine No. 117278 (2017, June). Retrieved from https://uapatents.com/4-117278-mostovijj-zasib-z-regulovanoyu-tekhnologichnoyu-koliehyu.html.
[16] Ivanovs, S., Bulgakov, V., Pascuzzi, S., Santoro, F., & Bulgakova, O. (2023). Research of the possibilities to improve the quality of potatoes harvesting by including an experimental heap leveler-distributor in the design of harvesting machines. In S. Pascuzzi, F. Santoro (Eds.), *Farm machinery and processes management in sustainable agriculture. FMPMSA 2022. lecture notes in civil engineering* (pp. 37-47). Cham: Springer. doi: 10.1007/978-3-031-13090-8_4.
[17] Antoshchenkov, R.V. (2017). *Dynamics and energy of the turn of rich-element machine-tractor units*. Kharkiv: KhNTUSG, Miskdruk.
[18] Adamchuk, V.V., Bulgakov, V.M., Holovach, I.V., & Kuvachov, V.P. (2018). Studying the conditions of assembling traction-drive soil-processing aggregates with tractors of traction-energy concept. *Agricultural Science and Practice*, 5(2), 27-36.
[19] Pedersen, H.H. (2011). Harvest capacity model for a wide span onion bunker harvester. In *Automation and system technology in plant production, CIGR section V & NJF section VII conference* (pp. 27-36). Uppsala, Sweden.
[20] Popp, K., & Schiehler, W. (2010). *Ground vehicle dynamics*. Berlin: Springer. doi: 10.1007/978-3-540- 68553-1.

Христо Белоєв

Доктор технічних наук, професор
Русенський Університет «Ангел Кенчев»
7017, вул. Студентська, 5, м. Русе, Болгарія
https://orcid.org/0000-0002-8644-2947

Методика експериментального дослідження мікрорельєфу ґрунту на коліях при мостовому землеробстві

Анотація. Вивчення питань, пов'язаних з дослідженням стану ґрунту на поверхні найбільш постійної технологічної колії є актуальним, оскільки рух ходових коліс по вузьких коліях визначає тягово-зчіпні властивості машинно-тракторних агрегатів, їх вібрації, стійкість руху і керованість рухом. Метою даного дослідження було підвищення ефективності процесу профілювання мікронерівностей поверхні ґрунту, розташованих на ділянках, що утворюють колію, по якій рухатимуться ходові колеса машинно-тракторних агрегатів, шляхом обґрунтування нової схеми автоматизованого профілографа та розробка методики його використання. Для даного дослідження були використані сучасні методи експериментальних досліджень на основі IT-технологій. Зокрема, розроблено автоматизований комплекс для вимірювання та оцінки мікропрофілю нерівностей поверхні ґрунту на самій колії технологічної колії. Результати експериментальних досліджень у цьому питанні показали, що стандартне відхилення нерівностей поверхні ґрунту досягає ±0,84 см. Це дає підстави розглядати гармонічні складові цих функцій як затухаючі, що мають нормовані кореляційні функції. Побудовані за допомогою ПК графіки показали, що більшість дисперсій нерівностей поверхні ґрунту на самих коліях зосереджено в діапазоні 0…0,3 см$^{-1}$. Встановлено, що генератором утворення нерівностей поздовжнього профілю слідів постійної технологічної колії є параметри протекторів коліс машин, що рухаються по ній. Отримані результати дослідження можуть бути використані при виборі протекторів пневматичних шин ходових коліс машинно-тракторних агрегатів, що рухаються по двох коліях

Ключові слова: колійний засіб; нерівності; коливання; кореляційна функція; спектральна щільність

Machinery & Energetics
Vol. 13, No. 4. 2022

Journal homepage:
https://technicalscience.com.ua/en

UDC 658.562.2:635.11:633.63
DOI: 10.31548/machenergy.13(4).2022.16-27

Myroslav Budzanivskyi*
Postgraduate Student
Institute of Mechanics and Automatics of Agroindustrial Production
National Academy of Agrarian Sciences of Ukraine
08631, 11/1 Vokzalna Str., Glevakha, Kyiv region, Ukraine
https://orcid.org/0000-0002-0508-3816

Mathematical modelling of oscillations of a machine for cutting tops of root crops

Abstract. High-quality cutting of root crop tops at the root ensures both a high yield and determines the condition of the root crops before they are extracted from the soil. Therefore, the search for conditions that will ensure this is an important and urgent problem for the production of these crops. The purpose of this research was to determine, through an analytical study, the optimal parameters of a new design of a machine for harvesting root crop tops, which is mounted in front of an aggregating tractor and performs oscillatory movements in the longitudinal-vertical plane. Methods related to the modelling of complex dynamic systems consisting of an aggregating tractor and a front-mounted machine, the development and solution of the final form of differential equations of oscillatory motion and computer modelling of the oscillatory process were used. According to the developed equivalent scheme, a new differential equation of angular vibrations of the machine was solved in the final form. In addition, numerical modelling was performed on a PC, which allowed constructing graphical dependencies of the machine's turning angle φ at different speeds V of its forward movement and values of the c stiffness coefficient and μ damping coefficient of the pneumatic tyres of the copying wheels, and at different values of the unevenness of the soil surface and the main design parameters of the machine. It was established that with an increase V from 1.5 m·s^{-1} to 2.5 m·s^{-1}, the amplitude of oscillations of the machine's turning angle φ increased from 0.88° to 1.18°. However, at V 1.5 m·s^{-1}, the duration of the transient process is 0.22 s, and at a speed of 2.5 m·s^{-1}, this figure is already 0.14 s, i.e., a decrease of 36%. The positive amplitude of oscillations φ of the machine's steering angle reaches 1.2°, and the negative amplitude does not exceed 0.3°, i.e., the oscillation range is insignificant. In the range of values considered V, preference should be assigned to its higher value. The structural and kinematic parameters of the system examined were determined using computer simulation. The presented method of mathematical modelling of the oscillatory process can be used in the research of any machines that are hitched in front of the aggregating tractors

Keywords: sugar beet; harvesting; oscillations; differential equation; solving on a PC; graphs

Article's History: Received: 15/08/2022; Revised: 14/10/2022; Accepted: 02/11/2022.

INTRODUCTION

The tops of most root crops (sugar, fodder and table roots, carrots, turnips, rutabagas, etc.), if produced in sufficient quantities, can be of significant benefit both as organic fertiliser and as livestock feed and raw material for biogas production. Therefore, cutting, collecting and using root crop tops is an urgent task in the field of agricultural mechanisation.

Since many root crops are grown using modern technologies that involve harvesting the tops of these crops on the root, the machines that will perform these operations must comply with the relevant requirements to prevent damage and loss of root crop bodies and their damage, dislodging the root crops themselves from the soil, complete harvesting of the tops and preventing their contamination with soil impurities. In addition, accurate and high-quality pruning of tops from the heads of root crops reduces the loss of their upper parts, which will significantly increase the full yield of root crops per hectare of their crops [1].

Suggested Citation:
Budzanivskyi, M. (2022). Mathematical modelling of oscillations of a machine for cutting tops of root crops. *Machinery & Energetics,* 13(4), 16-27.

*Corresponding author

Thus, the most common multistage method of harvesting root crop tops involves first making a continuous main cut of the entire crop, followed by harvesting and unloading into a vehicle or scattering it across the field. Next, the heads of the root crops are cleaned or trimmed (or simultaneously cleaned and trimmed with different working tools) from the remaining tops on the root.

Therefore, this sequence must be followed before removing the root crops from the soil, and the tops harvesting machines, either as independent agricultural machines or as top harvesting modules of various combines, must be attached to the front of the power vehicle (i.e., to the aggregating tractor or the front of the frame of self-propelled combines) [2].

Analysing the studies published on this subject [2-4], it can be stated that the results of experimental studies indicate that during operation, the machines for cutting tops frontally attached to the aggregating tractor perform oscillatory movements, which are determined by the relief of uneven field surfaces, the forward speed of the aggregating tractor, the location of the copy wheels relative to the machine suspension system, etc. Using the latter causes oscillatory movements of machines for harvesting root crops, which significantly worsens the quality indicators of the process in question. Namely, it is necessary to improve the quality of cutting the tops from each head of root crops over the entire working width of the machine and to collect and unload them without significant losses. And this should be the case in any condition of the location of the heads of root crops in terms of their height. It requires precise and sensitive reproduction of soil surface irregularities and the height of root crop heads.

Despite the widespread use of front-mounted machines for harvesting root crop tops, there is virtually no fundamental analytical research into their oscillatory movements over uneven soil surfaces. Works [1; 4; 5] present theoretical studies of oscillations of a machine for cutting tops of root crops frontally attached to an aggregating tractor using the equations of dynamics of mechanical systems in generalised coordinates. Therewith, these studies do not always consider some important parameters. For example, the forces acting on topsy-turvy machines are not always considered, oscillatory movements are considered in the presence of unnecessary generalised coordinates, and unjustified simplifications are made when solving the resulting differential equations. In addition, when solving this problem, a dynamic system consisting of two differential equations of oscillatory motion is explored, i.e., in the presence of an extra generalised coordinate. Having just one coordinate will be enough.

In studies [6-8], it was demonstrated that the issues of high-quality sugar beet tops harvesting are solved based on other conditions not related specifically to the oscillatory processes of top harvesting machines and their working bodies.

The issues of exploring the energy performance of harvesting root crops and processing raw materials are discussed in [9-11]. However, they do not consider the dynamics of harvesting machines. The study of the stability of a ploughing unit mounted frontally on an aggregating tractor is devoted to [12-14], the methodology for constructing graphical dependencies of oscillatory processes is given in [15-17], and the controllability of movement is reflected in [18]. The issues of changes in soil properties that affect the oscillations of harvesting machines are discussed in [19; 20]. The studies presented in well-known works provide grounds for the development of a mathematical model that would accurately describe the oscillatory process of a machine for harvesting root crops mounted in front of an aggregating tractor.

Based on the above and using the methodology discussed in [3], it is possible to build a more accurate mathematical model of the movement of a machine for cutting root crops in the longitudinal-vertical plane when it moves along uneven soil surfaces. It will allow for a more accurate study and determination of such kinematic and structural parameters, using which will contribute to a significant improvement of the technological process under consideration.

The purpose of the study was to determine the optimal structural and kinematic parameters of a machine for cutting tops of various root crops, which is attached to the front of a wheeled aggregating tractor, by analytically exploring the dynamics of its oscillatory movements in the longitudinal-vertical plane.

MATERIALS AND METHODS

The mathematical modelling was performed using the methods of constructing computational mathematical models of agricultural machines and machine units. Theoretical studies of the obtained differential equation of oscillatory motion are conducted using the basic provisions of the dynamics of complex dynamic systems based on the methods of analytical mechanics, vibration theory and higher mathematics (in particular, the method of uncertain coefficients is used to solve the differential equation). The numerical solution was performed using a personal computer and PTC Mathcad 15 software.

At the Department of Mechanics of the National University of Life and Environmental Sciences of Ukraine, and the Institute of Mechanics and Automation of Agricultural Production of the National Academy of Agrarian Sciences of Ukraine, under the guidance of Prof. V.M. Bulgakov, a new design of a machine for cutting root crop tops was developed, which works like a mower and can be used to cut tops of both many root crops on the root and perennial grasses, as it is frontally attached to the aggregating tractor [1]. Several prototypes of machines for harvesting root crop tops were manufactured in industrial conditions and tested in the field, with positive results. Comprehensive theoretical and experimental studies are conducted to optimise its structural and kinematic parameters.

This machine uses a rotary cutting unit that is positioned over the entire working width of the machine. The rotary cutting machine has arc-shaped cutting blades that are pivotally mounted on the drive drum in an appropriate pitch. The drive drum rotates in the opposite rotation to the forward motion of the entire machine. The sharp blades of the arcuate cutting knives cover the entire working width of the cutter bar. The arc-shaped cutting knives rotating in the longitudinal-vertical plane provide a free-flowing cut of the main mass of the tops along the entire working width of the machine and ensure that it is transferred to the screw conveyor, which collects and transports it to the end part of the machine. Here, using an unloading mechanism and a spigot of the appropriate height, the cut tops are unloaded into a vehicle moving alongside the harvested area of the field [1; 4; 6]. If necessary, the discharge mechanism and the nozzle can be detached from the machine, and the cut stubble is then discharged onto the harvested area of the field and used as fertiliser. The rotary cutter bar (i.e. the actual sharp ends of its arc-shaped cutting blades) is positioned at the appropriate cutting height relative to the surface established by the root crops (in the crop rows) using two tracking wheels (with screw mechanisms for their installation relative to the machine frame). The tracking wheels are positioned in the row spacing of the root crops and roll over uneven soil surfaces in the row spacing but track the general unevenness in the machine's working area. Considering the fact that root crops are harvested at the root, and the heads of these crops can be located at different heights relative to the soil surface itself, the rotary cutter is set to a higher cutting height using the screw mechanisms of the copy wheels. It prevents the bodies of the root crops themselves from being removed along with the tops, damaging them, which is extremely undesirable and knocking the root crops out of the soil. Therefore, the operations of complete and final harvesting of root crop tops are performed by other machines, in particular, root crop head cleaners for removing tops from the crops or passive (sometimes active) head trimmers.

Figure 1 presents a general overview of this machine for cutting the tops of root crops at the root.

Figure 1. Root crop peeling machine with rotary cutting unit

The qualitative performance of the machine for cutting the tops of root crops, namely the completeness of the cut, the absence of damage and the dislodging of root crops from the soil, will be determined by the stability of the movement of its rotary cutting unit in the longitudinal-vertical plane. And this will be positively influenced by the sensitivity of the machine's tracking system, which will be able to track all the unevenness of the surface of the field with root crops, and by the design parameters of the machine and the device for connecting it to the wheeled tractor. Mathematical modelling of the oscillations of a machine for cutting the tops of root crops can be performed if differential equations of its oscillatory movements in the corresponding plane are compiled. For this purpose, first of all, an equivalent diagram of this machine for cutting the tops of root crops in the longitudinal-vertical plane was built, which is presented in Figure 2.

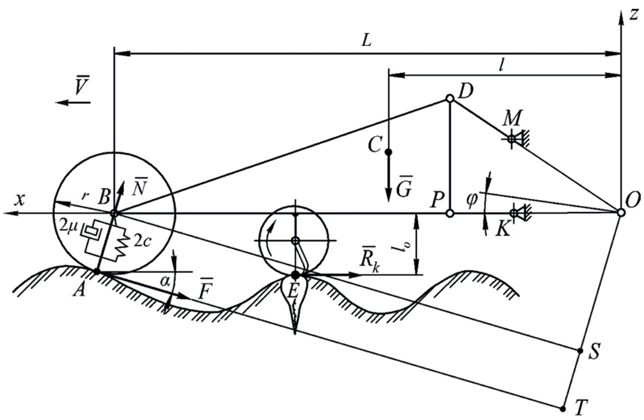

Figure 2. An equivalent diagram of a machine for cutting off the tops of root crops φ – generalised coordinate (the angle of rotation by which the machine deviates in the longitudinal-vertical plane); α – the angle of deviation of the friction force ($\bar{F}$) from the horizontal, which changes its value in different areas of the uneven ground surface on which the copy wheel moves; c – coefficient of stiffness of the pneumatic tyre of the copy wheel; μ – coefficient of damping of the pneumatic tyre of the copy wheel

The features of this equivalent arrangement are that the root crop top dresser is connected to the aggregating tractor at the front. For this purpose, two lower (*PK*) and one upper (*MD*) linkages are used, i.e. the central linkage of the tractor's front linkage. When performing the technological process of harvesting tops with a root crop tops harvester, the connecting rods of the front linkage of the implement are unlocked. It is in this position that the root crop top dresser uses its pneumatic tracking wheels, which are positioned and move in the row spacing of the root crops, to effectively follow the unevenness of the soil surface and set its rotary cutter bar to the desired cutting height. The equivalent diagram represents the movement of a root crop topping machine in the longitudinal-vertical plane when its front tracking wheel moves over an uneven soil surface that has the form of a harmonic function. Figure 2 demonstrates all the external forces acting on the pneumatic copy wheels (two wheels combined into one and represented as elastic-damping models) and the rotary cutter and provides the main linear and angular dimensions.

RESULTS AND DISCUSSION

In the mathematical modelling of the movement of the machine for cutting the tops of root crops, equations in the Lagrange form of the 2nd kind were used, all the necessary transformations were performed, and the differential equation of its movement was obtained in the following form [1; 3]:

$$A_2\cdot\ddot{\varphi}+A_1\cdot\dot{\varphi}+A_o\cdot\varphi=B_1\cdot\dot{h}+B_o\cdot h+C, \quad (1)$$

where the coefficients A_o, A_1, A_2, B_o, B_1 are constant values, which are equal to each other:

$A_2=I_{oy}$ – is the moment of inertia of the machine relative to the axis O_y (this axis is not presented in the diagram of Fig. 2), which is perpendicular to the longitudinal-vertical plane zOx and passes through the point O, kg·m^2; $A_1=2\mu\cdot L^2$, (μ is the damping coefficient of the pneumatic tyre of the copying wheel); $A_o=2c\cdot L^2$, (c is the stiffness coefficient of the pneumatic tyre of the copying wheel); $B_1=2\mu\cdot L$; $B_o=2c\cdot L$. φ is the angle of rotation of the machine in the longitudinal-vertical plane relative to the centre of rotation (point O); h – is the ordinate of the unevenness of the soil surface.

Equation (1) belongs to the class of second-order differential equations with constant coefficients and a right-hand side.

In this case, the term C included in equation (1) is determined from the following expression:

$$C=N\cdot[L-f(r+L\cdot\alpha)]-R_k\cdot l_o-G\cdot l, \quad (2)$$

where N – unknown normal reaction of the bunch (i.e. normal reaction of the soil to the tracking wheel at point A); L – distance from the conditional point O of machine turning to the axis of the tracking wheels (point B); r – radius of the tracking wheel; α – angle of deviation of the friction force $\bar{F}$ from the horizontal, provided that $\sin\alpha=\alpha$ i.e. when the angle is small α; R_k – the total force of cutting the tops of root crops, reduced to point E, i.e. the end of the arcuate knife of the rotary top cutter; l_o – the height of the cut of the tops of root crops (or the distance from the end of the arcuate knife of the rotary top cutter to the lower base of the machine); G – the weight of the machine for cutting the tops of root crops; l – the distance from the conditional point O of rotation of the machine to its centre of mass.

Thus, equation (1) contains two unknowns, namely φ and N.

However, N can be determined to a first approximation from the static equilibrium equation of the mechanical system under consideration with sufficient accuracy for practice. Namely:

$$N=\frac{R_k\cdot l_o+G\cdot l}{L-f(r+L\cdot\alpha)}. \quad (3)$$

It is easy to confirm that after substituting expression (3) into expression (2), the value of C will turn to zero, i.e. C=0.

Thus, equation (1), with sufficient accuracy, is transformed into the following equation:

$$A_2\cdot\ddot{\varphi}+A_1\cdot\dot{\varphi}+A_o\cdot\varphi=B_1\cdot\dot{h}+B_o\cdot h. \quad (4)$$

Since the harmonic function h, which is included in the right-hand side of equation (4), determines the unevenness of the soil surface over which the machine's copy wheel moves, it is determined according to the following expression [6]:

$$h=h_o\left(1-\cos\frac{2\pi\cdot x}{l_1}\right)=h_o\left(1-\cos\frac{2\pi\cdot V\cdot t}{l_1}\right), \quad (5)$$

along with its first derivative, whose value at time t will be equal to:

$$\dot{h}=\frac{2\pi\cdot h_o\cdot V}{l_1}\cdot\sin\frac{2\pi\cdot V\cdot t}{l_1}, \quad (6)$$

where h – the actual current ordinate of the unevenness of the soil surface, m; h_o – the amplitude of the unevenness of the facet surface; l_1 – the period of oscillation of the unevenness of the soil surface, m; $x=V\cdot t$ – the current abscissa of the unevenness of the soil surface, m; V – the forward speed of the machine, m·s^{-1}, then after substituting (5) and (6) into equation (4), the following differential equation is obtained:

$$A_2\cdot\ddot{\varphi}+A_1\cdot\dot{\varphi}+A_o\cdot\varphi=\frac{2\pi\cdot B_1\cdot h_o\cdot V}{l_1}\cdot$$
$$\cdot\sin\frac{2\pi\cdot V\cdot t}{l_1}-B_o\cdot h_o\cdot\cos\frac{2\pi\cdot V\cdot t}{l_1}+B_o\cdot h_o\ , \quad (7)$$

which can be converted to the following equation:

$$\ddot{\varphi}+\frac{A_1}{A_2}\cdot\dot{\varphi}+\frac{A_o}{A_2}\cdot\varphi=\frac{2\pi\cdot B_1\cdot h_o\cdot V}{A_2\cdot l_1}\cdot$$
$$\cdot\sin\frac{2\pi\cdot V\cdot t}{l_1}-\frac{B_o\cdot h_o}{A_2}\cdot\cos\frac{2\pi\cdot V\cdot t}{l_1}+\frac{B_o\cdot h_o}{A_2}. \quad (8)$$

Firstly, consider the general solution of the homogeneous differential equation of the following form:

$$\ddot{\varphi}+\frac{A_1}{A_2}\cdot\dot{\varphi}+\frac{A_o}{A_2}\cdot\varphi=0. \quad (9)$$

Its characteristic equation is as follows:

$$k^2 + \frac{A_1}{A_2} \cdot k + \frac{A_o}{A_2} = 0, \quad (10)$$

where k – roots of the characteristic equation.

Determine the roots of the quadratic equation (10). Have:

$$k_1 = -\frac{A_1}{2A_2} + \sqrt{\frac{A_1^2}{4 \cdot A_2^2} - \frac{A_o}{A_2}}. \quad k_2 = -\frac{A_1}{2A_2} - \sqrt{\frac{A_1^2}{4 \cdot A_2^2} - \frac{A_o}{A_2}}. \quad (11)$$

Natural oscillations of the mechanical system examined are possible when the roots k1 and k2 are complex numbers.

It will be the case if:

$$\frac{A_1^2}{4 \cdot A_2^2} - \frac{A_o}{A_2} < 0. \quad (12)$$

It can be demonstrated that within the real parameters of the machine for cutting the tops of root crops under consideration, inequality (12) is always performed. Indeed, inequality (12):

$$\frac{A_1^2}{4 \cdot A_2^2} - \frac{A_o}{A_2} = \frac{A_1^2 - 4A_2 \cdot A_o}{4 \cdot A_2^2} < 0, \quad (13)$$

is summarised in the following inequality:

$$A_1^2\text{-}4A_2 \cdot A_o<0, \quad (14)$$

or, considering the expressions for the coefficients included in this inequality, obtain:

$$(2\mu \cdot L^2)^2\text{-}4I_{oy} \cdot 2c \cdot L^2<0, \quad (15)$$

At 2μ=150 N·s·m^{-1}, I_{oy}=30 kg·m^2, $2c$=4000 N·m^{-1}, L=1.8 m, there are:

(150·1.8^2)^2-4·30·4000·1.8^2=236196-1555200=-1319004<0.

Thus, the roots of the characteristic equation (10) are always complex and equal:

$$k_1 = -\frac{A_1}{2A_2} + \sqrt{\frac{A_o}{A_2} - \frac{A_1^2}{4 \cdot A_2^2}} \cdot i, \quad k_2 = -\frac{A_1}{2A_2} - \sqrt{\frac{A_o}{A_2} - \frac{A_1^2}{4 \cdot A_2^2}} \cdot i, \quad (16)$$

where i – imaginary unit.

In this case, the general solution $\bar{\varphi}$ of the homogeneous equation (9) will be as follows:

$$\bar{\varphi} = e^{-\frac{A_1}{2A_2} t} \cdot \left[\begin{array}{l} C_1 \cdot \sin\left(\sqrt{\frac{A_o}{A_2} - \frac{A_1^2}{4 \cdot A_2^2}} \cdot t\right) + \\ +C_2 \cdot \cos\left(\sqrt{\frac{A_o}{A_2} - \frac{A_1^2}{4 \cdot A_2^2}} \cdot t\right) \end{array} \right], \quad (17)$$

where C_1 and C_2 – arbitrary constants that are obtained from the initial conditions.

Next, determine the partial solution φ^* of the heterogeneous equation (8). Considering the right-hand side of the differential equation (8), its partial solution φ^* is found in the following form:

$$\varphi^* = M \cdot \sin\frac{2\pi \cdot V \cdot t}{l_1} + N \cdot \cos\frac{2\pi \cdot V \cdot t}{l_1} + R, \quad (18)$$

where M, N and R – uncertain coefficients.

To find the coefficients M, N, and R, use the method of uncertain coefficients. To do this, determine the first and second derivatives of time t for expression (18).

$$\dot{\varphi}^* = M \cdot \frac{2\pi \cdot V}{l_1} \cdot \cos\frac{2\pi \cdot V \cdot t}{l_1} - N \cdot \frac{2\pi \cdot V}{l_1} \cdot \sin\frac{2\pi \cdot V \cdot t}{l_1}, \quad (19)$$

$$\ddot{\varphi}^* = -M \cdot \frac{4\pi^2 \cdot V^2}{l_1^2} \cdot \sin\frac{2\pi \cdot V \cdot t}{l_1} - N \cdot \frac{4\pi^2 \cdot V^2}{l_1^2} \cdot \cos\frac{2\pi \cdot V \cdot t}{l_1}. \quad (20)$$

Substituting expressions (18) and (19) into the differential equation (8), obtain:

$$\begin{array}{c} -M \cdot \frac{4\pi^2 \cdot V^2}{l_1^2} \cdot \sin\frac{2\pi \cdot V \cdot t}{l_1} - N \cdot \\ \cdot \frac{4\pi^2 \cdot V^2}{l_1^2} \cdot \cos\frac{2\pi \cdot V \cdot t}{l_1} + \frac{A_1}{A_2} \cdot \\ \cdot M \cdot \frac{2\pi \cdot V}{l_1} \cdot \cos\frac{2\pi \cdot V \cdot t}{l_1} - \frac{A_1}{A_2} \cdot N \cdot \frac{2\pi \cdot V}{l_1} \cdot \\ \cdot \sin\frac{2\pi \cdot V \cdot t}{l_1} + \frac{A_o}{A_2} \cdot M \cdot \sin\frac{2\pi \cdot V \cdot t}{l_1} + \frac{A_o}{A_2} \cdot N \cdot \\ \cdot \cos\frac{2\pi \cdot V \cdot t}{l_1} + \frac{A_o}{A_2} \cdot R = \frac{2\pi \cdot B_1 \cdot h_o \cdot V}{A_2 \cdot l_1} \cdot \\ \cdot \sin\frac{2\pi \cdot V \cdot t}{l_1} - \frac{B_o \cdot h_o}{A_2} \cdot \cos\frac{2\pi \cdot V \cdot t}{l_1} + \frac{B_o \cdot h_o}{A_2}. \end{array} \quad (21)$$

By equating the coefficients of the same trigonometric functions and the free terms in the left and right sides of expression (21), obtain the following system of linear algebraic equations with respect to the unknowns M, N, and R:

$$\left. \begin{array}{c} \left(-\frac{4\pi^2 \cdot V^2}{l_1^2} + \frac{A_o}{A_2}\right) \cdot M - \frac{2 \cdot A_1 \cdot \pi \cdot V}{A_2 \cdot l_1} \cdot N = \frac{2\pi \cdot B_1 \cdot h_o \cdot V}{A_2 \cdot l_1}, \\ \frac{2 \cdot A_1 \cdot \pi \cdot V}{A_2 \cdot l_1} \cdot M + \left(-\frac{4\pi^2 \cdot V^2}{l_1^2} + \frac{A_o}{A_2}\right) \cdot N = \frac{B_o \cdot h_o}{A_2}, \\ \frac{A_o}{A_2} \cdot R = \frac{B_o \cdot h_o}{A_2}. \end{array} \right\} \quad (22)$$

From the third equation of system (22), the unknown R is determined:

$$R = \frac{B_o \cdot h_o}{A_o}. \quad (23)$$

To reduce the cumbersomeness of the equations, the following notation will be used:

$$-\frac{4\pi^2 \cdot V^2}{l_1^2} + \frac{A_o}{A_2} = S, \quad (24)$$

$$\frac{2 \cdot A_1 \cdot \pi \cdot V}{A_2 \cdot l_1} = T, \quad (25)$$

$$\frac{2 \cdot \pi \cdot B_1 \cdot h_o \cdot V}{A_2 \cdot l_1} = Q, \quad (26)$$

$$-\frac{B_o \cdot h_o}{A_2} = K. \quad (27)$$

Then the system of the first two equations of system (22) will be written in the following form:

$$\left. \begin{array}{l} S \cdot M - T \cdot N = Q, \\ T \cdot M + S \cdot N = K. \end{array} \right\} \quad (28)$$

Determine the principal determinant of the system (28):

$$\Delta = \begin{vmatrix} S & -T \\ T & S \end{vmatrix} = S^2 + T^2 \neq 0. \quad (29)$$

Therefore, to find the unknowns M and N from the system of equations (28), the Kramer rule can be applied. Calculate the necessary determinants:

$$\Delta_M = \begin{vmatrix} Q & -T \\ K & S \end{vmatrix} = Q \cdot S + K \cdot T, \tag{30}$$

and

$$\Delta_N = \begin{vmatrix} S & Q \\ T & K \end{vmatrix} = S \cdot K - T \cdot Q. \tag{31}$$

Then:

$$M = \frac{\Delta_M}{\Delta} = \frac{Q \cdot S + K \cdot T}{S^2 + T^2}, \tag{32}$$

and

$$N = \frac{\Delta_N}{\Delta} = \frac{S \cdot K - T \cdot Q}{S^2 + T^2}. \tag{33}$$

Substituting expressions (24)-(27) into expressions (32) and (33), accordingly, obtain:

$$M = \frac{\frac{2\pi \cdot B_1 \cdot h_o \cdot V}{A_2 \cdot l_1} \cdot \left(-\frac{4\pi^2 \cdot V^2}{l_1^2} + \frac{A_o}{A_2}\right) - \frac{2B_o \cdot h_o \cdot A_1 \cdot \pi \cdot V}{A_2^2 \cdot l_1}}{\left(-\frac{4\pi^2 \cdot V^2}{l_1^2} + \frac{A_o}{A_2}\right)^2 + \frac{4A_1^2 \cdot \pi^2 \cdot V^2}{A_2^2 \cdot l_1^2}}, \tag{34}$$

and

$$N = \frac{\left(\frac{4\pi^2 \cdot V^2}{l_1^2} - \frac{A_o}{A_2}\right) \cdot \frac{B_o \cdot h_o}{A_2} - \frac{4A_1 \cdot B_1 \cdot \pi^2 \cdot h_o \cdot V^2}{A_2^2 \cdot l_1^2}}{\left(-\frac{4\pi^2 \cdot V^2}{l_1^2} + \frac{A_o}{A_2}\right)^2 + \frac{4A_1^2 \cdot \pi^2 \cdot V^2}{A_2^2 \cdot l_1^2}}. \tag{35}$$

Considering (34) and (35), the partial solution (18) of the differential equation (8) will be as follows:

$$\varphi^* = \frac{\frac{2\pi \cdot B_1 \cdot h_o \cdot V}{A_2 \cdot l_1} \cdot \left(-\frac{4\pi^2 \cdot V^2}{l_1^2} + \frac{A_o}{A_2}\right) - \frac{2B_o \cdot h_o \cdot A_1 \cdot \pi \cdot V}{A_2^2 \cdot l_1}}{\left(-\frac{4\pi^2 \cdot V^2}{l_1^2} + \frac{A_o}{A_2}\right)^2 + \frac{4A_1^2 \cdot \pi^2 \cdot V^2}{A_2^2 \cdot l_1^2}} \cdot$$
$$\cdot \sin\frac{2\pi \cdot V \cdot t}{l_1} + \frac{\left(\frac{4\pi^2 \cdot V^2}{l_1^2} - \frac{A_o}{A_2}\right) \cdot \frac{B_o \cdot h_o}{A_2} - \frac{4A_1 \cdot B_1 \cdot \pi^2 \cdot h_o \cdot V^2}{A_2^2 \cdot l_1^2}}{\left(-\frac{4\pi^2 \cdot V^2}{l_1^2} + \frac{A_o}{A_2}\right)^2 + \frac{4A_1^2 \cdot \pi^2 \cdot V^2}{A_2^2 \cdot l_1^2}} \cdot$$
$$\cdot \cos\frac{2\pi \cdot V \cdot t}{l_1} + \frac{B_o \cdot h_o}{A_o}. \tag{36}$$

Then the total solution of the differential equation with the right-hand side of (8), considering (17) and (36), will be equal:

$$\varphi = \bar{\varphi} + \varphi^* = e^{-\frac{A_1}{2A_2} \cdot t} \cdot \left[C_1 \cdot \sin\left(\sqrt{\frac{A_o}{A_2} - \frac{A_1^2}{4A_2^2}} \cdot t\right) + C_2 \cdot \cos\left(\sqrt{\frac{A_o}{A_2} - \frac{A_1^2}{4A_2^2}} \cdot t\right) \right] +$$
$$+ \frac{\frac{2\pi \cdot B_1 \cdot h_o \cdot V}{A_2 \cdot l_1} \cdot \left(-\frac{4\pi^2 \cdot V^2}{l_1^2} + \frac{A_o}{A_2}\right) - \frac{2B_o \cdot h_o \cdot A_1 \cdot \pi \cdot V}{A_2^2 \cdot l_1}}{\left(-\frac{4\pi^2 \cdot V^2}{l_1^2} + \frac{A_o}{A_2}\right)^2 + \frac{4A_1^2 \cdot \pi^2 \cdot V^2}{A_2^2 \cdot l_1^2}} \cdot \sin\frac{2\pi \cdot V \cdot t}{l_1} +$$
$$+ \frac{\left(\frac{4\pi^2 \cdot V^2}{l_1^2} - \frac{A_o}{A_2}\right) \cdot \frac{B_o \cdot h_o}{A_2} - \frac{4A_1 \cdot B_1 \cdot \pi^2 \cdot h_o \cdot V^2}{A_2^2 \cdot l_1^2}}{\left(-\frac{4\pi^2 \cdot V^2}{l_1^2} + \frac{A_o}{A_2}\right)^2 + \frac{4A_1^2 \cdot \pi^2 \cdot V^2}{A_2^2 \cdot l_1^2}} \cdot \cos\frac{2\pi \cdot V \cdot t}{l_1} + \frac{B_o \cdot h_o}{A_o}. \tag{37}$$

To determine the arbitrary constants C_1 and C_2, the following initial conditions are set: since the motion starts from a state of rest, i.e. at t=0, then:

$$\varphi=0,\ \dot{\varphi}=0.$$

Next, find the first derivative of expression (37) in time t. Have:

$$\varphi = \dot{\bar{\varphi}} + \dot{\varphi}^* = -\frac{A_1}{2A_2} \cdot e^{-\frac{A_1}{2A_2} \cdot t} \cdot \left[C_1 \cdot \sin\left(\sqrt{\frac{A_o}{A_2} - \frac{A_1^2}{4A_2^2}} \cdot t\right) + \right.$$
$$\left. + C_2 \cdot \cos\left(\sqrt{\frac{A_o}{A_2} - \frac{A_1^2}{4A_2^2}} \cdot t\right)\right] + e^{-\frac{A_1}{2A_2} \cdot t} \cdot$$
$$\cdot \left[C_1 \cdot \sqrt{\frac{A_o}{A_2} - \frac{A_1^2}{4A_2^2}} \cdot \cos\left(\sqrt{\frac{A_o}{A_2} - \frac{A_1^2}{4A_2^2}} \cdot t\right) - \right.$$
$$\left. - C_2 \cdot \sqrt{\frac{A_o}{A_2} - \frac{A_1^2}{4A_2^2}} \cdot \sin\left(\sqrt{\frac{A_o}{A_2} - \frac{A_1^2}{4A_2^2}} \cdot t\right)\right] +$$
$$+ \frac{\frac{2\pi \cdot B_1 \cdot h_o \cdot V}{A_2 \cdot l_1} \cdot \left(-\frac{4\pi^2 \cdot V^2}{l_1^2} + \frac{A_o}{A_2}\right) - \frac{2B_o \cdot h_o \cdot A_1 \cdot \pi \cdot V}{A_2^2 \cdot l_1}}{\left(-\frac{4\pi^2 \cdot V^2}{l_1^2} + \frac{A_o}{A_2}\right)^2 + \frac{4A_1^2 \cdot \pi^2 \cdot V^2}{A_2^2 \cdot l_1^2}} \cdot \frac{2\pi \cdot V}{l_1} \cdot \tag{38}$$
$$\cdot \cos\frac{2\pi \cdot V \cdot t}{l_1} - \frac{\left(\frac{4\pi^2 \cdot V^2}{l_1^2} - \frac{A_o}{A_2}\right) \cdot \frac{B_o \cdot h_o}{A_2} - \frac{4A_1 \cdot B_1 \cdot \pi^2 \cdot h_o \cdot V^2}{A_2^2 \cdot l_1^2}}{\left(-\frac{4\pi^2 \cdot V^2}{l_1^2} + \frac{A_o}{A_2}\right)^2 + \frac{4A_1^2 \cdot \pi^2 \cdot V^2}{A_2^2 \cdot l_1^2}} \cdot$$
$$\cdot \frac{2\pi \cdot V}{l_1} \cdot \sin\frac{2\pi \cdot V \cdot t}{l_1}.$$

Considering the initial conditions, the following expression is obtained from (37):

$$C_2 + \frac{\left(\frac{4\pi^2 \cdot V^2}{l_1^2} - \frac{A_o}{A_2}\right) \cdot \frac{B_o \cdot h_o}{A_2} - \frac{4A_1 \cdot B_1 \cdot \pi^2 \cdot h_o \cdot V^2}{A_2^2 \cdot l_1^2}}{\left(-\frac{4\pi^2 \cdot V^2}{l_1^2} + \frac{A_o}{A_2}\right)^2 + \frac{4A_1^2 \cdot \pi^2 \cdot V^2}{A_2^2 \cdot l_1^2}} + \frac{B_o \cdot h_o}{A_o} = 0\,. \tag{39}$$

Under the same initial conditions, the following is obtained from (38):

$$-\frac{A_1}{2A_2} \cdot C_1 + C_2 \cdot$$
$$\cdot \sqrt{\frac{A_o}{A_2} - \frac{A_1^2}{4A_2^2}} + \frac{\frac{2\pi \cdot B_1 \cdot h_o \cdot V}{A_2 \cdot l_1} \cdot \left(-\frac{4\pi^2 \cdot V^2}{l_1^2} + \frac{A_o}{A_2}\right) - \frac{2B_o \cdot h_o \cdot A_1 \cdot \pi \cdot V}{A_2^2 \cdot l_1}}{\left(-\frac{4\pi^2 \cdot V^2}{l_1^2} + \frac{A_o}{A_2}\right)^2 + \frac{4A_1^2 \cdot \pi^2 \cdot V^2}{A_2^2 \cdot l_1^2}} \cdot \tag{40}$$
$$\cdot \frac{2\pi \cdot V}{l_1} = 0.$$

From expression (39), the value of the arbitrary constant C_2 is obtained:

$$C_2 = -\frac{\left(\frac{4\pi^2 \cdot V^2}{l_1^2} - \frac{A_o}{A_2}\right) \cdot \frac{B_o \cdot h_o}{A_2} - \frac{4A_1 \cdot B_1 \cdot \pi^2 \cdot h_o \cdot V^2}{A_2^2 \cdot l_1^2}}{\left(-\frac{4\pi^2 \cdot V^2}{l_1^2} + \frac{A_o}{A_2}\right)^2 + \frac{4A_1^2 \cdot \pi^2 \cdot V^2}{A_2^2 \cdot l_1^2}} - \frac{B_o \cdot h_o}{A_o}\,. \tag{41}$$

Substituting (41) into (40), the value of the arbitrary constant C_1 is obtained:

$$C_1 = \left\{ \frac{A_1}{2A_2} \left[-\frac{\left(\frac{4\pi^2 \cdot V^2}{l_1^2} - \frac{A_o}{A_2}\right) \cdot \frac{B_o \cdot h_o}{A_2} - \frac{4A_1 \cdot B_1 \cdot \pi^2 \cdot h_o \cdot V^2}{A_2^2 \cdot l_1^2}}{\left(-\frac{4\pi^2 \cdot V^2}{l_1^2} + \frac{A_o}{A_2}\right)^2 + \frac{4A_1^2 \cdot \pi^2 \cdot V^2}{A_2^2 \cdot l_1^2}} - \frac{B_o \cdot h_o}{A_o} \right] - \right.$$
$$\left. - \frac{\frac{2\pi \cdot B_1 \cdot h_o \cdot V}{A_2 \cdot l_1} \cdot \left(-\frac{4\pi^2 \cdot V^2}{l_1^2} + \frac{A_o}{A_2}\right) - \frac{2B_o \cdot h_o \cdot A_1 \cdot \pi \cdot V}{A_2^2 \cdot l_1}}{\left(-\frac{4\pi^2 \cdot V^2}{l_1^2} + \frac{A_o}{A_2}\right)^2 + \frac{4A_1^2 \cdot \pi^2 \cdot V^2}{A_2^2 \cdot l_1^2}} \cdot \frac{2\pi \cdot V}{l_1} \right\} \times \left(\frac{A_o}{A_2} - \frac{A_1^2}{4A_2^2}\right)^{-\frac{1}{2}}. \tag{42}$$

Substituting expressions (41) and (42) into the general solution (37) of equation (8), a partial solution of this equation satisfying the initial conditions is obtained:

$$\varphi = e^{-\frac{A_1}{2A_2}\cdot t}\cdot\left\{\left\{\frac{A_1}{2A_2}\left[-\frac{\left(\frac{4\pi^2\cdot V^2}{l_1^2}-\frac{A_o}{A_2}\right)\cdot\frac{B_o\cdot h_o}{A_2}-\frac{4A_1\cdot B_1\cdot\pi^2\cdot h_o\cdot V^2}{A_2^2\cdot l_1^2}}{\left(-\frac{4\pi^2\cdot V^2}{l_1^2}+\frac{A_o}{A_2}\right)^2+\frac{4A_1^2\cdot\pi^2\cdot V^2}{A_2^2\cdot l_1^2}}-\frac{B_o\cdot h_o}{A_o}\right]-\frac{\frac{2\pi\cdot B_1\cdot h_o\cdot V}{A_2\cdot l_1}\cdot\left(-\frac{4\pi^2\cdot V^2}{l_1^2}+\frac{A_o}{A_2}\right)-\frac{2B_o\cdot h_o\cdot A_1\cdot\pi\cdot V}{A_2^2\cdot l_1}}{\left(-\frac{4\pi^2\cdot V^2}{l_1^2}+\frac{A_o}{A_2}\right)^2+\frac{4A_1^2\cdot\pi^2\cdot V^2}{A_2^2\cdot l_1^2}}\cdot\frac{2\pi\cdot V}{l_1}\right\}\cdot\right.$$

$$\cdot\left(\frac{A_o}{A_2}-\frac{A_1^2}{4A_2^2}\right)^{-\frac{1}{2}}\cdot\sin\left(\sqrt{\frac{A_o}{A_2}-\frac{A_1^2}{4A_2^2}}\cdot t\right)-\left[-\frac{\left(\frac{4\pi^2\cdot V^2}{l_1^2}-\frac{A_o}{A_2}\right)\cdot\frac{B_o\cdot h_o}{A_2}-\frac{4A_1\cdot B_1\cdot\pi^2\cdot h_o\cdot V^2}{A_2^2\cdot l_1^2}}{\left(-\frac{4\pi^2\cdot V^2}{l_1^2}+\frac{A_o}{A_2}\right)^2+\frac{4A_1^2\cdot\pi^2\cdot V^2}{A_2^2\cdot l_1^2}}+\frac{B_o\cdot h_o}{A_o}\right]\cdot\cos\left(\sqrt{\frac{A_o}{A_2}-\frac{A_1^2}{4A_2^2}}\cdot t\right)\right\}+$$

$$+\frac{\frac{2\pi\cdot B_1\cdot h_o\cdot V}{A_2\cdot l_1}\cdot\left(-\frac{4\pi^2\cdot V^2}{l_1^2}+\frac{A_o}{A_2}\right)-\frac{2B_o\cdot h_o\cdot A_1\cdot\pi\cdot V}{A_2^2\cdot l_1}}{\left(-\frac{4\pi^2\cdot V^2}{l_1^2}+\frac{A_o}{A_2}\right)^2+\frac{4A_1^2\cdot\pi^2\cdot V^2}{A_2^2\cdot l_1^2}}\cdot\sin\frac{2\pi\cdot V\cdot t}{l_1}+\frac{\left(\frac{4\pi^2\cdot V^2}{l_1^2}-\frac{A_o}{A_2}\right)\cdot\frac{B_o\cdot h_o}{A_2}-\frac{4A_1\cdot B_1\cdot\pi^2\cdot h_o\cdot V^2}{A_2^2\cdot l_1^2}}{\left(-\frac{4\pi^2\cdot V^2}{l_1^2}+\frac{A_o}{A_2}\right)^2+\frac{4A_1^2\cdot\pi^2\cdot V^2}{A_2^2\cdot l_1^2}}\cdot\cos\frac{2\pi\cdot V\cdot t}{l_1}+\frac{B_o\cdot h_o}{A_o}. \quad (43)$$

And finally, substituting the expressions for the coefficients A_o, A_1, A_2, B_o, B_1 in (43), finally obtaining a partial solution φ of the differential equation (8):

$$\varphi = e^{-\frac{\mu\cdot L^2}{I_{oy}}\cdot t}\left\{\left\{\frac{\mu\cdot L^2}{I_{oy}}\cdot\left[-\frac{\left(\frac{4\pi^2\cdot V^2}{l_1^2}-\frac{2c\cdot L^2}{I_{oy}}\right)\cdot\frac{2c\cdot L\cdot h_o}{I_{oy}}-\frac{16\mu^2\cdot L^3\cdot\pi^2\cdot h_o\cdot V^2}{I_{oy}^2\cdot l_1^2}}{\left(-\frac{4\pi^2\cdot V^2}{l_1^2}+\frac{2c\cdot L^2}{I_{oy}}\right)^2+\frac{16\mu^2\cdot L^4\cdot\pi^2\cdot V^2}{I_{oy}^2\cdot l_1^2}}-\frac{h_o}{L}\right]-\frac{\frac{4\pi\cdot\mu\cdot L\cdot h_o\cdot V}{I_{oy}\cdot l_1}\cdot\left(-\frac{4\pi^2\cdot V^2}{l_1^2}+\frac{2c\cdot L^2}{I_{oy}}\right)-\frac{8c\cdot L^3\cdot h_o\cdot\mu\cdot\pi\cdot V}{I_{oy}^2\cdot l_1}}{\left(-\frac{4\pi^2\cdot V^2}{l_1^2}+\frac{2c\cdot L^2}{I_{oy}}\right)^2+\frac{16\mu^2\cdot L^4\cdot\pi^2\cdot V^2}{I_{oy}^2\cdot l_1^2}}\cdot\frac{2\pi\cdot V}{l_1}\right\}\left(\frac{2c\cdot L^2}{I_{oy}}-\frac{\mu^2\cdot L^4}{I_{oy}^2}\right)^{-\frac{1}{2}}\cdot\right.$$

$$\sin\left(\sqrt{\frac{2c\cdot L^2}{I_{oy}}-\frac{\mu^2\cdot L^4}{I_{oy}^2}}\cdot t\right)-\left[\frac{\left(\frac{4\pi^2\cdot V^2}{l_1^2}-\frac{2c\cdot L^2}{I_{oy}}\right)\cdot\frac{2c\cdot L\cdot h_o}{I_{oy}}-\frac{16\mu^2\cdot L^3\cdot\pi^2\cdot h_o\cdot V^2}{I_{oy}^2\cdot l_1^2}}{\left(-\frac{4\pi^2\cdot V^2}{l_1^2}+\frac{2c\cdot L^2}{I_{oy}}\right)^2+\frac{16\mu^2\cdot L^4\cdot\pi^2\cdot V^2}{I_{oy}^2\cdot l_1^2}}+\frac{h_o}{L}\right]\cdot\cos\left(\sqrt{\frac{2c\cdot L^2}{I_{oy}}-\frac{\mu^2\cdot L^4}{I_{oy}^2}}\cdot t\right)\right\}+\frac{\frac{4\pi\cdot\mu\cdot L\cdot h_o\cdot V}{I_{oy}\cdot l_1}\cdot\left(-\frac{4\pi^2\cdot V^2}{l_1^2}+\frac{2c\cdot L^2}{I_{oy}}\right)-\frac{8c\cdot L^3\cdot h_o\cdot\mu\cdot\pi\cdot V}{I_{oy}^2\cdot l_1}}{\left(-\frac{4\pi^2\cdot V^2}{l_1^2}+\frac{2c\cdot L^2}{I_{oy}}\right)^2+\frac{16\mu^2\cdot L^4\cdot\pi^2\cdot V^2}{I_{oy}^2\cdot l_1^2}}\cdot$$

$$\sin\frac{2\pi\cdot V\cdot t}{l_1}+\frac{\left(\frac{4\pi^2\cdot V^2}{l_1^2}-\frac{2c\cdot L^2}{I_{oy}}\right)\cdot\frac{2c\cdot L\cdot h_o}{I_{oy}}-\frac{16\mu^2\cdot L^3\cdot\pi^2\cdot h_o\cdot V^2}{I_{oy}^2\cdot l_1^2}}{\left(-\frac{4\pi^2\cdot V^2}{l_1^2}+\frac{2c\cdot L^2}{I_{oy}}\right)^2+\frac{16\mu^2\cdot L^4\cdot\pi^2\cdot V^2}{I_{oy}^2\cdot l_1^2}}\cdot\cos\frac{2\pi\cdot V\cdot t}{l_1}+\frac{h_o}{L}. \quad (44)$$

The amplitude of the free (natural) oscillations of the dynamical system examined is determined from the expression:

$$A = e^{-\frac{\mu\cdot L^2}{I_{oy}}\cdot t}\cdot\sqrt{C_1^2+C_2^2}, \text{Rad}, \quad (45)$$

where C_1 and C_2 can be determined from expressions (41) and (42), respectively. In the final expression (44), C_1 and C_2 – the coefficients of functions $\sin\left(\sqrt{\frac{2c\cdot L^2}{I_{oy}}-\frac{\mu^2\cdot L^4}{I_{oy}^2}}\cdot t\right)$ and $\cos\left(\sqrt{\frac{2c\cdot L^2}{I_{oy}}-\frac{\mu^2\cdot L^4}{I_{oy}^2}}\cdot t\right)$.

Therewith:

$$k = \sqrt{\frac{2c\cdot L^2}{I_{oy}}-\frac{\mu^2\cdot L^4}{I_{oy}^2}}, \quad (46)$$

is the circular frequency of natural oscillations of the dynamic system considered, s^{-1}.

As can be seen from expression (45), these fluctuations are damped with time t, since the factor before the square root in this expression tends to zero, i.e: $\lim_{t\to\infty} e^{-\frac{\mu\cdot L^2}{I_{oy}}\cdot t} = 0$.

The amplitude B of the forced oscillations arising from the influence of soil surface irregularities on the movement of the root crop tops cutter is equal to the root of the square of the sum of the squared coefficients in expression (44) for functions $\sin\frac{2\pi\cdot Vt}{l_1}$ and $\cos\frac{2\pi\cdot Vt}{l_1}$, respectively. This amplitude B of forced oscillations is measured in radians. Based on the above, the analytical expression for determining B is as follows:

$$B = \sqrt{\left[\frac{\frac{4\pi\cdot\mu\cdot L\cdot h_o\cdot V}{I_{oy}\cdot l_1}\cdot\left(-\frac{4\pi^2\cdot V^2}{l_1^2}+\frac{2c\cdot L^2}{I_{oy}}\right)-\frac{8c\cdot L^3\cdot h_o\cdot\mu\cdot\pi\cdot V}{I_{oy}^2\cdot l_1}}{\left(-\frac{4\pi^2\cdot V^2}{l_1^2}-\frac{2c\cdot L^2}{I_{oy}}\right)^2+\frac{16\mu^2\cdot L^4\cdot\pi^2\cdot V^2}{I_{oy}^2\cdot l_1^2}}\right]^2+\left[\frac{\left(\frac{4\pi^2\cdot V^2}{l_1^2}-\frac{2c\cdot L^2}{I_{oy}}\right)\cdot\frac{2c\cdot L\cdot h_o}{I_{oy}}-\frac{16\mu^2\cdot L^3\cdot\pi^2\cdot h_o\cdot V^2}{I_{oy}^2\cdot l_1^2}}{\left(-\frac{4\pi^2\cdot V^2}{l_1^2}-\frac{2c\cdot L^2}{I_{oy}}\right)^2+\frac{16\mu^2\cdot L^4\cdot\pi^2\cdot V^2}{I_{oy}^2\cdot l_1^2}}\right]^2}. \quad (47)$$

The circular frequency of forced oscillations of the dynamic system considered will be equal to:

$$v = \frac{2\pi\cdot V}{l_1}, \text{s}^{-1}. \quad (48)$$

Thus, finally, based on the analytical study, a closed-form solution of the differential equation of motion of the machine for cutting the tops of root crops in the longitudinal-vertical plane was performed and specific expressions were obtained to determine the main indicators of the oscillatory process. Namely, the rotation angle φ, the amplitudes of natural A and forced B oscillations and the natural frequency k and v – the forced frequency.

Using the final analytical expressions obtained with a personal computer and the PTC Mathcad 15 software developed for this purpose, numerical calculations were performed, and new graphical dependencies were built based on them, as presented in Figure 3-Figure 7.

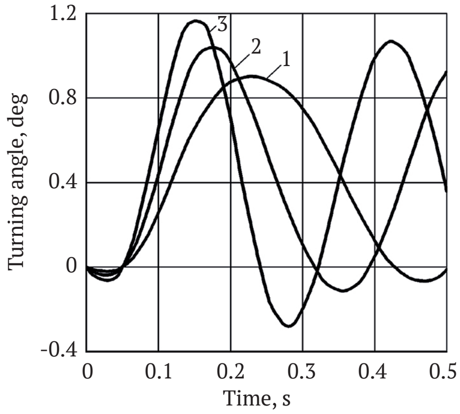

Figure 3. Dynamics of fluctuations in the angle φ of rotation of a machine for cutting tops of root crops at different speeds V of its working movement: 1 – 1.5 m·s^{-1}; 2 – 2.0 m·s^{-1}; 3 – 2.5 m·s^{-1}

Thus, the analysis of the mathematical modelling data, represented by the curves in Figure 3, demonstrates that a change in the speed V of the working translational movement of the machine for cutting the tops of root crops has two consequences.

Thus, the essence of the first consequence is that when the speed V of the translational movement of the machine increases from 1.5 to 2.5 m·s^{-1}, the amplitude of oscillations of the angle φ of rotation of the machine for cutting the tops of root crops in the examined plane undesirably increases (Fig. 3). The first maximum of this process indicates that this increase is 0.3°: from 0.88° at a travel speed of V=1.5 m·s^{-1} (curve 1 on the graph) to 1.18o, when the forward speed V of the machine for cutting the tops of root crops at the root is already 2.5 m·s^{-1} (curve 3 on the graph).

The second consequence is related to the dynamics of changes in such an estimation parameter as the time when the considered dynamic system reaches the first maximum of the oscillations of angle φ. In this case, this time can be assumed to be the duration of the transitional process of the system's reaching a stable mode of operation. The analysis of the curves in Figure 3 demonstrates that when the machine for cutting root crop tops moves with a translational speed of V, equal to 1.5 m·s^{-1}, the duration of the transient process is 0.22 s (curve 1 on the graph). During the translational movement of the machine for cutting the tops of root crops with a movement speed of V, equal to 2.5 m·s^{-1}, the value of the estimated indicator decreases to 0.14 s, i.e. by 36%, which is desirable.

As can be observed from the graphs of Figure 3, the positive amplitude of oscillations of the angle φ of rotation of the machine for cutting the tops of root crops in the investigated plane is no more than 1.2°, and the negative amplitude does not even reach 0.3°. As a result, the oscillation range of the considered oscillatory process is insignificant and does not exceed 1.4°.

It indicates that in the considered range of speeds of the V machine for cutting the tops of root crops, equal to 1.5...2.5 m·s^{-1}, preference should be given to higher values of this parameter. Therewith, consider that an increase in the speed of movement V of this machine will ensure the appropriate performance, albeit with a slight increase in the amplitude of angular oscillations and a small (in absolute value) reduction in the transient process, which will bring this dynamic system to a stable mode of operation, which will be extremely desirable.

Therewith, the negative amplitudes of the oscillations of the angle φ (refer to the graphs in Fig. 3) are conditioned upon the elastic properties of the copy wheels, which are quantified by the value of the coefficient c of the stiffness of their pneumatic tyres. Therewith, it is observed that the smaller it is, the more noticeable the response of the root crop cutting machine (through its support and copying wheels) in response to fluctuations in the longitudinal profile of field surface irregularities represented by dependence (5).

Further analysis of the mathematical modelling results fully confirms this. Setting the stiffness coefficient of the c pneumatic tyres of the copy wheels of the root crop tops cutter at 550 kN·m causes its angular oscillatory movements with smaller negative and larger positive amplitudes (curve 2 in Fig. 4).

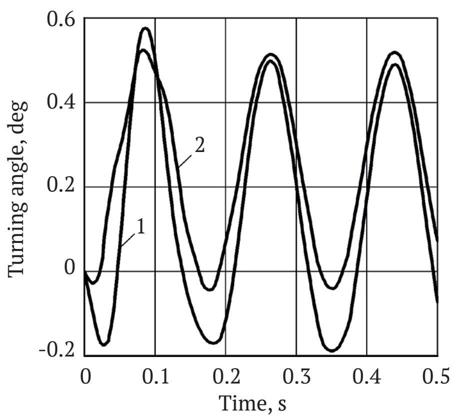

Figure 4. Dynamics of fluctuations in the angle φ of rotation of a machine for cutting tops of root crops at different values of the stiffness coefficient c of its copy wheels: 1 – 115 kN·m; 2 – 550 kN·m

In contrast, when the stiffness *c* of the pneumatic tyres of the machine's copy wheels is 115 kN·m, the part of the amplitude curve in the positive zone of this graph (curve 1 of Fig. 4) decreases. The negative component of the amplitude increases more significantly: by a factor of 7-8 compared to the situation with a tyre stiffnessc of 550 kN·m.

The damping coefficient μ of the tyres of the root crop top dresser is as follows. Thus, increasing the value of this parameter from 350 to 1350 kN·s·m^{-1} has very little effect on the change in the negative component of the angle oscillation amplitude φ, which for both values of the coefficient μ does not exceed 0.2° (see Fig. 5).

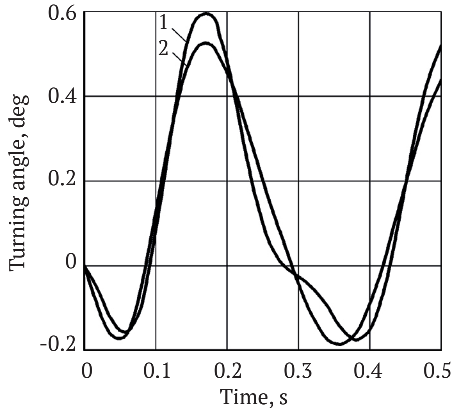

Figure 5. Dynamics of oscillations of the angle φ of rotation of a machine for cutting tops of root crops at different values of the damping coefficient μ of its copy wheels:1 – 350 kN·s·m^{-1}; 2 – 1350 kN·s·m^{-1}

As for the positive component of the amplitude of the process examined, it is 15...17% lower in the case of a larger parameter value μ (curve 2 in Fig. 5). Thus, the stiffer the tyres of the root crop peelers, the smaller the angle φ (in the positive zone of this graph) of deviation from the static position. Therewith, considering the relatively small value of this deviation, it can be stated that the machine for cutting tops of root crops is invariant to changes in the values of the damping coefficient μ of the tyres of its support and copying wheels.

Thus, there is every reason to consider this machine for cutting the tops of root crops as a dynamic system that can be represented by a physical pendulum that makes angular oscillations relative to the point *O* (Fig. 2). These angular oscillations are specifically determined by the amplitude of the vertical movement of the machine's copy wheels (point *B* in the diagram in Fig. 2). However, point *B*, which performs these oscillations, has an amplitude that depends entirely on the length *L*. Thus, it is the length that connects point *B* with the centre of instantaneous rotation (point *O*) of the oscillatory system considered.

Therewith, a change in the design parameter *L* causes a simultaneous change in the parameter *l*, which is the longitudinal coordinate of the centre of mass of the root crop top cutter (point *C* in Fig. 2). Thus, it is necessary to consider a mutually agreed change in the parameters *L* and *l*.

Finally, based on the calculations, it was found that an increase in the distance *L* (and, therewith, *l*; denoted as *L*(*l*) in the graphs) leads to a desirable and logical decrease in the amplitude of angular oscillations of the root crop tops machine (Fig. 6). Moreover, these changes mainly relate to amplitude values that are in the positive range. From the curves presented in these graphs, it can be seen that its first maxima indicate that an increase in the values of the parameters *L* and *l* by 1 m causes a decrease in the angle φ from 0.72 to 0.44°, i.e. a decrease of almost 39%.

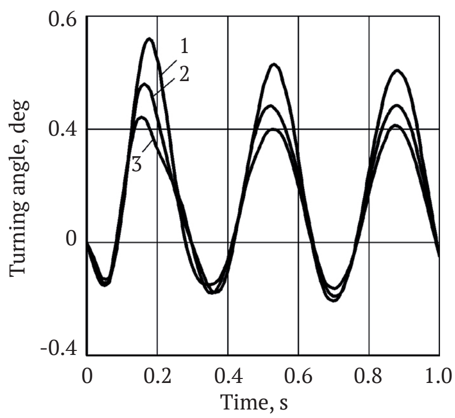

Figure 6. Dynamics of oscillations of the angle φ of rotation of the machine for cutting the tops of root crops at different values of parameters *L*(*l*): 1 – 3.8(2.8) m; 2 – 4.3(3.3) m; 3 – 4.8(3.8) m

This result indicates the necessity of designing a machine for cutting the tops of root crops with the highest possible value of the *L* parameter. It can be accomplished by connecting the machine to the tractor in such a way that $\angle MDP$ (see Fig. 2) of the central linkage *MD* of the front hitch is as high as possible concerning the vertical. It should be noted that the value of the *DP* parameter must in any case be greater than the value of the *MK* parameter, which is the shortest distance between the attachment points of the centre and lower links of the front hitch to the implement. With *DP=MK*, the latter becomes a parallelogram, thus lifting the mounted front machine into the transport position without turning it in the longitudinal-vertical plane. From the standpoint of aggregation, it is an undesirable outcome. The variant when *DP<MK* is completely unacceptable, since in this case it becomes impossible to raise the frontal stubble harvester (and other trailed agricultural machines) to the transport position at all [7; 19].

In addition, the factors that affect the dynamics of the angle φ of rotation of the machine for cutting the tops of root crops include the period of fluctuations in the longitudinal profile of unevenness of the field surface l_1. The most common values of this parameter for fields where root crops are grown are 0.70 and 1.75 m.

The analysis of the calculations demonstrates that an increase in the value of the period l_1 of disturbing oscillations from 0.70 to 1.75 m, although insignificant, reduces the amplitude of angular oscillations of the machine for cutting root crop tops (Fig. 7).

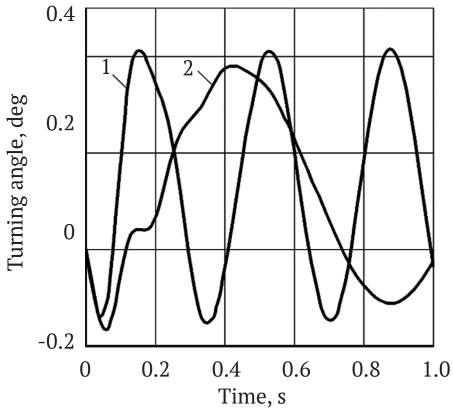

Figure 7. Dynamics of oscillations of the angle φ of rotation of the machine for cutting tops of root crops at different values of parameter l_1:1 – 0.70 m; 2 – 1.75 m

It follows that this desired reduction will be greater the larger the value of the parameter l_1. It can be achieved by carefully levelling the longitudinal profile of the field in preparation for sowing root crops.

Other calculations using a personal computer demonstrated that the influence of different values of the remaining design parameters on the dynamics of angular vibrations of the machine for cutting the tops of root crops is insignificant.

Thus, the results of the analytical study indicate the achievement of the goal, which was related to determining the optimal kinematic and design parameters of a new machine for cutting root crop tops on the root by exploring the dynamics of its oscillatory movements in the longitudinal-vertical plane.

The previously obtained results are thematically close to the present study and published scientific works of other researchers [1; 2; 4], which contain the constructed mathematical models of frontally mounted stubble harvesters on an aggregating tractor. What is common in this, and these published works is that oscillations of soil surface irregularities in the form of a harmonic function are used as an input external forced disturbance. Another common feature is the representation of the copy wheels of buncher machines in the form of elastic-damping models.

If comparing the differences between the results obtained in this research and the subject of the study and the results of other authors [1; 2; 4], it can be observed that the fundamental difference is related to the fact that the dynamics of oscillatory motion is considered here only in the presence of a single generalised coordinate φ. Thus, the absence of unnecessary generalised coordinates significantly improves the accuracy of numerical calculations on a personal computer. It is known that the study of oscillatory movements, provided that they are added by two extra coordinates related to each other, actually reflects the true nature of the processes occurring with distortions. It significantly reduces the accuracy of the results. In addition, numerical calculations on a personal computer were performed in previously published works under the assumption of constant values of many parameters, which may be of a statistical (probabilistic) nature.

None of the works [1; 2; 4], and works close to this subject [7-9], do not provide detailed transformations and the final solution of the resulting differential equation in closed form, i.e., obtaining the final solution in the form of new ordinary linear dependencies, which allow for high accuracy to conduct relatively simple numerical calculations in the future and do it for a wide class of stubble harvesting and other agricultural machines (reapers, mowers, shredders of plant residues, etc.), of various designs and rows, which are hung in front of the aggregating tractor.

The subject of research contained in works [12; 14; 15; 21] and concerning related issues presented in this research, generally relate to the quality of technological processes of mechanised harvesting of root crops, which confirms the importance of this study, since the design and kinematic parameters of the machine for harvesting root crop tops on the root obtained here only improve the process.

In addition, the methodology presented in this research for solving a differential equation that belongs to the class of second-order differential equations with constant coefficients and a right-hand side that is not available in any previously published works can be widely used to explore the dynamics of front- and rear-mounted multiple structures of various agricultural machines as part of machine-tractor units.

CONCLUSIONS

If the machine for cutting root crop tops moves at a forward speed of up to 2.5 $m \cdot s^{-1}$, the time for this oscillatory system to reach a stable mode of operation will be reduced to 0.14 s. This circumstance will contribute both to an increase in the productivity of the tops harvesting and to a slight increase in the amplitude of its angular oscillations.

The coefficient c of stiffness of the tyres of the copy wheels of a root crop peeling machine, if reduced, causes angular vibrations of the machine with slightly higher positive and significantly lower negative amplitudes in the longitudinal-vertical plane.

It was established that the stiffer the pneumatic tyres of the copying wheels of the machine for cutting the tops of root crops, the smaller the angle φ of deviation from its static position. However, the relative smallness of this deviation allows stating that the machine for cutting tops of root crops on the root is invariant to changes in the values of the coefficient μ of damping of pneumatic tyres of its copy wheels.

Reducing the amplitude of angular oscillations in the longitudinal-vertical plane of the root crop tops cutter can be achieved by increasing the distance L from the axles of the tracing wheels (point B) to point O, which is the centre of rotation of the front linkage of the aggregating tractor. Therewith, the central linkage MD of the tractor's front linkage should be inclined at the greatest possible angle to the vertical position.

A more stable movement in the longitudinal-vertical plane of the root crop top dresser can be achieved by increasing the periods l_1 of oscillation of the longitudinal profile of the uneven soil surface. And it is possible due to a more thorough levelling of the field surface, with surface tillage, where root crops will be grown.

Further research should be focused on determining the parameters of oscillatory movements of the rotary cutting unit of the machine for cutting root crop tops (possibly its springing relative to the main frame of the machine), which will increase the number of tops harvested and the quality of cutting root crop heads. In addition, it is necessary to further consider the automation of the copying process, the accuracy and reliability of obtaining information on soil surface irregularities in the rows of crops, with the possibility of further obtaining and using the information on the location of root crop heads relative to the soil surface in height.

REFERENCES

[1] Bulgakov, V.M., Golovach, V.I., Ruzhilo, Z.V., Ignatiev, E.I., Adamchuk, O.V., & Trokhanyak, O.M. (2021). *Theory and technical means for harvesting sugar beet pulp*. Kyiv: Agrarian Science.

[2] Bulgakov, V., Pascuzzi, S., Anifantis, A.S., & Santoro, F. (2019). Oscillations analysis of front-mounted beet topper machine for biomass harvesting. *Energies*, 12, article number 2774. doi: 10.3390/en12142774.

[3] Vasilenko, P. (1996). *Introduction to agricultural mechanics* (1st ed.). Kyiv: Agricultural Education.

[4] Ihnatiev, Y. (2017). Theoretical research and development of new design of beet tops harvesting machinery. *Mechanization in Agriculture & Conserving of the Resources*, 63(4), 137-139.

[5] Ihnatiev, Y.I. (2016). Development of a new structural and technological scheme for harvesting sugar beet stalks using a rowing tractor. *Bulletin of Agrarian Science*, 8, 67-71.

[6] Morozov, B.I., & Gringauz, N.M. (2019). Calculation of the movement of a wheeled vehicle on a rough road. *Mechanization and Electrification of Socialist Agriculture*, 7, 11-14.

[7] Nadykto, V.T. (2011). Features of the aggregation of the frontal projectiles. *Technics and Technologies of the Agro-Industrial Complex*, 8, 8-11.

[8] Pogorely, L.V. (Ed.). (1983). *Beet harvesters: Design and calculation*. Kyiv: Technique.

[9] Bell, B., & Rickatson, M. (2015). *Farm Machinery* (6th ed.). Sheffield: 5M Publishing Ltd.

[10] Bzowska-Bakalarz, M., & Ostroga, K. (2012). The capacity of sugar beet farms' machinery and equipment. *Journal of Central European Agriculture*, 13, 769-781.

[11] Finkenstadt, V. (2013). A review on the complete utilization of the sugarbeet. *Sugar Tech*, 16, 339-346.

[12] Fang, Z., Zhu, Z., Wu, P., & Moradi, Z. (2023). Vibration and damping analysis of sandwich electrorheological fluid deep arches with bi-directional FGM containers. *Engineering Structures*, 276, article number 115325. doi: 10.1016/j.engstruct.2022.115325.

[13] Zhou, L., Moradi, Z., Al-Tamimi, H.M., & Ali, H.E. (2022). On propagation of elastic waves in an embedded sigmoid functionally graded curved beam. *Steel & Composite Structures*, 44(1), 17-31. doi: 10.12989/scs.2022.44.1.017.

[14] Nadykto, V.T., & Kistechok. O.D. (2015). Study of the stability of the movement of the plow MTA according to the "push-pull" scheme. *Mechanization and Electrification of Agriculture*, 101(2), 273-280.
[15] Battiato, A., & Diserens, E. (2013). Influence of tyre inflation pressure and wheel load on the traction performance of a 65 kW MFWD tractor on a cohesive soil. *Journal of Agricultural Science*, 5(8), 197-215.
[16] Adamchuk, V., Bulgakov V., Korenko M., Boris, A., Boris, M., & Ihnatiev, Ye. (2018). Laboratory and field equipment workingout and the results of experimental studies of pre-harvesting sugar beet field. *Mechanization in Agriculture & Conserving of the Resources*, 64(6), 188-190.
[17] Prikner, P., Kotek, M., Jindra, P., & Prazhan, R. (2017). Field compaction capacity of agricultural tyres. *Agronomy Research*, 15(3), 806-816.
[18] Ivanov, S., Bulgakov, V., Nadykto, V., Ihnatiev, Ye., Smolinskyi, S., & Kiernicki, Z. (2020). Experimental study of the movement controllability of a machine-and-tractor aggregate of the modular type. *INMATEH – Agricultural Engineering*, 61(2), 9-16.
[19] Nadykto, V.T. (2017). *Fundamentals of scientific research*. Kherson: TDATU.
[20] Boldrin, D., Knappett, J.A., Leung, A.K., Brown, J.L., Loades, K.W., & Bengough, A.G. (2022). Modifying soil properties with herbaceous plants for natural flood risk-reduction. *Ecological Engineering*, 180, article number 106668. doi: 10.1016/j.ecoleng.2022.106668.
[21] Bigan, Z., Derechkei, P., Mazur, V., & Pop, O. (2022). Study of the cross-section for the 122Te(γ, n)121Te reaction by the activation method. *Scientific Herald of Uzhhorod University. Series "Physics"*, 51, 18-23.

Мирослав Ігорович Будзанівський
Аспірант
Інститут механіки та автоматики агропромислового виробництва
Національна академія аграрних наук України
08631, вул. Вокзальна, 11/1, смт. Глеваха, Київська область, Україна
https://orcid.org/0000-0002-0508-3816

Математичне моделювання коливань машини для зрізання гички коренеплідних культур

Анотація. Високоякісне зрізання гички коренеплідних культур на корені обумовлює не тільки збирання її високого врожаю, а й визначає кондиційні властивості коренеплодів перед їх викопуванням з ґрунту. Тому пошук умов, які будуть це забезпечувати є важливою і актуальною проблемою виробництва цих культур. Метою даної статті було визначення шляхом аналітичного дослідження оптимальних параметрів нової конструкції машини для збирання гички коренеплідних культур, яка навішується попереду агрегатуючого трактора і здійснює коливальні рухи у повздовжньо-вертикальній площині. Були використані методи, які пов'язані з моделюванням складних динамічних систем, що складаються з агрегатуючого трактора та передньонавішеної машини, складання та розв'язування в кінцевому вигляді диференційних рівнянь коливального руху та комп'ютерного моделювання коливального процесу. Згідно розробленої еквівалентної схеми було розв'язане у кінцевому вигляді нове диференціальне рівняння кутових коливань машини. Здійснено також числове моделювання на ПК, яке дало можливість побудувати графічні залежності кута φ повороту машини за різної швидкості V її поступального руху та значень коефіцієнта c жорсткості та коефіцієнта μ демпфірування пневматичних шин копіювальних коліс, а також за різних значень нерівностей поверхні ґрунту і основних конструктивних параметрів машини. Було встановлено, що при збільшенні V з 1,5 м·с$^{-1}$ до 2,5 м·с$^{-1}$1 амплітуда коливань кута φ повороту машини зростає з 0,88° до 1,18°. Однак, при V 1,5 м·с$^{-1}$ тривалість перехідного процесу становить 0,22 с, а за швидкістю 2.5 м·с$^{-1}$ – 1 цей показник вже становить 0,14 с, тобто зменшується на 36 %. Позитивна амплітуда коливань кута φ повороту машини досягає 1,2°, а від'ємна амплітуда не перевищує 0,3°, тобто розмах коливань є незначним. У діапазоні розглянутих V перевагу слід надавати її більшим значенням. Шляхом моделювання на ПК визначені конструктивні й кінематичні параметри досліджуваної системи. Наведена методика математичного моделювання коливального процесу може бути використаною при дослідженні будь-яких машин, які начіплюються попереду агрегатуючого трактора

Ключові слова: буряк цукровий; збирання; коливання; диференціальне рівняння; розв'язування на ПК; графіки

Machinery & Energetics
Vol. 13, No. 4. 2022

Journal homepage:
https://technicalscience.com.ua/en

UDC 620.19
DOI: 10.31548/machenergy.13(4).2022.28-37

Georgy Pysarenko
Full Doctor in Technical Sciences, Professor
G.S. Pisarenko Institute for Problems of Strength of the National Academy of Sciences of Ukraine
01014, 2 Timiryazevs'ka Str., Kiyv, Ukraine
https://orcid.org/0000-0001-9557-9710

Oleksandr Voinalovych*
PhD in Technical Sciences, Associate Professor
National University of Life and Environmental Sciences of Ukraine
03041, 15 Heroiv Oborony Str., Kyiv, Ukraine
https://orcid.org/0000-0002-9321-2672

Andriy Mailo
PhD in Technical Sciences
G.S. Pisarenko Institute for Problems of Strength of the National Academy of Sciences of Ukraine
01014, 2 Timiryazevs'ka Str., Kiyv, Ukraine
https://orcid.org/0000-0002-4762-0886

Stepan Pysarenko
Postgraduate Student
G.S. Pisarenko Institute for Problems of Strength of the National Academy of Sciences of Ukraine
01014, 2 Timiryazevs'ka Str., Kiyv, Ukraine
https://orcid.org/0000-0003-4295-6687

A methodical approach to determining the damage characteristics of cyclically loaded samples of metal structures

Abstract. The article deals with an actual task of developing engineering methods for predicting the durability of modern long-life machines should be based on the methodology for determining the degree of fatigue damage to materials and structural elements. In the development of such a methodology, the work proposes to use modern optical and computer tools that allow analyzing the parameters of the deformed surface of metal structure samples and, on this basis, to estimate the residual resource of the metal structure. The purpose of the article was to substantiate a methodical approach for determining the limit state of damage using photometric analysis of the topography of the micro-deformed surface of cyclically loaded metal structure samples. To analyze the fatigue damage characteristics of metals and alloys, an experimental information system was developed based on the method of coherent optical scanning of the deformed surface of metal structure samples with a resolution of 0.2 μm/px. The obtained specklograms of the photodiode matrix, corresponding to the two-dimensional image of the micro-deformed surface of the sample in shades of gray 0-255, were computer analyzed. This made it possible to construct diagrams of the kinetics of the process of accumulation of the amplitude of the deformation microrelief of the surface of the laboratory samples for the studied steels St 45 and St 20. It is shown that the kinetics of speckle brightness obtained in the work by the correlation method, which corresponds to the evolution of the accumulation of fatigue damage on the surface of the studied structural steel samples, is characterized by a nonlinear function, which is consistent with the results of

Article's History: Received: 28.06.2022; Revised: 20.10.2022; Accepted: 23.11.2022.

Suggested Citation:
Pysarenko, G., Voinalovych, O., Mailo, A., & Pysarenko, S. (2022). A methodical approach to determining the damage characteristics of cyclically loaded samples of metal structures. *Machinery & Energetics,* 13(4), 28-37.

*Corresponding author

deformation microrelief studies obtained by other methods. The proposed methodology for analyzing the discrete distribution of specklogram brightness can be used to predict the onset of the limit state of a metal structure before failure due to fatigue

Keywords: fatigue of metals and alloys; correlational analysis;, microplastic deformation of the surface; deformation microrelief; photometric scanning

INTRODUCTION

Modern requirements for the operational resource of machines and equipment provide for their long-term operation [1], which can reach 109 cycles based on the declared duration of operation of machines based on cyclic loading. It is also necessary to develop new approaches to create a methodology for tracking fatigue damage of materials and structural elements on large load bases, as a basis for developing scientifically based engineering methods for predicting the durability of modern machines and equipment.

In the calculations of the residual resource of metal structures, the kinetics of scattered fatigue damage accumulation are analyzed depending on the model concept of the material structure. Diffuse fatigue damage develops mainly in the surface layers of the material, so it is important to study the changes in relief amplitudes under the action of cyclic loading [2].

The majority of scientifically based approaches to assessing the degree of damage to metal structures are based on models that use the parameters of the limit sizes of crack-like defects [3], the determination of which is a complicated resource-consuming task in the case of the need to predict the durability of materials and structural elements under multi-cycle fatigue. There is a need to develop alternative methods of research that allow obtaining parameters of the limit state of damage of highly stressed metal structures regardless of the limit characteristics of local centers of destruction. Such approaches include the methodology of determining the parameters of inelastic deformations, the kinetic characteristics of which contain information about the stages of fatigue and the residual resource of metal structures under multi-cycle fatigue in the range of 107-109 cycles [4].

It was shown in [5] that the plastic deformation of a metal from the microyield point to local destruction develops as a result of its dynamic localization at the mesoscopic level. In [6], it was established that in the case of repeated impact periodic loading of metal samples, local destruction occurs as a result of a certain limit accumulation of microplastic deformations in the surface layer. According to the results obtained in work [7], microplastic deformation is realized even under cyclic stresses that are somewhat lower than the endurance limit of the material, determined on the bases of loading recommended by fatigue standards.

This phenomenon is a prerequisite to substantiate the criteria of the limit state of the integrity of the surface of the metal structure based on the amplitude characteristics of microdeformation. The accumulation of inelastic deformations on the surface of the structural material allows the use of optical computer tools for direct measurement of the characteristics of the local deformation of the surface layer of the metal structure [8]. Optical methods, in which remote scanning of the metal structure surface is implemented, are characterized by the appropriate selectivity of detecting defects and their isolation.

Traces of microplastic deformation on the surface of a material cyclically loaded at a stress level close to the endurance limit in the initial stages of the accumulation of fatigue damage can be determined by the methods of atomic force or laser microscopy [9]. The analysis of damage kinetics assessed by such methods is accompanied by methodological difficulties, therefore, in order to assess the accumulated damage on the surface of a metal structure sample in the stages of fatigue before its localization, it is advisable to use correlational statistical characteristics of deformation surface defects. This will lead to a simplification of the method of tracking the transition of the damaged state of the metal structure to the limit with a satisfactory degree of reliability of the forecast under multi-cycle fatigue.

The purpose of the research is to substantiate the methodical approach to determining the characteristics of the physico-mechanical limit state of damage of cyclically loaded samples of metal structures, which precedes the local destruction of the material, evaluated according to the deformation criterion, using photometric analysis of the topography of the deformed surface.

The objectives of the study were to obtain and analyze the regularities of the effect of multicycle deformation on the intensity of changes in the parameters of the microrelief formed on the surface of the steel samples under fatigue.

LITERATURE REVIEW

In the study [10], it was found that the kinetics of propagation of surface and subsurface damage in metal structures depends on the dissipative properties of the material under multicycle loading at the level of 10-4-10-6 relative deformation, which causes the appearance and growth of local microplastic deformations. The achievement of their parameter limit values leads to the local destruction of the metal structure under stresses that do not exceed the elastic limits, i.e. in such places, the destruction is preceded by local microplastic deformation of the metal, as shown in [11].

In [12] it is stated that the limit state of a structural element can be determined by the state of the surface layer formed under external influence, when due to deformation the state of the mesovolume is characterized by a certain parameter of physical and mechanical properties. In multi-cycle fatigue, which is characterized by staged process, diffuse fatigue damage in the form of microscopic cells mainly accumulates in the first stage before the next stage of localized damage formation.

The authors of the work [13] established that the change in physical and mechanical properties under cyclic loading causes the inhomogeneity of local deformation, as a result of which different structural elements of the material are at different stages of damage development, which determines the discreteness of the characteristics of periods of fatigue damage. Likewise, when analyzing the degree of fatigue damage of an elastic-plastic polycrystal, it is necessary to take into account the kinetics of changes in properties during cyclic loading.

The kinetics of microplastic deformations of the polycrystal, initiated by structural mechanisms that depend on the nature of the material, determines the durability of the metal structure. The authors of the work [14] pointed out the importance of studying the structure of surface discrete deformation defects on the metal surface during cyclic deformation. The distribution function of deformation defects reveals the properties of a normal distribution due to the random nature of the localization of shifts in the sliding planes of the polycrystalline structure of the surface of the deformed sample.

It was shown in [15] that slip bands form a deformation microrelief on the surface of a deformed sample as a result of repeated sliding in the crystallographic planes of the surface layer of the material. The amplitude of the deformation relief, which accumulates on the surface of the deformed metal structure sample, corresponds to the degree of structural material damage. The density of deformation defects depends on the parameters of cyclic loading: amplitude and duration of action. Plastic deformation occurs in a limited number of microvolumes, but their number increases with an increase in the number of loading cycles, that is, the specific density of slip bands increases. The parameter of the accumulated damage of structural material samples characterizes the exhaustion of the resource of its plastic properties.

The application of scanning and transmission electron microscopy and methods of quantitative fractography to determine the characteristics of the physical and mechanical limit state of fatigue damage to the surface of structural materials is demonstrated in works [16; 17]. It was shown that the use of these methods allows to investigate certain stages of damage initiation and its development to cracks of critical size, which can be used to estimate the service life of metal structures. In particular, the authors of [18] introduce a certain number of parameters to describe the geometry of the surface microrelief created during cyclic loading, which allows for a more accurate description of the topography of the deformed surface. According to the international standard [19], it is proposed to introduce a system of normative parameters for measuring roughness amplitudes in the case of measuring the characteristics of vertical deviations of the geometric surface of a metal. Taking into account the requirements of this standard provides a summarized determination of the durability indicators of the metal structure according to the criterion of the surface roughness parameter of microplastic deformations.

In published works [8; 20; 21] it is shown that the use of such computerized methods as, respectively, wavelet analysis, fractal parameterization, and the synergistic approach allows to identify patterns of accumulation of fatigue damage on the surface of structural materials and to establish their correlation dependences with fatigue characteristics. In particular, work [22] states that the statistical kinetic characteristics of the accumulation of damage in austenitic steels due to their cyclic loading are correlated with certain parameters of the microstructure, and the revealed correlation depends on the sensitivity of the method used to control the fatigue damage of the material.

So, from the above analysis of publications, it can be concluded that scientists are currently paying significant attention to the issues of assessing the kinetics of fatigue damage accumulation in structural materials, modern computerized methods of measurement and analysis are involved in the study, but research into the possibilities of using engineering methods to control the deformed state of the surface of structural the material is not enough now.

MATERIALS AND METHODS

In this work, the surfaces of flat samples of St 45 and St 20 steels (corset shape, length of the working part – 50 mm, width of the narrowest cross-section of the working part of the sample 10 mm, thickness 3 mm) cyclically loaded on the Amsler testing machine under zero cycles were investigated tension-compression. For the indicated sizes of the samples, fatigue tests were carried out at loading frequencies of about 230 Hz, which made it possible to analyze the kinetics of the formed fatigue microrelief based on cyclic loading up to 5·107 cycles at stresses above and below the endurance limit.

Changes in the microrelief of the surface layer of samples of St 45 and St 20 steels under study were analyzed step by step during the termination of the fatigue tests by the method of evaluating the diffuse scattering of a laser beam reflected from the surface, the brightness of which correlates with the characteristic of the distribution of the spectral density of deformation defects, in particular slip bands [23]. Quantitative assessment of the degree of brightness of the spectrograms, which corresponds to changes in the deformation relief on the surface of the studied samples, was used for calculation and experimental control of changes in the deformed state, which can cause the loss of integrity of the surface of the metal structure due to cyclic loading [24].

The method of atomic force microscopy (AFM) was used to obtain the deformation relief of the surface of the steel sample (Fig. 1).

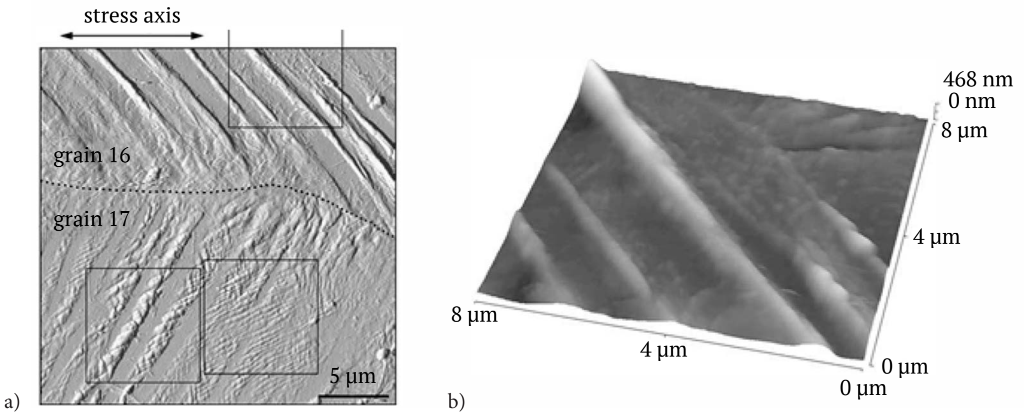

Figure 1. Electronic photograms of the deformation topography of the sample surface:
a – slip bands on the surface; b – AFM image of the relief of microplastic deformations of the surface
Source: [14]

According to the method [25], in this work, the microrelief of developed sliding bands formed on the surface of laboratory steel samples was illuminated by a coherent beam during the intervals of stopping cyclic loading, and in the direction of the beam reflected from the surface, a field of virtual speckles (specklegram) appeared on the LED matrix with discrete brightness distribution. The analysis of the structure of the spectrograms makes it possible to quantitatively assess the degree of accumulation of defects on the surface of the sample. The resolution of the developed experimental information system for the analysis of quantitative characteristics of diffuse damage of elastic-plastic material by the method of coherent optical scanning is up to 0.2 µm/px. [4].

The beam of a coherent light source reflected from a heterogeneously deformed surface contains information about the current state of the physical and mechanical properties of the material surface. The parameters of the two-dimensional image of the surface microrelief with a random distribution of deformation amplitudes characterize the damage of the material, and the brightness parameters of the deformed surface planes of the samples are correlated with discrete deformations, that is, they characterize the deformed state of the surface layer of the material in the case of cyclic loading according to a certain mode [26].

In this work, in order to evaluate the changes in the microplastic deformations of the surface of elastic-plastic materials, which include the studied steels, the metrological characteristics of the angle of reflection of the laser beam were used. Cyclic loading of a certain duration causes a change in the current value of the spatial orientation angle of some local zones of the deformed surface relative to the angle of inclination of the normal vector to the plane of the local surface of the image and the optical axis of the matrix, which leads to a decrease in the intensity of the beam reflected from the surface. The angles of inclination of the surfaces of the deformation relief of the sample, which can be considered as light-reflecting microplates, correlate with the brightness of the virtual speckles of the image on the LED brightness matrix.

The results of determining brightness changes on the photodiode matrix were processed using the PAST program using mathematical statistics methods in accordance with the requirements of the ISO 25178-1:2016 standard [27] regarding the roughness of the engineering surface. In particular, for individual samples of the numerical matrix of luminances corresponding to a certain duration of cyclic loading, the average value of n measurements, dispersion, kurtosis and other statistical characteristics of the sample were calculated. The results of determining the statistical characteristics of changes in the brightness of the deformed surface of the samples made it possible to construct correlational dependences of the degree of cyclic loading of the studied samples with the amplitude of the relief of surface deformation defects.

In order to reduce the dispersion of the analysis results, in the developed photometric method of studying the correlation dependence of the brightness of the speckle structure image with the amplitude spectrum of the relief of local deformation, the correspondence of the correlation parameter within the correlation sample of the general population of data is taken into account. This condition can be fulfilled by stabilizing the homogeneity parameter of the distribution of deformation amplitudes in the local area of one measurement for each sample located within the correlation zone of the general data set. Taking into account the inherent structural heterogeneity of the studied steels, this condition was implemented by reducing the area of the active zone of scanning by a coherent beam to the same average value of the size of the structural element of the sample surface under investigation.

RESULTS AND DISCUSSION

In Figure 2 presents images of spectrograms of the surface of the C 45 steel sample at individual stages of fatigue loading and diagrams of the brightness distribution functions of these spectrograms, constructed along the imaginary intersections of the numerical matrix of the spectrograms corresponding to the imaginary intersections of the sample surface. From the presented images of brightness spectrograms and the corresponding spectral distributions calculated from the data of the numerical brightness matrix, it can be seen that an increase in the number of load cycles is characterized by a significant decrease in the degree of brightness of the images due to a decrease in the number of extremely bright speckles on the spectrograms. That is, the deformation accumulation of damage to the surface of the sample, estimated in this paper by the correlation method, is characterized by a certain nonlinear function, which is consistent with the results obtained by other methods [28].

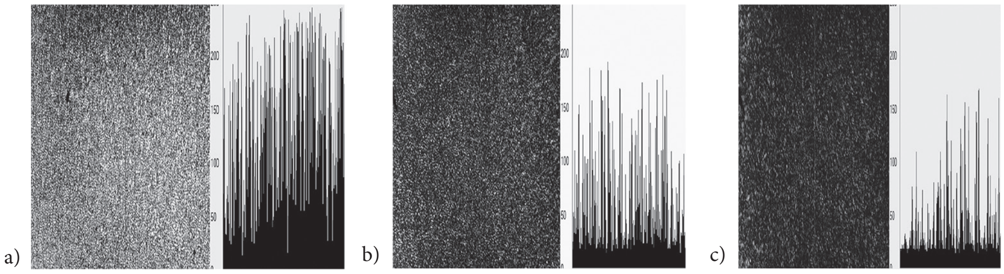

Figure 2. Image of spectrograms and corresponding spectra of speckle brightness in shades of gray 0-255 of the surface of the St 45 steel sample: a – initial state (before cyclic loading); b – the number of loading cycles N=5·105; c – the number of loading cycles N=5·107

Qualitative analysis of spectrograms presented in Figure 2, was clarified by statistical analysis of the numerical matrix of spectrogram brightness in the range of shades of gray 0-255 (Table 1). Presented in the Table 1, the descriptive statistical characteristics of the brightness distribution of the spectrograms at different stages of fatigue are calculated for individual columns of the numerical matrix corresponding to the imaginary cross-sections of the surface of the samples.

Table 1. Statistical characteristics of the brightness distribution of the spectrograms of the micro-deformed surface of the St 45 steel sample under stresses σa=120 MPA (below the endurance limit by 30%)

The number of sample loading cycles N	0	$5\cdot10^5$	$1\cdot10^6$	$5\cdot10^6$	$5\cdot10^7$
The maximum value of ***I***	255	200	125	123	140
The average value of ***I***	130.81	116.76	74.52	84.86	89.10
Standard error	7.958	6.065	4.350	5.247	4.501
Sampling variance	3526.26	1365.99	397.46	378.73	425.49
Standard deviation	59.38	36.96	19.94	19.46	20.63
Asymmetry	1.0133	0.6261	0.4065	0.3993	0.3062
Median	113	116	77	90	91
Kurtosis	-0.1992	-0.3548	0.9067	-0.3132	0.4991

Note: *N* is the number of sample loading cycles; *I* – the brightness of speckles in shades of gray
Source: developed by the authors

In the Table 1 shows the generalized results of calculating the statistical characteristics of the number of speckles of the selected gradation of brightness *I* (in the range of shades of gray 0-255), which correspond to the formed microrelief of discrete deformations of the studied surface of St 45 steel samples under different number of loading cycles *N*. The analysis of these data shows that in absolute terms, the kinetics of the degree of brightness of the spectrograms (both with respect to the average and maximum brightness values) is not monotonic in the considered range of loading cycles up to 5·107 cycles. In the case of reaching such a loading base, an increase in the average value of the spectrogram brightness by 5% is observed in the case of an increase in the duration of cyclic loading by almost an order of magnitude, which reflects a certain enlargement of the microrelief of the sample surface at large loading bases close to the endurance limit. At the same time, the effect of cyclic loading was also found for other statistical characteristics of brightness (sharpness and asymmetry of the normal distribution function).

In Figure 3 shows how the shape of the brightness histograms of spectrograms constructed for individual stages of cyclic loading of the sample, specified in Table 1, changes. The value of speckle brightness in shades of gray (0-255) is plotted on the abscissa axis, and the number of speckles n of the sample is plotted on the ordinate axis. From Figure 3 shows how the sharp peaks of the histograms increase, i.e. the number of brightly luminous speckles decreases. Therefore, the sequence of 1 2 3 brightness histograms corresponds to an increase in the specific area of the accumulated deformation of the metal of the surface layer of the sample.

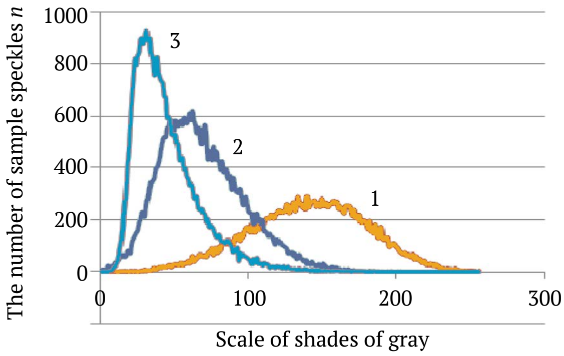

Figure 3. Histograms of the brightness of the spectrograms of the micro-deformed surface of the St 45 steel sample at different stages of cyclic loading: 1 – initial state; 2 – 5·105 cycles; 3 – 5·107 cycles
Source: developed by the authors

Therefore, in order to identify the trends of changes in the deformation microrelief parameters of the studied samples during the stages of multi-cycle fatigue, the statistical characteristics of the brightness distribution of spectrograms in the form of histograms are more informative in contrast to the absolute brightness values.

The system of correlation diagrams that characterize the effect of cyclic loading on changes in the brightness of spectrograms, as a manifestation of the accumulation of the amplitude of the deformation microrelief of the surface of the studied St 45 samples, as well as their trend lines, is shown in Figure 4.

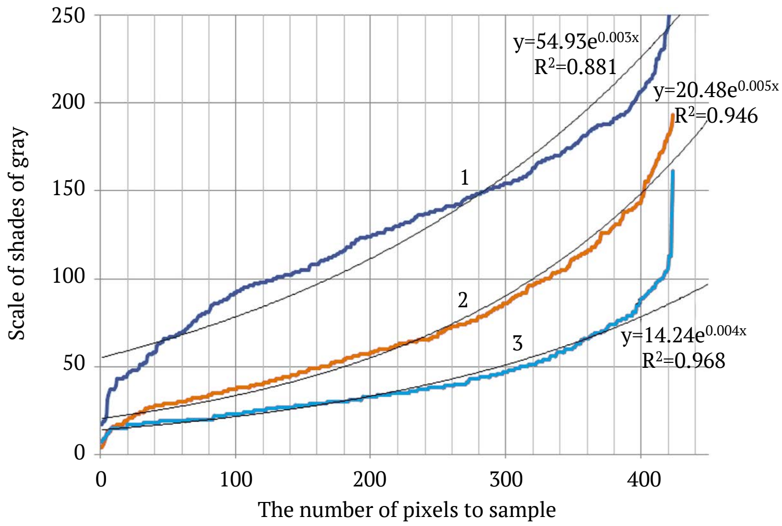

Figure 4. Correlation diagrams of changes in the degree of brightness of spectrograms based on the number of pixels of the sample taken into account, as a manifestation of the accumulation of surface deformations during fatigue of St 45 samples for different stages of cyclic loading: 1 – initial state; 2 – N=5·105; 3 – 5·107 cycles (thin lines depict trend lines with corresponding exponential equations and R2 confidence level)
Source: developed by the authors

Constructed according to the principle of Pareto diagrams, the diagrams in fig. 4 show the monotony of the location with an increase in the duration of cyclic loading and a significant increase in the current state of the instantaneous value of the angle of inclination of the graph in the coordinates of the diagram, as signs of the dynamics of the process of non-localized destruction under multi-cyclic loading. The obtained data are consistent with the results of the study of the accumulation of fatigue damage of metals, which present the stages of the process and a significant increase in damage parameters at the stage before the formation of local macro damage [29; 30]. The peculiarities of the results of the quantitative analysis of the correlation diagrams revealed in this work indicate the expediency of determining the state of fatigue damage of the metal structure according to the criterion of the limit accumulation of the parameter characterizing changes in the brightness of certain (light and dark) elements of spectrograms.

Currently, in the thematic publications on the accumulation of fatigue damage in metallic materials, in particular those mentioned above in this article, insufficient attention is paid to the study of the correlation between the rate of metal damage and the large-scale hierarchy of multi-level damage at the stages of fatigue. The importance of the study of correlation relations under fatigue loading of metal structure samples is indicated in [4], which describes a statistical method for determining the degree of damage under variable loading based on the data of profilometric measurement of the fatigue topography of the sample surface in the range of amplitudes up to 1.0 μm. Based on the calculation and experimental results of the analysis of the morphology of the fracture surface of samples of materials with isotropic and anisotropic mechanical properties, it is proposed to determine a certain constant as a spatial parameter of the surface relief of a solid body characterized by scale invariance. This makes it possible to monitor the general laws of fatigue failure, since the constant relates the parameters of the local and general profile of the surface to the kinetic parameters of fatigue failure. The research results obtained in this work correspond to these principles.

Zones of elastoplastic deformation appear on the surface of the sample under fatigue, which are localized as discrete manifestations of inelastic deformations. The fatigue failure of the metal of the sample is preceded by the accumulation of local macrodisplacements of the surface, that is, local plastic deformation occurs, which leads to local failure [31]. The comparison of microhardness at the fracture sites after monotonic and cyclic loading of the metal showed their close values, which indicates the uniformity of the limit plastic deformations leading to fracture. These deformations are characterized by a diagram of the spectrum of instantaneous values of scattered damage, which relates the topogram of the surface (amplitude of the range of local maxima of the relief) with the duration of cyclic loading. It has been experimentally shown that such a diagram reflects the current state of local strengthening and weakening of metal under cyclic loading [28].

The information presented in Figure 3 and 4, as well as in Table. 1, shows that the correlation method of digital analysis of the surface relief [11] provides experimental and computational means that allow to evaluate critical changes in the deformation microrelief of the samples based on the criterion of the brightness intensity of spectrograms. The digital representation of the brightness spectrum of the spectrogram is correlated with the amplitude spectrum of discrete deformations of the surface microrelief, which create the microrelief of slip bands on the surface of the polycrystalline structure sample. Therefore, the application of coherent optical scanning of the deformed surface of metal structure samples is an effective tool for studying the accumulation of fatigue damage in metal structure samples, as stated in [32].

From Figure 4, it follows that an increase in the duration of cyclic loading leads to a monotonous increase in the amplitude of the deformation relief, which can be represented by linear or exponential dependences, which is consistent with the kinetic dependences of the characteristics of the process of accumulation of microplastic deformation under dynamic loading of elastic-plastic structural materials [23], as well as during the previous cyclic loading of material samples [33], obtained using other methods of metal surface research (acoustic emission).

In order to quantitatively track the state of damage to the surface of structural metal materials, it is proposed to determine the damage (microplasticity) coefficient kD as a correlation characteristic of the deformation properties of the surface of the structural material. This coefficient, which is a quantitative measure of the deformation relief, surface, is calculated according to the formula:

$$k_D=(I_i-I_0)/I_i, \tag{1}$$

where the difference (I_i-I_0) characterizes the degree of damage to the surface area of microplastic deformations in the window area of the base matrix; I_0 – the value of the damage area parameter before loading; I_i is the current value of the damage area parameter. In the case of digital analysis of spectrograms, parameter I should be considered as brightness values of spectrograms in the range of shades of gray (0-255) for the investigated stages of cyclic loading.

In Figure 5 presents the kinetic diagrams of the coefficient of damage of St 45 and St 20 steel samples, constructed based on the results of tests with cyclic stress levels above and below the corresponding endurance limits, which led to different durations of cyclic loading. Testing of St 45 steel samples was carried out under cyclic stresses σa=120 MPa, and St 20 samples under cyclic stresses σa=240 MPa (Fig. 5a) and σa=200 MPa (Fig. 5b).

The presented diagrams can be described by exponential dependencies. From Figure 5b shows that the equations of the diagrams for both studied steels are similar, the slope depends on the magnitude of the cyclic stresses in their considered range, which is consistent with the low intensity of deformation microrelief accumulation on the surface of the samples under stresses close to the endurance limit. In particular, this applies to the laws obtained in [22], which relate the amplitudes of microplastic deformations of the surface of SUS316NG steel samples, determined as a result of direct measurement by atomic force microscopy methods, with the level of loading under low-cycle fatigue.

The results obtained in this work contribute to the creation of scientific and methodological foundations of experimental and calculation methods for determining the residual operational resource of metal structures under the conditions of cyclic loading, as well as methods for tracking the accumulation of deformation defects on the surface of the responsible elements of metal structures under the action of multi-cycle fatigue.

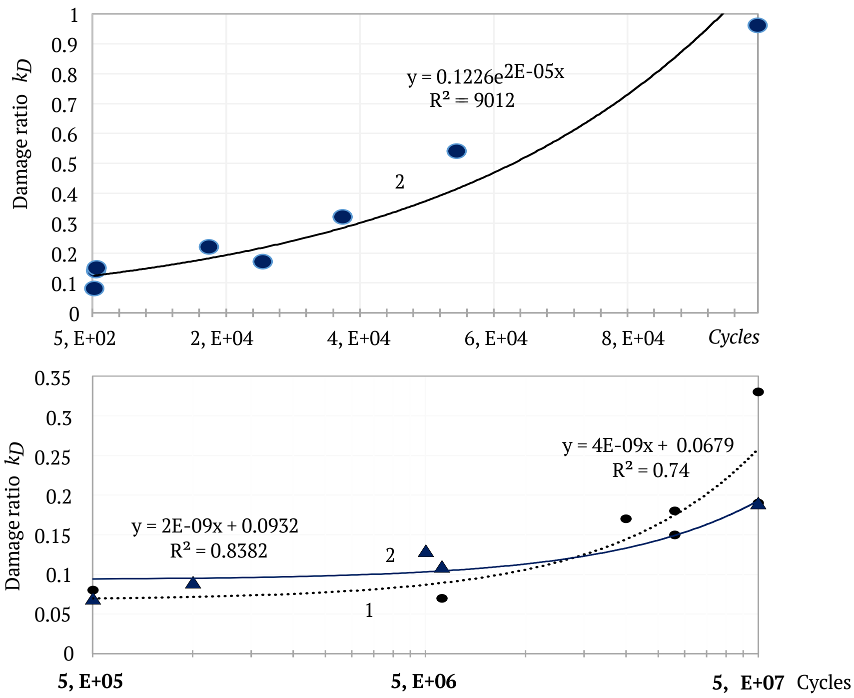

Figure 5. Damage characteristics of St 45 (diagram 1) and St 20 (diagram 2) steels under various cyclic stresses (R^2 – characterizes the degree of reliability of the approximation of experimental data by the equations shown in the figure)
Source: developed by the authors

CONCLUSIONS

An experimental and informational system for analyzing the quantitative characteristics of scattered damage of an elastic-plastic material by the method of coherent optical scanning of a deformed surface with a resolution of 0.2 μm/px has been developed.

The correlation characteristics of the distribution of speckles of the selected gradation of brightness I (in the gray range 0-255) corresponding to the formed microrelief of discrete deformations of the studied surface of St 45 steel samples under different number of loading cycles were calculated. It is shown that in absolute values, the kinetics of the degree of brightness of the spectrograms (both with respect to the average and maximum brightness values) is not monotonic in the considered range of loading cycles up to 5·107. The state of damage to the metal of the sample upon reaching such a loading base corresponds to a change in the average value of the amplitude of the spectrogram brightness by 5.0% due to an increase in the duration of cyclic loading by almost an order of magnitude, which correlates with the state of non-localized damage, determined by a controlled increase in the area of the microrelief of the sample's deformed surface under cyclic stresses close to to the limit of endurance.

The kinetics of the metrological parameters of the geometry of the deformation defects of the surface layer of the sample, formed as a result of cyclic loading at stresses below and above the endurance limit, were evaluated using scanning laser imaging microscopy. The obtained results, which are systematized in the form of correlation characteristics, contain information about the statistical process of microplastic deformation of the surface of St 45 and St 20 structural steels.

It was established that the components of the amplitude spectrum of the microrelief of deformation defects under fatigue, estimated by the parameters of spectrograms, are characterized by the criterion features of the limit state of the surface of the metal structure in the case of cyclic loading under stresses close to the endurance limit. In further research, it is necessary to consider the development of experimental and computational methods that will allow to substantiate the application of the optical-computer method presented in the article for establishing the limit values of the accumulation of fatigue damage on the surface of metal structures that are subjected to long-term cyclic loading during operation.

REFERENCES

[1] Chernousenko, O., Butovsky, L., Rindyuk, D., Granovska, O., & Moroz, O. (2017). Analysis of residual operational resource of high-temperature elements in power and industrial equipment. *Eastern-European Journal of Enterprise Technologies*, 1(8), 20-26.

[2] Pogrebniak, A., & Kasperska, V. (2022). Fatigue resistance of metal construction materials and its relationship with changes in the state of thin surface layers. *Mechanics and Advanced Technologies*, 6(2), 143-150.

[3] Shi, Y., Yang, X., Yang, D., Shi, D, Miao, G., & Wang, Z. (2020). Evaluation of the influence of surface crack-like defects on fatigue life for a P/M nickel-based superalloy FGH96. *International Journal of Fatigue*, 137, article number 105639.

[4] Pysarenko, G., Voynalovich, O., Maylo, A., & Pysarenko, S. (2022). Deformation defects of the structural material as a factor of life aging. *Procedia Structural Integrity*, 36, 30-35.
[5] Dequiedt, J.L., & Denoual, C. (2021). Localization of plastic deformation in stretching sheets with a crystal plasticity approach: Competition between weakest link and instable mode controlled process. *International Journal of Solids and Structures*, 210-211, 183-202.
[6] Froustey, C., Naimark, O., Bannikov, M., & Oborin, V. (2010). Microstructure scaling properties and fatigue resistance of pre-strained aluminium alloys (part 1: Al-Cu alloy). *European Journal of Mechanics. A/Solids*, 29, 1008-1014.
[7] Gajdoš, L., Šperl, M., Kaiser, J., & Mentl, V. (2013). Microplastic limit of steels as a means of fatigue limit determination. *Procedia Engineering*, 66, 635-642.
[8] Zhu, X.-K., & Joyce, J.A. (2012). Review of fracture toughness (G, K, J, CTOD, CTOA) testing and standardization. *Engineering Fracture Mechanics*, 85, 1-46.
[9] Bufford, D., Stauffe, D., Mook, W., Asif, S., Boyce, B., & Hattar, K. (2016). High cycle fatigue in the transmission electron microscope. *Nano Letters*, 16(8), 4946-4953.
[10] Liedmann, J., & Barthold, F.-J. (2017). Exploration of internal response sensitivities of materially nonlinear structures. *Proceedings in Applied Mathematics and Mechanics*, 17, 745-746.
[11] Al-Salih, H., Juno, M., Collins, W., Bennett, C., & Li,J. (2021). Application of a digital image correlation bridge inspection methodology on geometrically complex bifurcated distortion-induced fatigue crackin. *Fatigue & Fracture of Engineering Materials & Structure*, 44(11), 3186-3201.
[12] Algarni, M., Choi, Y., & Bai, Y. (2017). A unified material model for multiaxial ductile fracture and extremely low cycle fatigue of Inconel 718. *International Journal Fatigue*, 96, 162-177.
[13] Suhartono, H.A., Kirman, K., & Prawoto, Y. (2022). On the influence of the initial shear damage to the cyclic deformation and damage mechanism. *Metals*, 12(7), 1-24.
[14] Man, J., Vystavel, T., Weidner, A., Kuběna, I., Petrenec, M., Kruml, T., & Polák, J. (2012). Study of cyclic strain localization and fatigue crack initiation using FIB technique. *International Journal of Fatigue*, 39, 44-53.
[15] Radel, J.C., Belanger-Garnier, V., & Hegedus, M.P. (2018). Virtual image determination for mirrored surface. *Optics Express*, 26(3), 2599-2612.
[16] Babinský, T., Kuběna, I., Šulák, I., Kruml, T., Tobiáš, J., & Polák, J. (2021). Surface relief evolution and fatigue crack initiation in René 41 superalloy cycled at room temperature. *Materials Science and Engineering*, 819, article number 141520.
[17] Bannikov, M.V., Naimark, O.B., & Oborin, V.A. (2016). Experimental investigation of crack initiation and propagation in high- and gigacycle fatigue in titanium alloys by study of morphology of fracture. *Frattura ed Integrità Strutturale*, 10(35), 50-56.
[18] Shittu, A.A., Kolios, A., & Mehmanparast, A. (2020). A systematic review of structural reliability methods for deformation and fatigue analysis of offshore jacket structures. *Metals*, 11(50), 1-37.
[19] ISO 25178-2:2021. Geometrical product specifications (GPS) – Surface texture: Areal – Part 2: Terms, definitions and surface texture parameters. Retrieved from https:// www.iso.org/standard/74591.html.
[20] Ravanellia, R., Nascettia, A., Di Rita, M., Belloni, V., Mattei, D., Nisticò, N., & Crespi, M. (2017). A new digital image correlation software for displacements field measurement in structural applications. *The international archives of the photogrammetry, remote sensing and spatial information sciences: FOSS4G-Europe 2017, 18 – 22 July 2017: Academic Track. - Marne La Vallée, France*, XLII-4/W2, 139-145.
[21] Dodaran, M.S., Muhammad, M., Shamsaei, N., & Shao, S. (2022). Synergistic effect of microstructure and defects on the initiation of fatigue cracks in additively manufactured Inconel 718. *International Journal of Fatigue*, 162, article number 107002.
[22] Fujimura, N., Nakamura, T., & Takahashi, K. (2018). Changing mechanisms of surface relief and the damage evaluation of low cycle fatigued austenitic stainless steel. *MATEC Web of Conferences. 12th International Fatigue Congress (FATIGUE 2018)*, 165(2), 256-262.
[23] Pysarenko, G., Voynalovich, O., & Mailo, A. (2018). Stochastic regularities in the non-contact determination of local strains in the surface layer of steel 45 under high-cycle loading. *Mechanics and Advanced Technologies*, 84(3), 39-44. doi: 10.20535/2521-1943.2018.84.136382.
[24] Torabian, N., Favier, V., Dirrenberger, J., Adamski, F., Ziaei-Rad, S., & Ranc, N. (2017). Correlation of the high and very high cycle fatigue response of ferrite based steels with strain rate-temperature conditions. *Acta Materialia*, 134, 40-52. doi: 10.1016/j.actamat.2017.05.064ff. ffhal-01592775.
[25] Phung, N.L., Favier, V., Ranc, N., Valès, F., & Mughrabi, H. (2014). Very high cycle fatigue of copper: Evolution, morphology and locations of surface slip markings. *International Journal of Fatigue*, 63, 68-77.
[26] Polák, J., Mazánová, V., Heczko M., Petráš, R., Kuběna, I., Casalena, L., & Man, J. (2017). The role of extrusions and intrusions in fatigue crack initiation. *Engineering Fracture Mechanics*, 185, 46-60.
[27] ISO 25178-1:2016. Geometrical product specifications (GPS) – Surface texture: Areal – Part 1: Indication of surface texture. Retrieved from https://www.iso.org/standard/46065.html.
[28] Pysarenko, G., Voynalovich, O., & Mailo, A. (2020). Discrete properties of the inelasticity of steel and alloys based on Al and Ti under periodic deformation, *Metallophysics and Advanced Technologies*, 42(2), 261-279. doi: 10.15407/mfint.42.02.0261.
[29] Shanyavskiy, A., & Soldatenkov, A. (2022). Metallic materials fatigue behavior: Scale levels and ranges of transition between them. *International Journal of Fatigue*, 158, article number 106773.

[30] Wei, Y., Liao, H., Xu, H., & Tang, J. (2022). Microstructure evolution and mechanical properties of martensite stainless steel during repetitive high stress loading-unloading with small plastic deformation. *International Journal of Fatigue*, 158, article number 106750.
[31] Haghshenas, A., & Khonsari, M.M. (2018). Damage accumulation and crack initiation detection based on the evolution of surface roughness parameters. *International Journal of Fatigue*, 107, 130-144.
[32] Aulbach, L., Bloise, F., Lu, M., & Koch, A. (2017). Non-contact surface roughness measurement by implementation of a spatial light modulator. *Sensors*, 17(3), article number 596. doi: 10.3390/s17030596.
[33] Botvina, L., Tyutin, M., Sinev, I., & Bolotnikov, A. (2020). The effect of preliminary cyclic loading on acoustic emission parameters and damage of structural steels. *Procedia Structural Integrity*, 28, 2118-2125.

Георгій Георгійович Писаренко
Доктор технічних наук, професор
Інститут проблем міцності ім. Г.С. Писаренка НАН України
01014, вул. Тімірязєвська, 2, м. Київ, Україна
https://orcid.org/0000-0001-9557-9710

Олександр Володимирович Войналович
Кандидат технічних наук, доцент
Національний університет біоресурсів і природокористування України
03041, вул. Героїв Оборони, 15, м. Київ, Україна
https://orcid.org/0000-0002-9321-2672

Андрій Миколайович Майло
Кандидат технічних наук
Інститут проблем міцності ім. Г.С. Писаренка НАН України
01014, вул. Тімірязєвська, 2, м. Київ, Україна
https://orcid.org/0000-0002-4762-0886

Степан Георгійович Писаренко
Аспірант
Інститут проблем міцності ім. Г.С. Писаренка НАН України
01014, вул. Тімірязєвська, 2, м. Київ, Україна
https://orcid.org/0000-0003-4295-6687

Методичний підхід щодо визначення характеристик пошкодження циклічно навантажуваних зразків металоконструкцій

Анотація. В статті розглядається актуальна задача розроблення інженерних методів прогнозування довговічності сучасних машин тривалого ресурсу, яка має базуватися на методології відстеження ступеню втомного пошкодження матеріалів та конструкційних елементів. Мета статті – обґрунтувати методичний підхід для визначення граничного стану пошкодженості із застосуванням фотометричного аналізу топографії мікродеформованої поверхні циклічно навантажуваних зразків металоконструкції. У роботі було використано розроблену експериментально-інформаційну систему на основі методу когерентно-оптичного сканування деформованої поверхні зразків металоконструкції з виокремівністю 0,2 мкм/пкс. Комп'ютерно проаналізовано отримані спеклограми фотодіодної матриці, що у відтінках сірого 0-255 відповідають двовимірним зображенням мікродеформованої поверхні зразка для окремих етапів циклічного багатоциклового навантажування. Для досліджуваних конструкційних сталей Ст 45 і Ст 20 виявлено вплив тривалості циклічного навантажування на статистичні характеристики яскравості спеклограм (гостровершинність гістограм та асиметрію функції нормального розподілу). Побудовано діаграми змін ступеню яскравості спеклограм, що відповідають кінетиці накопичування амплітуди деформаційного мікрорельєфу поверхні лабораторних зразків за втоми. Показано, що отримана кореляційним методом кінетика яскравості спеклів, що корелює з еволюцією накопичення втомної пошкоджуваності на поверхні зразків досліджених сталей, характеризується нелінійною функцією, що узгоджується з результатами досліджень деформаційного мікрорельєфу, отриманих іншими методами. Результати дослідження (методологія аналізу дискретного розподілу яскравості спеклограм) можуть бути використані для прогнозування настання граничного стану металоконструкції перед її зруйнуванням внаслідок втоми

Ключові слова: втома металів і сплавів; кореляційний аналіз; мікропластичне деформування поверхні; деформаційний мікрорельєф; фотометричне сканування

Machinery & Energetics
Vol. 13, No. 4. 2022

Journal homepage:
https://technicalscience.com.ua/en

UDC 612.316.1.052.6:696.6-1
DOI: 10.31548/machenergy.13(4).2022.38-47

Viktor Kaplun*
Full Doctor in Technical Sciences, Professor
National University of Life and Environmental Sciences of Ukraine
03041, 15 Heroiv Oborony Str., Kyiv, Ukraine
https://orcid.org/0000-0001-7040-9344

Volodymyr Osypenko
PhD in Technical Sciences, Associate Professor
National University of Life and Environmental Sciences of Ukraine
03041, 15 Heroiv Oborony Str., Kyiv, Ukraine
https://orcid.org/0000-0002-9321-2672

Svitlana Makarevych
PhD in Technical Sciences, Associate Professor
National University of Life and Environmental Sciences of Ukraine
03041, 15 Heroiv Oborony Str., Kyiv, Ukraine
https://orcid.org/0000-0001-7040-9344

Forecasting the electricity pricing of energy islands with renewable sources

Abstract. The strategy for the development of local low-power systems involves the use of several sources. The efficiency of functioning such systems depends on the purposeful reliability management and it is based on the rational hierarchical connections of their structural components. Coordination of the structure of diversified sources and their participation in the formation of energy balance of micro-energy systems in the conditions of dynamic development of renewable energy is an actual research task. The purpose of research was to develop a method of reliability-cost optimization of structure of micro-energy systems with dissimilar sources, which is based on the use of reliability indicators and cost of electricity. The studies conducted are based on the modern methods of applied statistical analysis, the theory of reliability, the synthesis of complex multi-aggregate systems. Through the implementation of the Markov model and simulation modeling of the functioning of sources, it has been obtained the conditions for optimal formation of the energy balance of micro-energy system with the lowest cost of electricity, considering the reliability indicators. Computational experiments made it possible to obtain the regularities of cost evolution of electricity and to show its dependence on the structure and algorithms of the sources' functioning. Using a probabilistic modeling method, it has been proved for the first time that the cost of electricity is sensitive to the ratio availability of renewable sources of primary energy. The practical application of results lies in the increase in efficiency of energy islands through the structural and algorithmic optimization of diversified sources (traditional and renewable) based on determining the cost of electricity

Keywords: diversified sources of electricity; reliability-cost analysis; the Markov model; simulation modeling; efficiency of microgrids

Article's History: Received: 01.07.2022; Revised: 18.10.2022; Accepted: 23.11.2022.

INTRODUCTION

Future low capacity energy systems depend on the development of systems with distributed generation capacity using multiple energy sources, primarily, the renewable ones.

The study is devoted to the substantiation of need to use the renewable sources of electricity in energy islands with renewable sources (EIRS) with traditional sources, as

Suggested Citation:
Kaplun, V., Osypenko, V., & Makarevych, S. (2022). Forecasting the electricity pricing of energy islands with renewable sources. *Machinery & Energetics,* 13(4), 38-47.

*Corresponding author

well as considering the probabilistic nature of access to the primary natural factors (power of solar insolation, wind speed, etc.) for traditional and renewable sources. This approaching is due the expected economic effect, namely, a reduction in the primary fuel costs for internal combustion engines. At the same time, the instability of operation of the renewable sources (RES) over time (caused by seasonality, natural factors, geographical location, etc.), the problem of substantiating the installed capacity of sources (traditional and renewable) is a rather difficult research issue. Provided that the uninterrupted power supply in the EIRS is ensured.

The study is devoted to the development of power systems with small volumes of electricity consumption, having an installed capacity of electricity consumers of up to 15 kVA. The island or autonomous operating mode of such a micro-energy system is typical for the local facilities with limited access to main grid (centralized power system). The use of combined power supply with several dissimilar sources is a feasible solution for such systems.

Forecasting the electricity prices of EIRS is the important component for developing low capacity systems and designing the hybrid systems combining multiple sources. It is important to consider that the management of EIRS efficiency is a relevant problem and it depends on the structures and algorithms of analyzing the prime electricity cost of such systems.

In the study of complex multicomponent energy systems with a stochastic nature of the behavior of its elements, the mathematical modeling involves the description of random processes that develop depending on a number of random factors. Most models of discrete systems with a stochastic nature of functioning are built on the basis of queuing models, the processes of which are random, and in many cases, the Markov ones. Therefore, to solve such problems, it is expedient to use the mathematical apparatus of the theory of the Markov processes. Mathematical description of the Markov processes is usually represented as systems of differential (in the case of non-stationary mode) or algebraic (for stationary mode) equations, the solutions of which, in general, cannot be obtained explicitly. This necessitates the application of numerical methods for solving systems of differential or algebraic equations. In the power systems with multiple sources, it is possible to apply the processes of data transmission to the information network of dispatching systems of the corresponding levels, the performance of tasks and data exchange with external devices in the computer system, etc. for the analysis of reliability and efficiency of the use of generating capacities.

Low-power supply systems with several sources are created for the modernization of existing networks and they require technical and economical justifications to choose the composition of generating capacities [1; 2]. The hybrid micro-energy systems usually include solar and wind generators to reduce the use of hydrocarbons as primary fuel from traditional sources [3]. The research of hybrid power system recently requires new approaches to intelligent management of this kind of local power supply and forms a separate conceptual direction of microgrid development as a lower-level smart grid system. This is the feature of operation of such microgrids: the coordination of their modes with the load and possibility of parallel operation with the main network [4]. The autonomy class of such systems is primarily due to the insufficient reliability of the main network. The creation of micro-energy systems of energy island is both a solution of the problem of power supply reliability and the creation of prerequisites for the introduction of RES [5]. Management of the efficiency of the combined power supply system can be solved on the basis of optimal distribution of share in the energy balance between traditional and renewable sources according to the specific cost criterion for electricity. The introduction of renewable sources creates certain restrictions for the needs of autonomous power supply systems of industrial, residential or other objects. The combined use of heterogeneous sources allows both managing the reliability of power supply, and considering the stochastic supply of natural resources to coordinate the current load or using energy storage [6; 7]. Based on the well-known publications [2; 3; 6], it is possible to generalize the composition of local micro-energy systems (Fig. 1), which are built on the basis of the use of several heterogeneous sources.

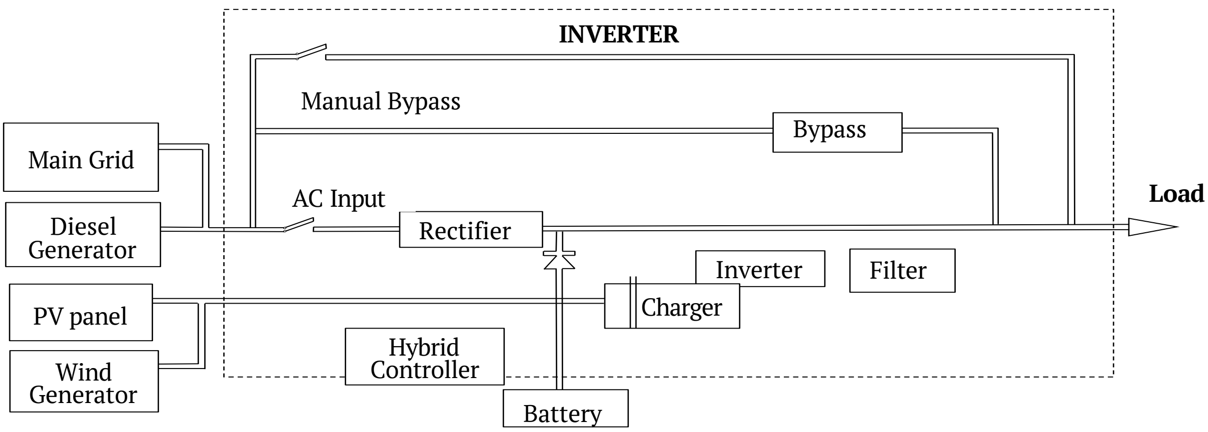

Figure 1. The principles of energy islands with renewable sources design

Publications [8-10] are devoted to the development of models for the search for optimal structures of autonomous power supply systems, as well as to the study of pricing of electricity in the energy islands with renewable sources.

The purpose of research was to increase the efficiency of island microgrid systems by means of structural optimization of traditional and renewable sources through the indicators of reliability and probability of supply of wind and solar energy with an assessment of the cost of electricity.

MATERIALS AND METHODS

For the analysis of EIRS, it is used the graph theory, which is one of the most convenient mathematical modeling tools to determine the reliability of complex systems. There are two sets of graph: (a) set of vertices and (b) set of edges [11].

The theories of the Markov processes is an effective tool for the analysis of reliability characteristics. It is used for estimating the probabilistic indicators of complex multicomponent systems [12-14]. The peculiarity of construction of the Markov models lies in the consideration of microgrid in different states such as operational and refusal ones. Each state is characterized by different operational efficiency and resources ensuring reliability. Transitions between system states occur at the times of refusal or restoration of one or another element of the system. It is described the process according to the models of discrete states for the selected time of system operation. A random process is called the Markov process, considering the following factors: if the probability of system transition during the time $t > t_0$ t for any moment t_0 depends only on the state at the moment $t = t_0$, and does not depend on the fact how the system entered this state. There are several conditions. Since the transitions statistically independent, the intensity of failures and the intensity of recovery are constant in time and different from state to state. The time intervals between the adjacent transitions are distributed according to the exponential law. Thus, for the Markov process, the probabilities of transitions from the *i*-th to the *j*-th state during the time Δt will be determined by the intensity of failure λ_{ij} as:

$$P_{ij}(\Delta t)=1-exp(-\lambda_{ij}\Delta t). \quad (1)$$

For short time intervals Δt:

$$P_{ij}(\Delta t)\approx 1\lambda_{ij}\Delta t. \quad (2)$$

A circle with the identification number can be represented for reliability graph of each EIRS state (vertex) of the system. The transition from one state to another will be depicted as the the lines (edges) connecting the states. For the numerical analysis of the EIRS reliability, the mathematical theory of graphs can be used [12; 15].

It is possible to perform the reliability analysis of EIRS with graphs. Random failures of system elements can be modeling with random graphs. The reliability characteristics of individual elements (blocks) are used to quantify the reliability of EIRS. It is assumed that the failures of elements are statistically independent.

The theories of the Markov and semi-Markov processes are also used. In this case, the Markov chains with states are considered, which can be represented in the form of matrix of transition probabilities [13; 14]:

$$P=\begin{bmatrix} p_{11} & p_{12} & \cdots & p_{1n} \\ p_{21} & p_{22} & \cdots & p_{2n} \\ p_{n1} & p_{n2} & \cdots & p_{nn} \end{bmatrix}. \quad (3)$$

The elements of transition matrix p_{ij} represents probability of the system transition to the state j from the state i in one step. The diagonal element pij represents the probability that the system will be constant.

The transition from one state to another is described according to the cumulative distribution function e_{EIRS}, for each state *k* for random variables. In case of the Markov processes, all distributions $F_{k(t)}$ are exponential ones. Knowing the transition probabilities such as: p_{ij}, parameters, λ_{ij} and distributions $F_{k(t)}$ of the time during which the process remains in state i , the weight of each edge is $\lambda_{ij} = p_{ij}\lambda_i$ The semi-Markov process is determined by the transition probabilities of the embedded Markov chain p_{ij} and conditional distribution $F_{k(t)}$ of the time duration; the system remains in state i provided that the system moves into the pre-defined state *j*.

Thus, the graph representing the semi-Markov process has to describe each edge transition probability p_{ij} and conditional distribution $F_{k(t)}$ of time, so that the process remains in the state corresponding to the state in transition of this edge.

Thus, one unreserved element can exist in three states: s_1 – the element is in order, s_2 – the element is out of order, it is not required the need to supply disconnection, and – s_0 the element is out of order (state of failure) (Fig. 2a). If the failure stream has intensity λ and restoration intensity μ, the system transits from state to state and back after a certain time [16]. The graph of state-to-state transitions of the time $d t\lambda$ and μ characteristics is shown in the Figure 2b.

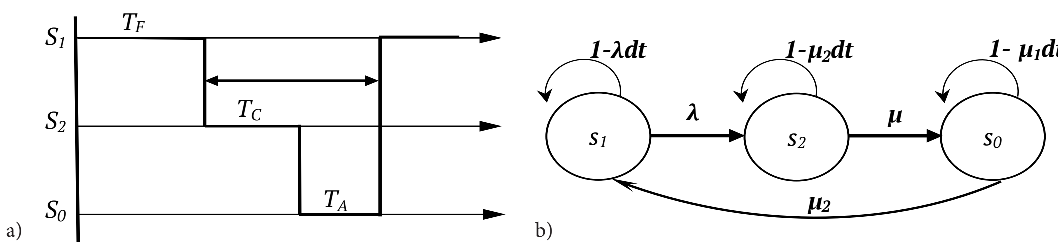

Figure 2. The time diagram of a single element transitions: from one state to another (a) and the graph of states (b)
Source: developed by the authors based on [16]

The graph of transitions of the Markov process allows system of differential equations of states [14]:

$$\frac{dp}{dt} = \sum_{j \in G} \lambda_{ij} p_j(t) - p_i(t) \sum_{j \in G} \lambda_{ij}, \tag{4}$$

where G_i is the subset of states of the Markov process which allows transition into state i, and G_i is the subset of states that may be achieved from state i, and λ_{ij} is intensity of the transitions.

The system (4) is linearly dependent, and therefore, it is required to add another equation (normality equation) to make the solution unique:

$$\sum_{i=n}^{n} p_i = 1. \tag{5}$$

Let's consider the structure of EIRS that combines three sources of electric power: R_1 is the supply from the network; R_2 is a set with electric energy consisting of static converters with accumulative features and a set with renewable primary energy.

R_3 is a set with combustion engines (gas/diesel, gas/petrol, diesel, biofuels, etc.). Automatization is a specific feature of these sources, enabling the required activation time (namely, the time from transition of unloaded/cold reserve to the operating mode).

Probably, the changing restoration process is a source, represented by two independent one-by-one variables. These variables are performed identically and are free as a set.

The research of EIRS reliability indicators should be reduced to structural optimization of sources [17]. There are two approaches to solving the optimization task. It is based on achieving the maximum reliability indicators. It will be adhere to the directivity of established resource costs, or it will minimize the average specific losses in the system according to the established limit indicators of reliability. Solving the optimization task will be guided to minimize the cost function by a set of variables corresponding to the selected constraints [18; 19]. The choice of the structure of EIIR sources has a significant impact on the reliability indicators of microgrid system, primarily on the current specific resource costs and system efficiency. It is obvious that in case of using the renewable energy sources, their share in the energy balance should be maximal, provided that the reliability (continuity) of power supply is ensured. This is exactly for achieving the maximum reduction in the specific cost of electricity [20]. In terms of reliability, the process of EIRS functioning is a stochastic recovery process (Fig. 3) [13]: The quantities are random, independent and have the same distribution.

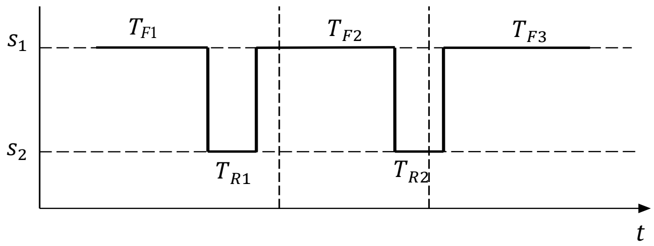

Figure 3. The alternating restoration process of EIRS operation
Source: developed by the authors based on [13]

If one source fails, another source out of the set ones is available and can operate. In general, the sequence of activation sources (if the source fails) is presented by the general EIRS algorithm. Sources of the set are operating in unloaded reserve with time delay and they are required for activation.

GPSS World (General Purpose Simulating System) simulation system [8] was used to build a simulation model of the studied system. The choice of this software environment is based on the availability of a specialized and object-oriented language with the ability to display dynamic processes in real systems, generate arbitrary laws of distribution of stochastic values, diagnose errors during the execution of a simulation program, etc.

RESULTS AND DISCUSSION

It is supposed that the time of failure, the time of system elements restoration (sources D_1, D_2, D_3, as well as the connection expiration time are distributed by an exponential law with parameters λ_1, λ_2, λ_3, μ_1, μ_2, μ_3, and λ_4, respectively. In fact, these parameters depend on the choice of a "candidate" among the selected sources from the sets $D_2^1,\dots, D_2^{n1}$ and $D_3^1,,\dots ,D_3^{n1}$ respectively.

That is $\lambda_i=\lambda_i(x_i)$, $i=\overline{1,4}$; $\mu i=\mu_i(x_i)$, $i=\overline{1,3}$, where x_i, $i=\overline{1,3}$ is the integer value characterizing the selected model of the source Di; and x_4 is the selected expiration time value to activate the source D_3.

Considering that all random variables of the model are distributed according to the exponential laws, the mathematical model of the process of EIRS operation with heterogeneous sources is presented as *a* semi-Markov process with *a* set of system states. The system states are represented by a vector with three components $d=(d_1, d_2, d_3)$, where

$$d_1 = \begin{cases} 1, \text{when } D_1 \text{ works} \\ 0, \text{when } D_1 \text{ is restored} \end{cases} \tag{6a}$$

$$d_2 = \begin{cases} 1, \text{when } D_1 \text{ works} \\ 0, \text{when } D_1 \text{ is restored} \end{cases} \tag{6b}$$

$$d_3 \begin{cases} 0, \text{when } D_3 \text{ is restored,} \\ 1, \text{when } D_3 \text{ operational and in unloaded mode,} \\ 2, \text{when } D_3 \text{ operational and is in standby mode,} \\ 3, \text{when } D_3 \text{ works.} \end{cases} \tag{6c}$$

This is a set of possible states of system D:

$$D=\{(d_1, d_2, d_3)\}=\{(0,0,0); (0,0,2); (0,0,3); (0,1,0);(0,1,2); (0,1,3); (1,0,0); (1,0,1); (1,1,0); (1,1,1)\}.$$

After analyzing the peculiarities of the system functioning, it is proved that:

- the state (0,0,1) of the system is impossible as the restoration of sources D_1, D_2 and D_3 must be in the state (2), in operating state (3), or in restoration state (0);
- the state (0,1,1) of the system is impossible during the restoration of source D_1 the source D_2 is in operating state, and the source D_3 cannot be in unloaded mode (1): the source D_3 must be prepared for activation (2), work (3), or restoration (0);
- the states (1,0,2) and (1,0,3) of the system cannot be considered when the source D_1 is in operating state and the source D_2 is in restoration state (0), the source D_3 cannot be prepared for activation (2) or work (3);
- system states (1,1,2), (1,1,3) are impossible, when the sources D_1 and D_2 are operating, that is, they are in state (1), the source D_3 cannot be prepared for activation (2) or work (3).

The graph of the system transitions from one state to another is represented in the Figure 4.

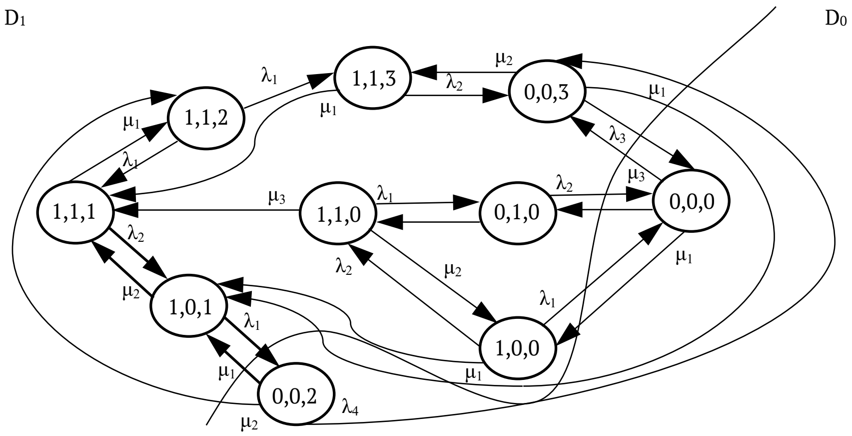

Figure 4. The graph of the system transitions from one state to another in one step

Continuing the analysis of the system functioning, it can be stated that some transitions from one state to another are simply impossible. For instance, only one source may fail at one point of time (therefore the transition is forbidden); the source D_3 may fail if it is activated (therefore the transition   is forbidden), etc.

In terms of system efficiency, the set of states of the system D can be divided into two subsets D_1 and D_0,

$$D=D_1\cdot\cup\cdot D_0,\ D_1\cdot\cap\cdot D\_0=\varnothing, \tag{7}$$

where:

$$D_1=\{(1,1,1);(0,1,2);(1,0,1);(0,1,3);(1,1,0);(0,0,3);(0,1,0);(1,0,0)\}$$

is the set of the system operating states;

$$D_0=\{(0,0,2);(0,0,0)\}$$

is the set of the system disabling states.

To calculate EIRS reliability indices (availability factor, average failure rate, average recovery time), it is necessary to determine:

- average time of the semi-Markov process in all possible states of the system;
- probabilities of transition from a state to the embedded Markov chain;

The average system time in states is as follows:

$$m(1,1,1)\frac{1}{\lambda_1+\lambda_2}, m(0,1,2)=\frac{1}{\lambda_4+\mu_1} \tag{8}$$

$$m(0,0,3)=\frac{1}{\lambda_3+\mu_1+\mu_2}, m(0,1,0)=\frac{1}{\lambda_2+\mu_1+\mu_3}.$$

The matrix of probabilities of transitions in one step of the embedded Markov chain is as follows:

$$P=\|P((d_1, d_2, d_3); (k_1, k, k_3))\|$$

To conclude, it is necessary to choose a source of electricity among a number of possible "candidates" in the structure of EIRS model. However, the types of sources must be selected by the system structure. Generally, one of the two approaches is considered in the formulation of optimization problem (although the others are possible): the first task is to maximize the reliability index; the second task is to minimize the average specific losses of the system operation.

The problem in such definition is considered below.

The problem of optimization is to find the minimum prime cost with a few variables with several constraints. The prime cost of electricity is the most important criterion for evaluation EIRS effectiveness (which was generated by it).

This is the calculation of electricity generation cost:

$$e_{EIRS}=\frac{Z_\Sigma}{W_{EIRS}}=\frac{(w_1B_{11}+w_2B_{22}+w_3B_{33}+...+w_iB_{im})+{}^{E}/_{q}}{W_{EIRS}}=\frac{qB+E}{W_{EIRS}} \tag{9}$$

where: Z_Σ is the total discounted expenses; W_{EIRS} is the average amount of electricity generated by *EIRS*; $B=w_1B_{11}+w_2B_{22}+w_3B_{33}+...+w_iB_{im}$ is a total cost of electricity generation from the sources of the first year of project implementation; E is total operational expenses; q is a rate of return on capital investments; E/q – the operational expenses given by the first year for n years.

The stationary distribution of the embedded Markov chain is found from the system of equations (10).

$$
\begin{gathered}
p(0,0,0)=\frac{\lambda_3}{\lambda_3+\mu_1+\mu_2},\, p(0,0,3)=\frac{\lambda_2}{\lambda_2+\mu_1+\mu_2},p(0,1,0)+\frac{\lambda_1}{\lambda_1+\mu_1+\mu_2}\rho(1,0,0);\\
p(0,0,2)=\frac{\lambda_1}{\lambda_1+\mu_2}\rho(1,0,1);\\
p(0,0,3)=\frac{\mu_3}{\mu_1+\mu_2+\mu_3}\rho(0,0,0)+\frac{\lambda_4}{\lambda_4+\mu_1+\mu_2}\rho(0,0,2)+\frac{\lambda_2}{\lambda_2+\lambda_3+\mu_1}\rho(0,1,3);\\
p(0,1,0)=\frac{\mu_2}{\mu_1+\mu_2+\mu_3}\rho(0,0,0)+\frac{\lambda_3}{\lambda_2+\mu_3+\mu_1}\rho(0,1,3)+\frac{\lambda_1}{\lambda_1+\lambda_2+\mu_3}\rho(1,1,0);\\
p(0,1,2)=\frac{\mu_2}{\lambda_4+\mu_1+\mu_2}\rho(0,0,2)+\frac{\lambda_1}{\lambda_1+\lambda_2}\cdot p(1,1,1)\\
p(0,1,3)=\frac{\mu_2}{\lambda_3+\mu_1+\mu_2}\rho(0,0,3)+\frac{\mu_3}{\lambda_2+\mu_1+\mu_3}\rho(0,1,0)+\frac{\lambda_4}{\lambda_4+\mu_1}\rho(0,1,2);\\
p(1,0,0)=\frac{\mu_1}{\mu_1+\mu_2+\mu_3}\rho(0,0,0)+\frac{\lambda_2}{\lambda_1+\lambda_2+\mu_3}\rho(1,1,0)\\
p(1,0,1)=\frac{\mu_1}{\lambda_4+\mu_1+\mu_3}\rho(0,0,2)+\frac{\mu_1}{\lambda_3+\mu_1+\mu_2}\rho(0,0,3)+\frac{\mu_3}{\lambda_1+\mu_2+\mu_3}\rho(1,0,0)\frac{\lambda_2}{\lambda_1+\mu_2}\rho(1,1,1);\\
p(1,1,0)=\frac{\mu_1}{\lambda_2+\mu_1+\mu_3}\rho(0,1,0)+\frac{\mu_2}{\lambda_1+\mu_2+\mu_3}\rho(1,0,0)\\
p(1,1,1)=\frac{\mu_1}{\lambda_4+\mu_1}\rho(0,1,2)+\frac{\mu_1}{\lambda_3+\lambda_3+\mu_1}\rho(0,1,3)+\frac{\mu_2}{\lambda_1+\mu_2}\rho(1,0,1)+\frac{\mu_3}{\lambda_1+\lambda_2+\mu_3}\rho(1,1,0).
\end{gathered}
\tag{10}
$$

Considering the above mentioned facts, it is important to solve two simulation optimization problems [20]:

1. To find the structures and algorithms of EIRS allowing the average specific costs of the EIRS electricity generation with the failure source R_1 attaining a minimum $C \to min$, under constraints imposed on system reliability. Herewith, the availability factor K_A (operative availability K_{OA}) should not be less than a normalized value $K_A (K_A > K)$.

2. To find such structures and algorithms of EIRS, allowing the availability factor of the system to achieve the maximum $K_A \to max$ by limiting the average specific costs of the EIRS for electricity generation. It should not be more than the preset value.

3. Further research will focus on the study of structures and algorithms of EIRS with RES (Fig. 5).

The software algorithm consists of three stages, the procedure and the content represented graphically in the Figure 5.

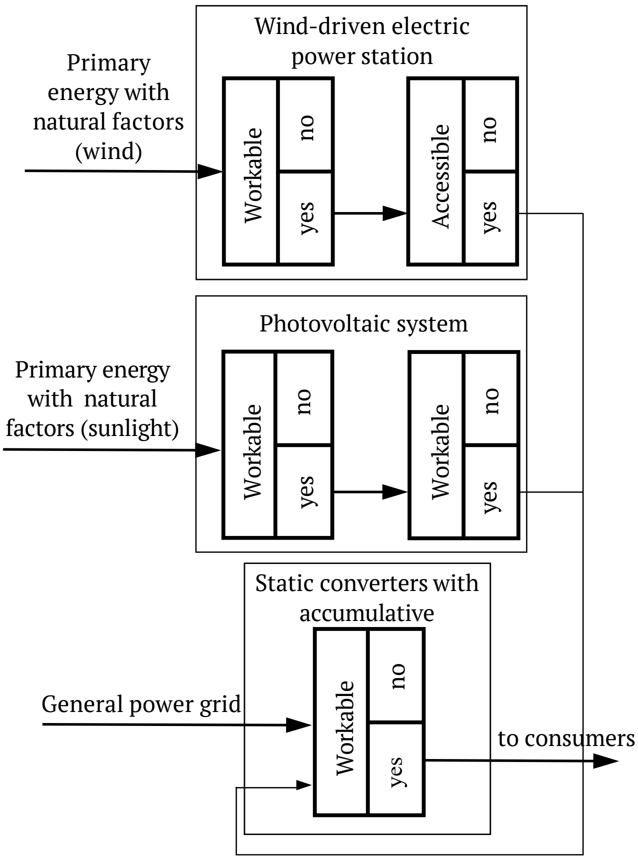

Figure 5. The structure and algorithms of EIRS operation

In the Figure 6, it is shown the algorithm of EIRS functioning through the simulation modeling with GPSS [18]. The study was performed within the following stages:

- development of a conceptual model;
- design and implementation of a simulation model software;
- checking the model adequacy;
- reliability evaluation of simulation results;
- planning and carrying out the experiment.

The adequacy of mathematical models of real system depends on the reliability of probability of distribution determination of random variables that describe the process of EIRS elements [21].

From a mathematical perspective, two procedures are important: solving the systems of linear algebraic equations and the procedure for generating the random variables (given in advance by the distribution functions of random variables) [12]. The Gaussian method is used to solve the systems of linear algebraic equations after eliminating the linear dependence of the equations [12]. As for the random variable generation procedure, the use of random variables lies in the basis of simulation modeling method. It is necessary to generate random variables with given distribution laws [12]. The inverse function method is used, which is based on the following statement of probability theory [12]. For example, $F(x)$ – a distribution function, and R – a random variable uniformly distributed in the interval [0, 1]. Then the random variable $X=F^{-1}$ – will have a distribution function $F(x)$:

$$P(X \leqslant x)=P(r \leqslant F(x))=\int_0^{F(x)} f(r)dr=F(x). \qquad (11)$$

The sequence of random numbers r_1, r_2, r_3... is converted into a sequence x_1, x_2, x_3..., which has a given law $F(x)$ (distribution density function $f(x)$. The general algorithm for modeling the random continuous variables with a given probability distribution function follows from this: a random number is generated $r_i \in [0\ 1]$; a random number is calculated $x_i=F^{-1}(r_i)$.

$F^{-1}(r_i)$F^(-1) (r_i), it is used a piecewise linear approximation of the corresponding continuous functions [21]. To obtain the function of normal distribution of a random variable X with mathematical expectation $m_x \neq 0$, the square deviation $\sigma_x \neq 1$ calculation is as follows:

$$X=m_x+\sigma_x Z, \qquad (12)$$

Z – a random variable with a standard normal distribution function, for which the function has been approximated $F^{-1}(z)$.

To specify other laws (non-exponential, non-uniform, and non-normal), special programs are used. It is allowed to perform the numerically tabulation of inverse functions, that is, to calculate the necessary values of the points of piecewise linear approximation functions.

This simulation does not impose restrictions on the types of the used probability distributions of random variables.

There is a problem of probabilistic description of the random processes with an incomplete statistical information (there are no reliable data of the energy potential of wind and sun and the principles of their distribution). It leads to significant errors in the simulation.

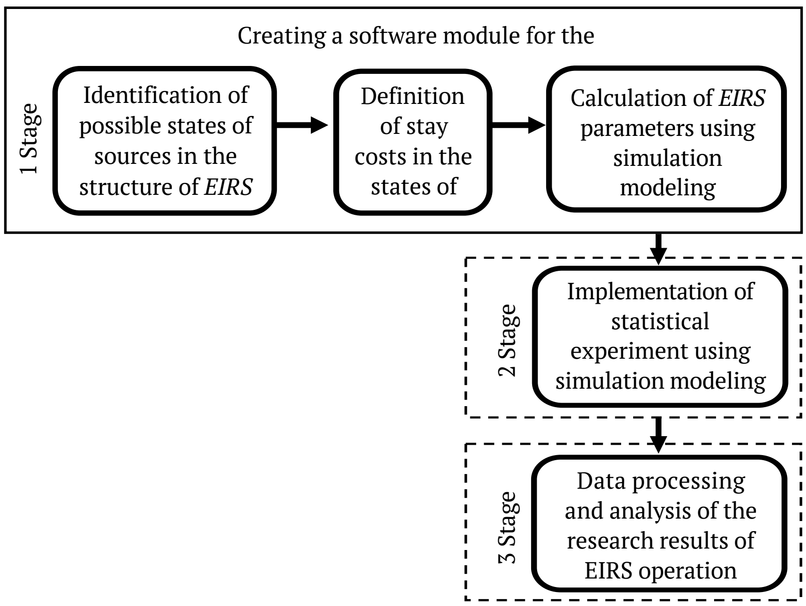

Figure 6. The operating algorithm of the software for researching EIRS using simulation modeling with GPSS

This is a solution to this problem: to determine the probability of a sufficient daily supply of wind or solar energy potential for Wind-driven electric power station (WEPS) and Photovoltaic station (PS), determined for a specific area. In the Table 1, it is shown the results of analytical solution and simulation modeling for some of 75 variants of the EIRS structures.

Table 1. The results of analytical solution and simulation modeling for some of 75 variants of the EIRS structures

Serial number of variant	Serial number of source (model series of source)		Specific cost of EIRS electricity, $		Error (%)
	R_2	R_3	The result of analytical solution	The result of simulation	
1	1	1	4.3084	4.2528	1.29
...	...	...	...	...	...
16	2	1	3.4453	3.5126	1.95
...	...	...	...	...	...
46	4	1	2.1530	2.2074	2.52
...	...	...	...	...	...
61	5	1	1.4255	1.4569	2.20
...	...	...	...	...	...
75	5	15	1.4149	1.4256	0.76

The research result of this work is the development of a method for the reliability management and functional analysis of systems of this class at the stage of preliminary design for solving the optimization problem, considering the specific cost of electricity. Moreover, this approach allows developing control algorithms for such systems, considering the power consumption levels of a local object.

Thus, the description of these sources as a scheme of reliability and functioning can be represented as a series of connections of two hypothetical elements (the EIRS structure with a set of sources is shown in the Figure 5). Using simulation results, it is shown that the system components are characterized by the period between failures, restoration time, cost of unit of electricity generation, specific losses due to power failure. The probabilities of availability of energy natural factors are added for WEPS and PS (throughout the year, the source ones are supplemented with delay time for activation). Every time, the parameters are described by the distribution of random variables.

EIRS, as a stochastic system, cannot be described by analytical mathematical models. In the further research, it is suggested to apply the method of simulation modeling. The simulation model and algorithms of functioning of autonomous systems with renewable energy sources are developed. The proposed approach provides for the use of probabilistic model of availability for renewable sources, which allows evaluating the reliability and efficiency of the system, given that it is impossible to obtain them analytically.

Based on the analysis of simulation results of 75 investigated variants of the system structure (Table 1), it has been found that the use of renweable sourse leads to a reduction in the cost of electricity. At the same time, the formation of energy balance by increasing the share of renweable sourse leads to an increase in the efficiency of EIRS by more than 13%.

Finally, it is important to emphasize that EIRS structures are characterized by a set of possible states of each element of the system, the set of possible states of the system and matrix of transition probabilities (transition graph).

The results obtained can be used to develop a methodology for determining the economic efficiency with implementation of local energy systems. Reliability-cost indicators can be additional indicators of investment efficiency of long-term projects, based on the projected total volume of electricity generation, as shown in the figure [5]. The principles and approaches for evaluating the effectiveness of investments and adapted for transitional market economies are the basis of the development of technical and economic indicators [20-22]. It is proved that the projection of island microgrid systems with renewable sources is possible with two compromise approaches to determining investment efficiency indicators: deterministic levels of power supply reliability and cost of electricity. The first approach is based on the calculation of present value of EIRS implementation, which includes all costs for n years of project implementation; the second one – on obtaining a specific indicator – the reduced cost of electricity at the beginning of investment project, based on the projected total volume of electricity generation and analysis of structural implementation in terms of its economic efficiency – comparing NPV (Net Present Value) with possible losses (loss of profits) in the interruptions in energy supply during the project.

CONCLUSIONS

On the basis of Markov model and simulation model of EIRS functioning with two dissimilar sources through the computational experiments, the evolution of the prime cost of electricity was developed and its dependence on the structural composition and algorithms for sources operation was proved. To obtain these results, the probabilistic method was used for modeling the availability energy potential of renewable sources. It is obvious that the prime cost of electricity is sensitive to the availability factor, which depends on the structure of EIRS. EIRS availability indexes (in particular availability factor) can vary in all structural variants of EIRS.

The prime cost of electricity varies widely from $1.42 to $4.31 per kWh throughout the simulation interval, and it is particularly sensitive to the reliability of the main source. The analysis of simulation results shows that the structural-algorithmic implementation of the EIRS using RES allows (at the pre-design stage) ensuring the given (directive-defined) levels of power supply reliability with restrictions on capital costs, and reaching the economically advantageous levels of cost of electricity, which will allow reducing the payback period of such systems by 18-20 months.

Further research related to the justification of choice of the model series, first of all, the installed generating capacities of traditional and renewable sources in the structure of EIRS and the improvement of analytical model of the reliability-cost analysis of microgrid system with the possibility of forecasting the generation levels of renewable sources in real time.

ACKNOWLEDGEMENT

This work was supported by the Ministry of Education and Science of Ukraine (№ 0120U102155).

REFERENCES

[1] Valenciaga, F., & Puleston, P.F. (2005). Supervisor control for a stand-alone hybrid generation system using wind and photovoltaic energy. *IEEE Transactions on Energy Conversion*, 20(2), 398-405.
[2] Mao, M., Jin, P., Hatziargyriou, N.D., & Chang, L. (2014). Multiagent-based hybrid energy management system for microgrids. *IEEE Transactions on Energy Conversion*, 5(3), 938-946.
[3] Kaplun, V., & Osypenko, V. (2019). About using electricity pricing for smart grid dynamic management with renewable sources. *IEEE International Conference on Energy Smart Systems (ESS)*, 2019, 256-261.
[4] Reddey, J.B., & Reddy, D.N. (2008). Probablistic performance assessment of a roof top wind, solar photo voltaic hybrid energy system. *Engineering Science & Education Journal*, 2(4), 281-298.
[5] Cecati, C., Citro, C., Piccolo, A., & Siano, P. (2011). Smart operation of wind turbines and diesel generators according to economic criteria. *IEEE Transactions on Industrial Electronics*, 58(10), 4514-4525.
[6] Choi, D., Kim, H., Won, D., & Kim, S. (2009). Advanced key management architecture for secure SCADA communications. *IEEE Transactions on Power Delivery*, 24(3), 1154-1163.
[7] Georgilakis, P. (2008). Technical challenges associated with the integration of wind power into power systems. *Renewable and Sustainable Energy Reviews*, 12, 852-863.
[8] Kondoh, J., Ishii, I., Yamaguchi, H., Murata, A., Otani, K., & Sakuta, K. (2000). Electrical energy storage systems for energy networks. *Energy Conversion and Management*, 41, 1863-1874.
[9] Deshmukh, M.K., & Deshmukh, S.S. (2008). Modeling of hybrid renewable energy systems. *Renewable and Sustainable Energy Reviews*, 12, 235-249.
[10] Roozbehani, M., Dahleh, M.A., & Mitter, S.K. (2011). *Volatility of power grids under real-time pricing*. Retrieved from https://arxiv.org/pdf/1106.1401.pdf.
[11] Osypenko V., & Kaplun V. (2017). About the intelligent decision making system for dynamic electricity pricing on renewable microgrids. In *Proceedings of the 9-th International Workshop on Inductive Modeling* (IWIM-2017) (pp. 348-350). Lviv: Lviv National Polytechnic University.
[12] Gross, J., & Yellen, J. (1999). *Graph theory and its applications*. Boca Raton: Chapman and Hall.
[13] Korolyuk, V.S., Brodi, S.M., & Turbin, A.F. (1975). Semi-Markov processes and their applications. *Journal of Soviet Mathematics*, 4(3), 244-280.
[14] Zbirko, M.D., Kuznetsov, V.N., & Turbin, A.F. (1980). On a semi-Markov model for reliability analysis of a system with restorable protection. *Automation Remote Control*, 41(6), 879-887.
[15] Mohsenian-Rad, A.-H., & Leon-Garcia, A. (2010). Optimal residential load control with price prediction in real-time electricity pricing environments. *IEEE Transactions on Smart Grid*, 1(2), 120-133.
[16] Ivakhnenko, G. (1971). Polynomial theory of complex system. *IEEE Transaction on Systems, Man and Cybernetics*, 1(4), 364-378.
[17] Holland, J., & Arbor, A. (1975). *Adaptation in natural and artificial systems*. Ann Arbor: The University of Michigan Press.
[18] Farlow, S.J. (1984). *Self-organizing methods in modeling: GMDH type algorithms*. Basel: Marcel Decker Inc.
[19] Zhao, Z., Lee, W.C., Shin, Y., Member, S., & Song, K. (2013). An optimal power scheduling method for demand response in home energy management system. *IEEE Transactions on Smart Grid*, 4(3), 1391-1400. doi: 10.1109/TSG.2013.2251018.
[20] Feroldi, D., & Zumoffen, D. (2014). Sizing methodology for hybrid systems based on multiple renewable power sources integrated to the energy management strategy. *International Journal of Hydrogen Energy*, 39(16), 8609-8620.
[21] Haddadian H., & Noroozian R. (2017). Multi-microgrids approach for design and operation of future distribution networks based on novel technical indices. *Applied Energy*, 185(1), 650-663.
[22] Ostanin, V. (2022). Effects of repulsion and attraction between rotating cylinders in fluids. *Scientific Herald of Uzhhorod University. Series "Physics"*, 51, 39-47.

Віктор Володимирович Каплун
Доктор технічних наук, професор
Національний університет біоресурсів і природокористування України
03041, вул. Героїв Оборони, 15, м. Київ, Україна
https://orcid.org/0000-0001-7040-9344
Володимир Васильович Осипенко
Доктор технічних наук, професор
Київський національний університет технологій та дизайну
01011, вул. Немировича-Данченка, 2, м. Київ, Україна
https://orcid.org/0000-0002-1077-1461
Світлана Сергіївна Макаревич
Кандидат технічних наук, доцент
Національний університет біоресурсів і природокористування України
03041, вул. Героїв Оборони, 15, м. Київ, Україна
https://orcid.org/0000-0002-9601-5156

Прогнозування ціноутворення на електроенергію енергетичних островів з відновлюваними джерелами

Анотація. Стратегія розвитку локальних енергосистем малої потужності передбачає використання декількох джерел. Ефективність функціонування таких систем залежить від цілеспрямованого управління надійністю і базується на раціональних ієрархічних взаємозв'язках їх структурних складових. Узгодження структури різнорідних джерел та їх участі у формуванні енергетичного балансу мікроенергетичних систем в умовах динамічного розвитку відновлюваної енергетики є актуальним науковим завданням. Метою дослідження було розроблення методу надійнісно-вартісної оптимізації структур мікроенергосистем з різнорідними джерелами, в основу якого покладено використання показників надійності та собівартості електроенергії. Проведені дослідження ґрунтуються на сучасних методах прикладного статистичного аналізу, теорії надійності, синтезу комплексних багатоагрегатних систем. Шляхом реалізації марковської моделі та імітаційного моделювання функціонування джерел одержані умови оптимального формування енергетичного балансу мікроенергосистеми з найменшою вартістю електроенергії та урахуванням показників надійності. Обчислювальні експерименти дозволили одержати закономірності еволюції вартості електроенергії та показати її залежність від структури та алгоритмів функціонування джерел. Шляхом використання ймовірнісного методу моделювання вперше доведено, що собівартість електроенергії чутлива до коефіцієнта доступності відновлюваних джерел до первинної енергії. Практичне застосування результатів полягає в підвищення ефективності енергетичних островів шляхом структурно-алгоритмічної оптимізації різнорідних джерел (традиційних та відновлюваних) на основі визначення собівартості електроенергії

Ключові слова: різнорідні джерела електроенергії; надійнісно-вартісний аналіз; марківська модель; імітаційне моделювання; ефективність мікронергосистем

Machinery & Energetics
Vol. 13, No. 4. 2022

Journal homepage:
https://technicalscience.com.ua/en

UDC 621.867.42
DOI: 10.31548/machenergy.13(4).2022.48-59

Mykola Klendii*

PhD in Technical Sciences, Associate Professor
Separated Subdivision of National University of Life and Environmental Sciences of Ukraine
"Berezhany Agrotechnical Institute"
47501, 20 Academichna Str., Berezhany, Ternopil region, Ukraine
https://orcid.org/0000-0001-8271-5381

Ivan Lohush

PhD in Technical Sciences, Associate Professor
Separated Subdivision of National University of Life and Environmental Sciences of Ukraine
"Berezhany Agrotechnical Institute"
47501, 20 Academichna Str., Berezhany, Ternopil region, Ukraine
https://orcid.org/0000-0001-5075-1054

Andrii Drahan

PhD in Technical Sciences
Separated Subdivision of National University of Life and Environmental Sciences of Ukraine
"Berezhany Agrotechnical Institute"
47501, 20 Academichna Str., Berezhany, Ternopil region, Ukraine
https://orcid.org/0000-0001-7195-1127

Igor Chvartatskiy

PhD in Technical Sciences, Associate Professor
Separated Subdivision of National University of Life and Environmental Sciences of Ukraine
"Berezhany Agrotechnical Institute"
47501, 20 Academichna Str., Berezhany, Ternopil region, Ukraine
https://orcid.org/0000-0001-5689-4603

Andrii Hrabar

Separated Subdivision of National University of Life and Environmental Sciences of Ukraine
"Berezhany Agrotechnical Institute"
47501, 20 Academichna Str., Berezhany, Ternopil region, Ukraine
https://orcid.org/0000-0001-8208-6212

Justification and calculation of structural-power parametersof screw loaders

Abstract. Existing designs of screw working bodies of transport and processing machines cannot always provide the required performance and avoid overloading, which causes deformation and damage to parts of the mechanisms. Thus, it is necessary to establish new efficient screw working bodies that would ensure the execution of the technological process. The purpose of the study was to substantiate and explore the design and methodology for calculating the main structural-power parameters of the developed screw loader, to synthesise screw loaders using the method of morphological analysis to obtain designs of mechanisms with better technical and economic characteristics.

Article's History: Received: 14.06.2022; Revised: 25.10.2022; Accepted: 23.11.2022.

Suggested Citation:
Klendii, M., Lohush, I., Drahan, A., Chvartatskiy, I., & Hrabar, A. (2022). Justification and calculation of structural-power parameters of screw loaders. *Machinery & Energetics,* 13(4), 48-59.

*Corresponding author

The methods of surface theory, analytical and differential geometry, computer graphics and mathematics were used to conduct the research. As a result of theoretical and experimental studies, the designs of screw conveyors with hopper loading and screw conveyors with nozzle loading are presented. In addition, a classification of loaders for screw transport and technological mechanisms is presented. The dependencies for calculating the design of screw conveyor loaders are determined. The synthesis of loaders and mixers by the method of morphological analysis was performed to obtain designs of mechanisms with the best technical and economic characteristics and competitive designs of mechanisms were established. A system of coding and synthesis of structural elements and mechanisms of screw implements with improved technological properties is proposed, and competitive designs of screw implement that perform technological processes efficiently and effectively are selected. A methodology for calculating the main structural and power parameters of a screw loader has been developed, which allows for determining the parameters of a screw loader. The materials of the research can be used in further studies of screw conveyors and, in particular, screw loaders to determine their design, technological, energy and power parameters

Keywords: screw conveyor; nozzle; transport and technological mechanism; structural elements; structural synthesis; morphological analysis; calculation method

INTRODUCTION

One of the most significant criteria for the operation of screw conveyors is the productivity of the transport-technological machine, which must be ensured with minimal energy consumption. Thus, to efficiently perform the technological process of reloading bulk materials using transport-technological machines in the form of screw conveyors, it is necessary to ensure their rational loading. In addition, note that screw conveyors can be loaded with hoppers, nozzles and loading devices.

The issues of theoretical design of screw reloading mechanisms with flexible lines and methods of designing and calculating their parameters, development of efficient designs of screw conveyors for transporting bulk materials along curved routes are discussed in [1; 2], and the issues of synthesis of machine structures by morphological analysis are discussed in [3] etc. Particular attention should be paid to the coverage in the literature of the issues of calculation and selection of parameters of screw working bodies and transportation of grain materials, mineral fertilisers and other bulk agricultural materials by screw conveyors [4; 5; 6] since the problem of injury to materials during the transportation is open.

The design calculations of mechanisms with screw working bodies are covered in many scientific works, in particular [7-9] and many others, but the presented calculations of each mechanism or part have their specifics since each of the given structures is characterised by the presence of certain structural details that affect the nature of their operation and operation. In addition, in [10; 11], studies were conducted on the development of working bodies for flexible screw conveyor lines, which significantly increase their length and expand technological capabilities.

The issues of exploring the functional, operational, and resource characteristics of screw conveyors in their interaction with agricultural materials are discussed in [12; 13]. The study of the movement of particles of agricultural materials by the screw surfaces of the working bodies of conveyors is devoted to [14; 15]. Works [16; 17] substantiate the design, kinematic and technological parameters of screw working bodies by considering their functional purpose. The possibility of using a helical surface for the manufacture of conveyor working bodies was considered in [18]. The theoretical foundations of the design and construction of linear screw surfaces are presented in [7; 19]. Research [20] justify using a helical surface in conveyor working bodies and reloading nozzles, and research [21] explored the injury of grain material by a screw conveyor working body. Works [22; 23] justify using elastic working bodies to minimise damage to grain material when it is overloaded by screw conveyors.

However, the known designs of the working bodies of screw conveyors do not fully satisfy the operational requirements, and therefore the task of developing new designs of working bodies of screw conveyors and justifying their competitive design and technological parameters that could provide better performance while reducing material consumption and simplifying the design is relevant.

The purpose of the research – justification, design of elements of screw conveyors, development of a methodology for calculating the main structural-power parameters of a screw loader and synthesis of screw loaders.

MATERIALS AND METHODS

The mathematical modelling of the processes of movement of bulk materials is described using the laws and postulates of analytical geometry, differential mathematics, theoretical and applied mechanics, surface theory and computer graphics systems. The study was conducted using the method of morphological analysis, elements of the theory of experiment, methods of mathematical statistics and mathematical methods of optimal experiment planning. The analysis of the results of the presented research was performed using applied computer programmes, in particular Excel, Word, and SolidWorks, and was conducted according to standard and developed methods, in particular, the methodology for systematisation and classification of research results, their analysis, preparation of tables and graphs reflecting the results of research, calculation of errors, literature analysis, modelling, experimentation, and work experience that require research.

The methods of morphological analysis and synthesis were used to effectively search for new constructive solutions since they are the most common methods for establishing new designs of mechanisms that use elements of classification and systematisation. Morphological analysis means that a specific number of the most characteristic functional or structural morphological features are identified for a given product, which allows for specific search options for these characteristic features. In the course of the analysis, a list of specific variants of particular designs is determined for each morphological feature. All defined variants of morphological traits are compiled in the form of a so-called morphological table or "matrix". The term "morphological" can be explained by the fact that variants of constructive features are defined by the letters of the Ukrainian alphabet. By designing random combinations of variants, new design options can be discovered that might be missed by simple searching. The search for the most appropriate variants of mechanism designs should be conducted using computer software (electronic computers). The method of morphological analysis uses elements of combinatorics, i.e. a systematic study of all theoretically possible variants of constructive schemes that arise from the specific patterns of construction of the mechanism considered. The synthesis of these mechanisms involves both well-known and new, unusual design options. The method of morphological analysis has several varieties and is designed to overcome bias in existing opinions about the possibility and ways of solving a problem. It allows the task to be described and analysed using a set of all possible structural (i.e. morphological) relationships and relationships between its elements. Before conducting a morphological analysis, morphological tables or graphs should be developed and compiled. Using the method of morphological analysis does not result in new or original ideas, but it does provide an opportunity to find new combinations of known structural parts. Therefore, it is advisable to use it when a mechanism or product consists of several structural parts. The classification of structures allows for faster and more accurate orientation in a large number of terms and factors, and therefore morphological analysis is based on classification.

RESULTS AND DISCUSSION

The functional purpose of screw conveyor hoppers is to accumulate, store and ship bulk material for a short period to the discharge line of screw conveyors, provided that the screw working body is not overloaded. The shape of the hoppers of screw conveyors can be square, rectangular, round, etc. The purpose of the nozzles for screw conveyors is to insert the screw spiral into the bulk material without deformation and to perform productive loading of the screw conveyor casing while preventing the phenomenon of technological overload and breakage of the working bodies. Nozzles for screw conveyors are available with adjustable openings or with permanent openings. Loading mechanisms are used to transfer bulk materials from flat surfaces and containers to screw conveyors by delivering them to the working body. The loading devices are divided into two types: for loading the conveyor with materials that spill out of containers and for picking up loose materials from flat surfaces and moving them into the conveyor.

Figure 1 demonstrates a typical screw conveyor equipped with a hopper load, which is described in detail in [24].

a)  b) c)

Figure 1. Hopper-fed screw conveyors: a) tractor PTO drive; b) and c) mobile screw conveyors

Figure 2 demonstrates screw conveyors with rigid and flexible shafts, in which the loading is performed using nozzles. All of them do not provide a process for regulating the loading of the lines, which can result in the overloading of the screw conveyors caused by the process.

a) 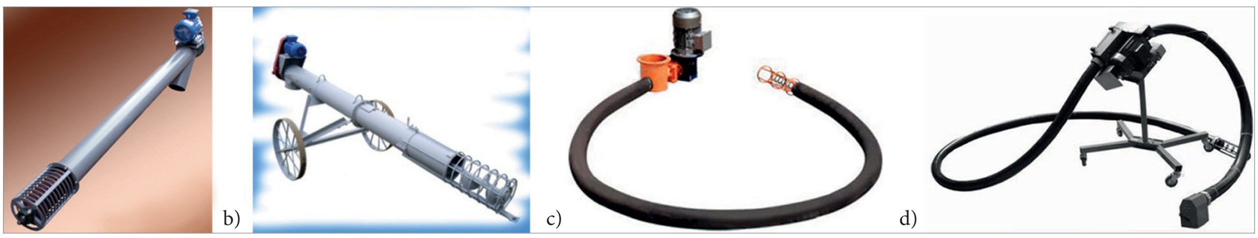 b) c) d)

Figure 2. Screw conveyors with nozzles for loading: a) manufactured by PJSC "Elevator Equipment Plant"; b) manufactured by LLC "Promstroykomplekt"; c) manufactured by LLC "TechResource"; d) manufactured by LLC TD "BMZ"

The transport-technological machines presented in Figures 3a-3g, it is possible to load conveyors with bulk materials from flat surfaces, and Figures 3e-3f presents wagon unloaders with screw working bodies.

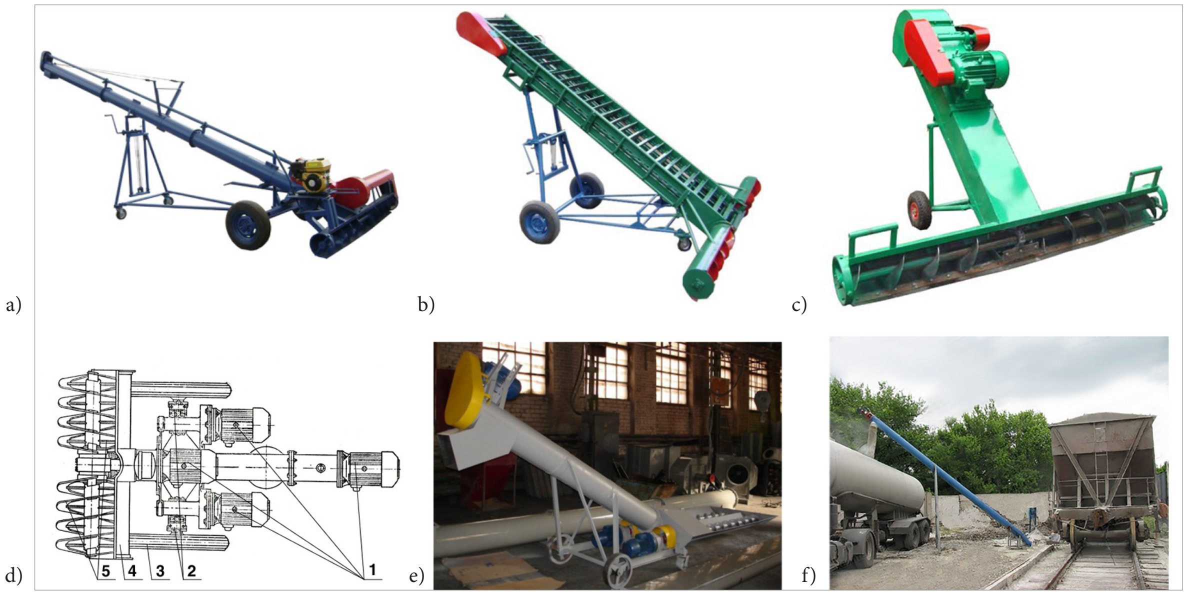

Figure 3. Loading mechanisms: a) auger loader; b) scraper-screw conveyor; c) auger working body for picking up bulk materials; d) auger pick-up trolley; e) screw wagon unloader; f) screw wagon unloader

To ensure the reliable and productive operation of screw conveyors and prevent their damage, which can be both accidental and as a result of the technological process, it is, therefore, necessary to use regulatory and protective mechanisms. For example, in screw conveyors, which are loaded through a hopper or nozzle, it is necessary to use regulating mechanisms in addition to protective grids, which can ensure that a specific volume of material enters the main line per unit of time.

It will ensure optimum loading of the main lines and maximum productivity when transporting various materials. In addition, for screw conveyors that are loaded with a nozzle, safety devices can be used to stop the loading of the main line if foreign material enters the nozzle, which can cause damage to the screw working body. It is difficult to ensure the optimum amount of material loaded in conveyors that have loading devices, therefore, their transport lines must be designed for maximum loading. In addition, loading mechanisms must be equipped with safety clutches. The classification of loaders of screw transport and technological mechanisms by design features is presented in Figure 4 [24].

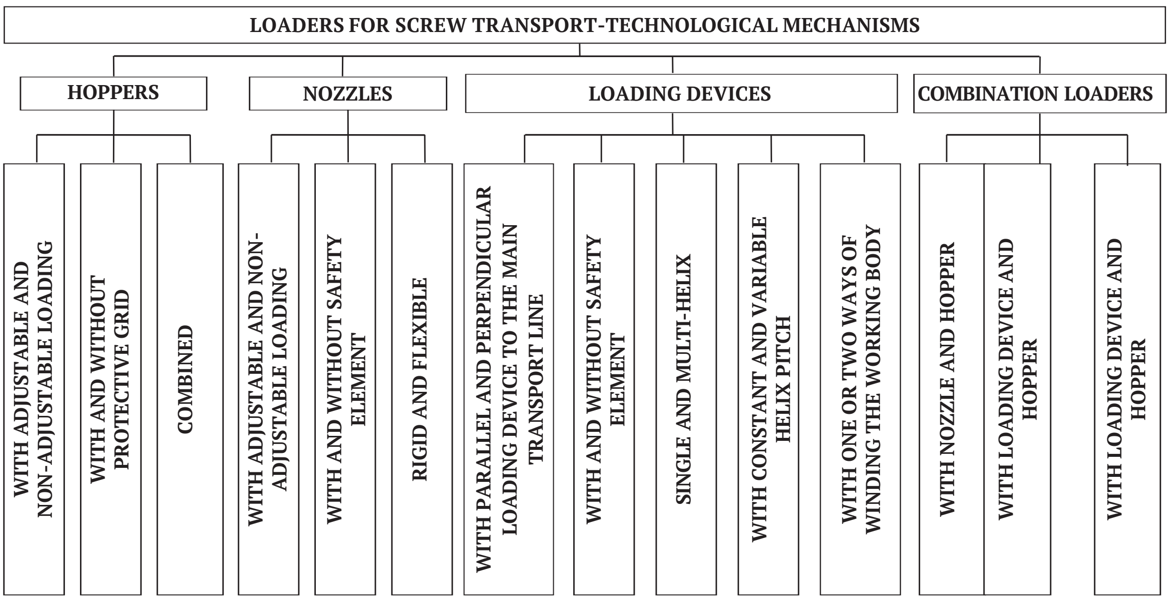

Figure 4. Classification of loaders of screw transport-technological mechanisms by design features
Source: developed by the authors based on [24]

Based on the above and considering the fact that the issue of material flow through the hopper gates has been thoroughly explored [25], it is necessary to address the problem of developing and researching screw conveyor nozzles that will ensure a regulated process of loading the main lines.

Loading and protective nozzles have been established for screw conveyors, the designs of which are presented in Figure 5 [24]. The design of the self-loading nozzle, presented in Figure 5a, protects the working body from deformation, and the presence of holes allows the transported material to penetrate it.

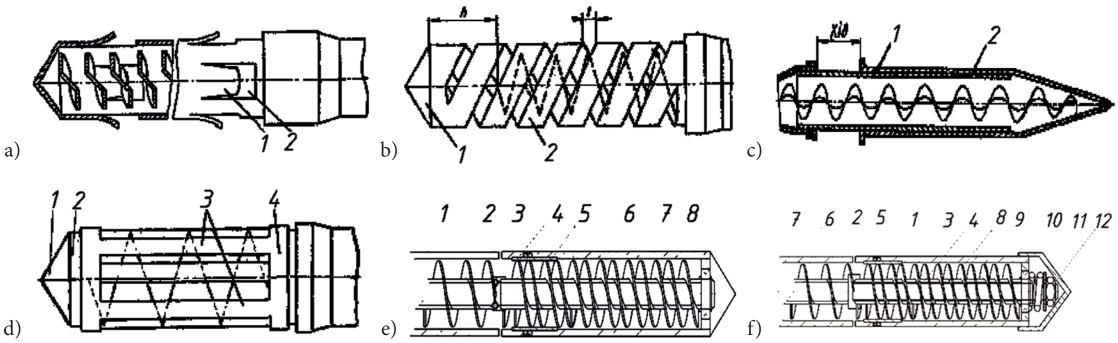

Figure 5. Designs of loading-protective nozzles for screw conveyors
Source: developed by the authors based on [24]

When the self-loading nozzle (Fig. 5b) is inserted into the bulk material, only the coils of the cylindrical spring 2 are deformed, not the auger working body. At the end of the injection process, spring 2 returns to its original position and moves the bulk material into the nozzle.

In the self-loading nozzle of screw conveyors (Fig. 5c), after insertion into the bulk material, the tip of the nozzle rests on the casing, and its petals open and allow the bulk material to penetrate the casing.

Figure 5d demonstrates a nozzle that can adjust the size of the material passage holes, which can ensure rational loading and compliance with the established standards for the transport process.

If foreign objects get into the nozzle presented in Figure 5e, which can cause damage to the working body, the western screw 5 of the nozzle stops and disconnects it from the screw of the retracting line using the balls 2 exiting the holes made on the line shaft 1 due to their axial displacement and deformation of the springs 3.

When foreign objects enter the nozzle presented in Figure 5f through the technological holes, which can cause damage to the screw working body, the 3-way screw of the safety nozzle stops and disconnects it from the working body of the transport line due to the axial displacement of the nozzle shaft and compression of the spring.

It has been established that to ensure the technological process of transporting by screw conveyors with retracting lines, it is necessary to determine the rational values of the dimensions of the holes for the passage of bulk material of nozzles. The capacity of a screw conveyor can be calculated using the formula:

$$Q=0{,}25\cdot\pi\cdot\varphi\cdot V_n\cdot(D^2-d), \qquad (1)$$

where D – diameter of the casing; d – diameter of the shaft of the working body; V_n – axial speed of movement of the load in the casing; φ – coefficient of filling the inter-turn space.

The reloading capacity must be equal to the bulk material loading capacity. If the bulk material is loaded through the nozzle, the capacity of the screw conveyor can be determined by the following equation:

$$Q=k\cdot F\cdot n\cdot V_z, \qquad (2)$$

where F – area of one hole; n – number of holes; V_z – the material filling rate; k – loading factor of the screw conveyor, k=0.7...0.5.

The rate of cargo spillage through the hole is determined by the formula [26]:

$$V=\lambda\cdot\sqrt{3.2\cdot g\cdot RR}, \qquad (3)$$

where λ – the coefficient of the passage of bulk material; R – the reduced radius of the conveyor outlet (the ratio of the outlet area to the perimeter of the outlet); g – the acceleration of free fall.

If the appropriate transformations are made, the following dependence is used to determine the size of the radius of the loading hole:

$$R=\sqrt[5]{\frac{\varphi^2\cdot V_n^2\cdot(D^2-d^2)}{25{,}6\cdot k^2\cdot n^2\cdot\lambda^2\cdot g}}. \qquad (4)$$

In addition, the width of the rectangular loading opening can be determined from the dependency:

$$l=\frac{\pi}{a}\left[\frac{\varphi^2\cdot V_n^2\cdot(D^2-d^2)}{25{,}6\cdot k^2\cdot n^2\cdot\lambda^2\cdot g}\right]^{\frac{-}{5}}. \qquad (5)$$

Using these dependencies, it is possible to determine the required design dimensions of the loading holes of the screw conveyor nozzles and obtain the maximum productivity of screw conveyors for the transport of bulk materials.

When developing progressive designs of screw conveyors with flexible working bodies, it is advisable to use the method of morphological analysis [27], which allows for obtaining a solution to the problem: obtaining the most rational and economical design solutions for establishing new mechanisms and their working bodies. Using the method of structural and schematic synthesis and morphological analysis [24], the constituent elements and the links between them were identified and a morphological matrix was compiled in the form of Table 1.

Table 1. Morphological table of features of structural elements of a flexible screw conveyor

Conveyor drive			Screw working body						Loading mechanism	
			Screw construction							
1. View	2. Type of movement	3. Quantity	4. Spiral profile	5. Partial	6. Solid	7. Spiral combination	8. Connection design	9. Gutter construction	10. Process	11. Type
1.1. Electric drive 1.2. Pneumatic drive 1.3. Internal combustion engine 1.4. Hydraulic drive	2.1. Continuous 2.2. Cyclic 2.3. With accelerations and decelerations	3.1. One 3.2. Two 3.3. Several	4.1. Narrowband 4.2. Wideband 4.3. Corrugated 4.4. L-shaped or inclined 4.5. Blade 4.6. With cut-outs or openings 4.7. Spring	5.1. Gimbal 5.2. Hinged 5.3. Sectional	6.1. Bulkhead 6.2. With flexible simple shaft 6.3. With flexible folding shaft	7.1. Single-type 7.2. Combined	8.1. Toothed 8.2. Riveting 8.3. Welded 8.4. Bolted 8.5. Finger 8.6. With internal section connection 8.7. With external section connection 8.8. With internal and external section connection 8.9. Elliptic 8.10. Ball	9.1. Solid 9.2. Sectional	10.1. Gravitational 10.2. orced 10.3. Separate 10.4. With calibration 10.5. With shredding 10.5. With additional technical operations 10.6. Multilink	11.1. Hopper 11.2. Nozzle 11.3. Loading device

Source: developed by the authors based on [24]

The main morphological features of screw conveyors have presented: types of drive, types of screw working bodies, designs of loading mechanisms, types of screw conveyor arrangement, and types of unloading mechanisms. The morphological model of spiral conveyors, which is presented in Table 1 [24], can be recorded by a morphological matrix, which was established by the method of designating the numbers of codes of the corresponding alternative designs, which are placed in the columns of the developed morphological table:

$$N = K_1 \cdot K_2 \cdot K_3 \cdot \ldots \cdot K_j = \prod_{j=1}^{n} K_j, \tag{6}$$

$$N_{\text{ГГК}} = \begin{vmatrix} 1.1 & & \\ 1.2 & 2.1 & 3.1 \\ 1.3 & 2.2 & 3.2 \\ 1.4 & 2.3 & 3.3 \end{vmatrix} \cap \begin{vmatrix} 4.1 & & & \\ 4.2 & & & \\ 4.3 & 5.1 & 6.1 & \\ 4.4 & 5.2 & 6.2 & 7.1 \\ 4.5 & 5.3 & 6.3 & 7.2 \\ 4.6 & & & \\ 4.7 & & & \end{vmatrix} \cap \begin{vmatrix} 8.1 \\ 8.2 \\ 8.3 \\ 8.4 \\ 8.5 \\ 8.6 \\ 8.7 \\ 8.8 \\ 8.9 \\ 8.10 \end{vmatrix} \cap \begin{vmatrix} 9.1 \\ 9.2 \end{vmatrix} \cap \begin{vmatrix} 10.1 & \\ 10.2 & 11.1 \\ 10.3 & 11.2 \\ 10.4 & 11.3 \\ 10.5 & \\ 10.6 & \end{vmatrix}. \tag{7}$$

The total number of design variants of flexible screw conveyors that make up the morphological matrix (7) is very significant, and therefore it is necessary to spend a lot of time selecting productive solutions, and therefore it is necessary to use the established variants by combinations of the presented method to synthesise hierarchical groups using the method of morphological analysis, which establishes conditions for dividing this system into a specific number of established hierarchical levels with their decomposition in each of the various established designs of this system [25].

For the presented variant, the combination of the first hierarchical level and the model of the established system "Flexible Screw Conveyor", presented in Figure 6, [24], can be divided into two subgroups.

The first presented subgroup includes designs of elements that demonstrate special morphological features of the design of the working body (5) and (7), and special morphological features of the design of the screw working body connection (8), and the second includes structural elements of screw working bodies (6). When using this method, the number of synthesised variants is determined by the formula:

$$N_{IГ}=\sum_{z=1}^{l}\sum_{x=1}^{q}\prod_{i=1}^{m}K_i, \quad (8)$$

where z – designation of the hierarchical level; l – number of levels; x – subgroup of a certain hierarchical level; q – number of subgroups of a certain hierarchical level; K_i – selection of a design feature of the mechanism of a subgroup of a certain hierarchical level; m – number of selections of design features of mechanisms of a particular subgroup of a specific hierarchical level.

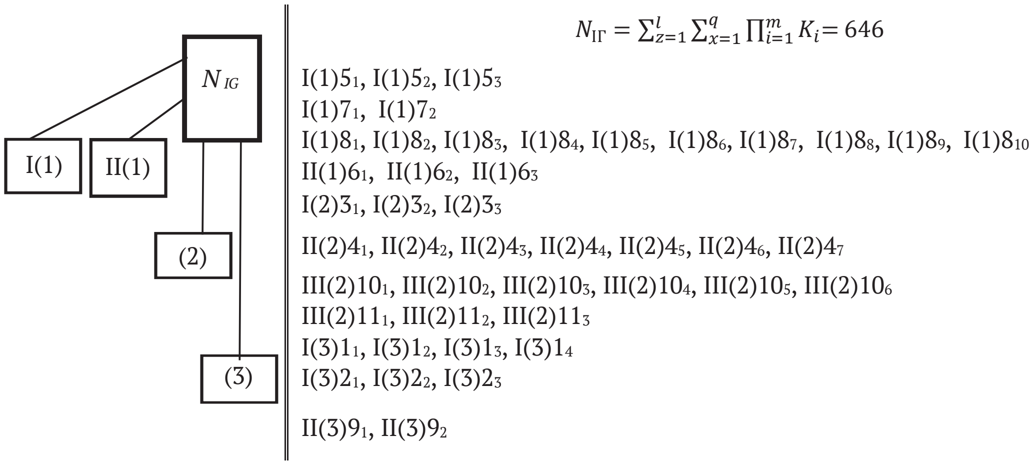

Figure 6. Diagram of the model of the mechanical system "Screw loader":
I – the first subgroup of the hierarchical level; II – the second subgroup of the hierarchical level;
III – the third subgroup of the hierarchical level; (2) – the second hierarchical level; (3) – the third hierarchical level

If the method of morphological analysis is used to calculate the number of alternative designs, the total number of generated variants of flexible spiral conveyors will be 1632960 variants, and if the method of synthesis of hierarchical groups with subsequent decomposition into separate subgroups is used, using the method of morphological analysis, the number of variants will be only 102, which is much less than using the conventional method of synthesis.

The choice of the established design variant of the screw working bodies of the reloader will depend on the transportation process and the amount of force load on the screw working body. If the main parameters in the design of working bodies are productivity and geometric dimensions and the quality indicators of the technological process are neglected, then in such a model of a mechanical system the number of coefficients will be reduced to two values, and the selection task will be to find designs that would ensure optimal strength and cost of screw working bodies. It will result in the search for rational solutions to establish equally strong structures of rigid and flexible screw working bodies, considering their technical and economic indicators. It will result in the search for rational solutions to establish equally strong structures of stiff and flexible screw working bodies, considering their technical and economic indicators.

As a result of the analysis of the design solutions of the generated variants, workable designs of flexible screw conveyors were obtained (Fig. 7) [27].

Since the design and kinematic parameters of these devices are interrelated, it is necessary to set a specific value of the loader's capacity Q, i.e. a value that would reflect the amount of material that will be periodically loaded into the device. This parameter is the initial value for setting the diameter of the spiral and its rotation frequency. According to the methodology for determining the performance of screw conveyors:

$$Q_p=Q_v\rho, \text{ t/h}, \quad (9)$$

where Q_v – volumetric capacity, m³/hour; ρ – bulk density of the transported material, t/m³.

The volumetric capacity is determined by the formula:

$$Q_v=47D_C^2\xi n_C\psi c_\beta, \quad (10)$$

where D_C – outer diameter of the working body, m; ξ – pitch ratio of the working body; n_C – rotational speed of the working body, rpm; ψ – conveyor filling rate; c_β – coefficient that considers the angle of inclination of the working body.

The estimated capacity is determined by the formula:

$$Q_p=47D_C^2\xi n_C\psi c_\beta\rho, \quad (11)$$

whence the calculated value of the outer diameter of the spiral is equal:

$$D_C \approx \sqrt{\frac{Q_p}{47\xi n_C\psi c_\beta\rho}}. \quad (12)$$

The final value of the outer diameter of the helix is determined according to DSTU 2763-94 [28], with the closest value to the calculated one being the largest.

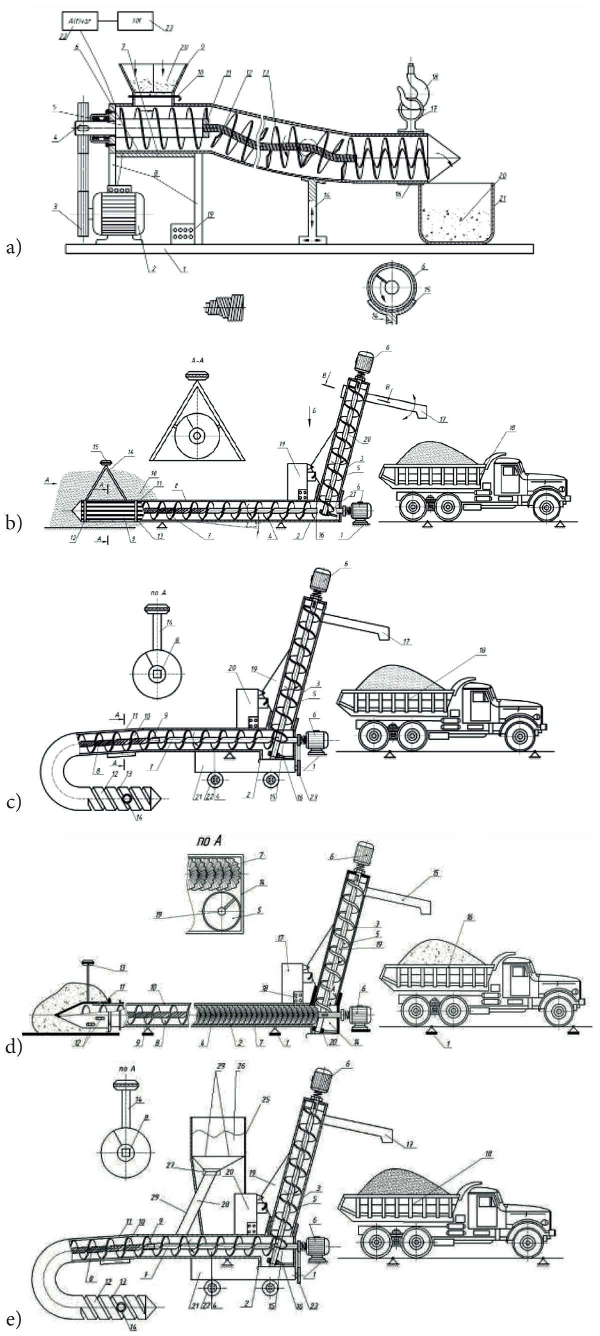

Figure 7. Synthesised models of screw conveyors and loaders

The drive power can be calculated based on the following considerations. The power of the drive motor is used to overcome the frictional resistance when the material is moved in the respective hose, for bearing losses and to lift the material to a specific height (vertical conveying section).

The total drag force W caused by the friction of the bulk material against the pipe walls and the inclination of the device at an angle β to the horizon (Fig. 8) [27] is equal:

$$W=qgf_pL_C\cdot \cos\alpha+qgf_pL_C\cdot \sin\alpha=qg(Lf_p+h), \tag{13}$$

where q – the distributed mass of the material, kg; g – free fall acceleration; f_p – coefficient of friction of the material against the walls of the hopper pipe; L_C, L, h – length of the spiral and its projections, m; α – the angle of inclination of the highway to the horizon.

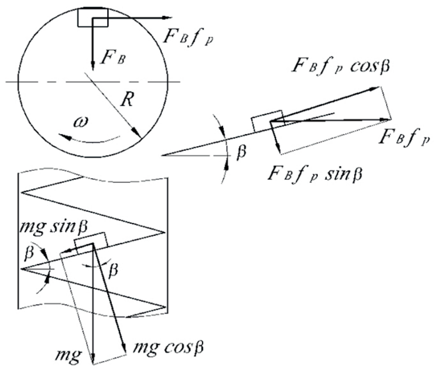

Figure 8. Calculation scheme for determining the critical speed of the helix

Note: m – mass of the material particle; f_p – coefficient of friction of the material against the walls of the hopper; R – radius of the spiral; β – angle of rise of the spiral; F_B – reaction force of the hopper

If the speed of material movement is expressed as:

$$v=t_Cn_C/60, \tag{14}$$

where t_C – the spiral pitch, and the distributed mass of material q through the productivity Q:

$$Q=3{,}6qt_Cn_C/60, \tag{15}$$

the necessary power N_1 is obtained, which is required to overcome the resistance force W:

$$N_1=\frac{Wv}{1000}=\frac{Qg(Lf_p+\mathrm{h})}{3600}. \tag{16}$$

If the drag force is considered to be the normal pressure on the surface of the propeller blade, without considering the angle of elevation, the friction force of the material against the helix can be calculated:

$$F_C=qgf_C(Lf_p+h), \tag{17}$$

where f_C – the coefficient of friction of the material to the helix.

Since the force acts in a cross-section approximately equal to 0.25 D_C, the power N_2 consumed by friction against the spiral is equal:

$$N_2=F_Cv=\frac{qgf_C(Lf_p+h)}{1000}\cdot\frac{\pi dn_C}{60}, \tag{18}$$

where d – diameter of the spiral shaft, m. After the appropriate transformations, the following will be obtained:

$$N_2=\frac{Qf_C(Lf_p+h)}{367}\cdot\frac{\pi d}{t_C}. \tag{19}$$

However, in production conditions, it is difficult to determine all the forces that oppose the movement of the working body, thus a well-known dependence is used to determine the drive power [2]:

$$N = \frac{Q_p L_C}{367\eta_\Pi} \cdot (k \pm \sin\alpha), \tag{20}$$

where η_p – actuator efficiency; k – material resistance coefficient.

Accordingly, the "+" ign is used when lifting the material, and the "-" sign when lowering it. For horizontal positioning of the hopper section:

$$N = \frac{Q_p L_C k}{367\eta_\Pi}. \tag{21}$$

In addition to the appropriate diameter and shape of the spiral blades, a certain spiral speed is required to lift material with the vertical section. To determine the minimum required helix rotation frequency, consider the kinematics of the material movement using the example of the scheme presented in Figure 8.

A particle of mass m on a helical surface is subject to two forces, one of which is downward $mg\sin\beta$, and the other – the frictional force of the particle against the surface of the spiral $mgf_C\cos\beta$. During the rotational movement of the particle along with the spiral at a certain speed υ along the radius R, a centrifugal force $m\upsilon^2/R$ arises, which presses the material particle against the fixed wall of the spiral sleeve, where the friction force of the particle against the sleeve $m\upsilon^2 f_p/R$ arises, which generates additional pressure on the helical surface of the spiral blade. The vertical component of this pressure is $m\upsilon^2 f_p\cos\beta/R$, and the normal pressure on the helical surface is $m\upsilon^2 f_p\sin\beta/R$.

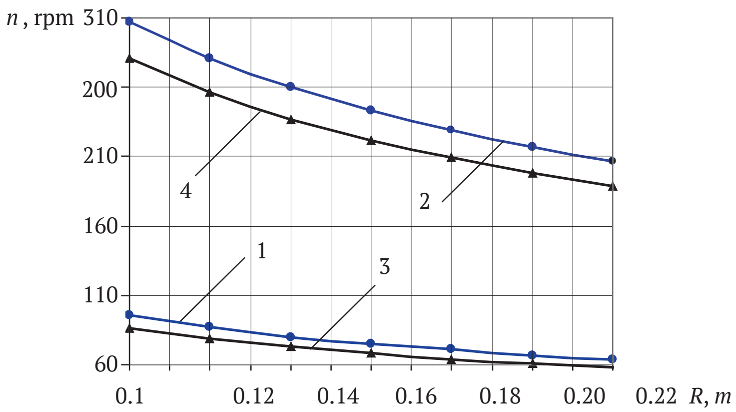

Figure 9. Dependence of the change in the critical rotation frequency of the working body of the loader on its radius $n=f(R)$ at different values of the process line elevation angle and the coefficient of friction of the material against the pipe walls: 1 – (β=16°, f_p=0.15); 2 – (β=20°, f_p=0,15); 3 – (β=16°, f_p=0,18); 4 – (β=20°, f_p=0.18)

The critical velocity, i.e. the velocity on the circumferential surface of the spiral at which the material fraction is in equilibrium, is found from the following condition:

$$mg\sin\beta + mgf_C\cos\beta + \frac{m\upsilon_{\text{кр}}^2 f_p f_C\sin\beta}{R} - \frac{m\upsilon_{\text{кр}}^2 f_p\cos\beta}{R} = 0, \tag{22}$$

where the critical velocity is equal:

$$\upsilon_{\text{кр}} = \sqrt{\frac{gR\sin\beta + f_C\cos\beta}{f_p\cos\beta - f_C\sin\beta}} = \sqrt{\frac{gR}{f_p}}tg(\beta + \rho_C), \tag{23}$$

where ρ_C – the angle of friction of the material particle to the surface of the spiral.

Considering that the critical speed is equal:

$$\upsilon_{kp} = \frac{\rho R n_{kp}}{30}, \tag{24}$$

the critical speed of the working body is equal:

$$n_{\kappa p} = \frac{30}{\pi R}\sqrt{\frac{gR}{f_p}}tg(\beta + \rho_C). \tag{25}$$

To determine the influence of the screw radius R, the angle of the rise of the process line β, and the coefficient of friction of the material against the pipe walls f_p on the value of the working body rotation frequency, we determined the dependence (25). According to the results obtained, which are presented in Figure 9, it was found that the frequency of rotation of the working body decreases with the growth of the screw radius, and, accordingly, the greater the value of the angle of the rise of the technological line and the smaller the value of its radius, the lower the value of the coefficient of friction of the material against the pipe walls.

The monograph [22] discusses new designs of mechanisms with screw working bodies for the mechanisation of labour-intensive processes of bulk materials handling. Progressive designs are presented, their technical characteristics are defined, but the designs with the best technical and economic indicators are not identified.

Work [24] is devoted to the design, manufacturing technology and experimental studies of flexible screw conveyors, the main characteristics of which are mobility and the possibility of reloading bulk materials along curved routes. The research provides a theoretical justification for the design of flexible screw conveyors, explores the processes of their manufacture, presents the results of experimental studies and optimises the design parameters of screw working bodies, but it is necessary to improve the methodology for designing the structures of working bodies of screw conveyors.

Research [25] describes the main methods of transporting bulk agricultural materials along curved routes in the closed elastic casing using nozzles. A theoretical substantiation of the structural and kinematic parameters of the proposed schemes of flexible screw conveyor nozzles has been performed, but it is necessary to determine the optimal parameters of these mechanisms.

Work [29] states that to ensure the growth of productivity and quality of technological processes using screw transport and technological mechanisms of machines, it is necessary to use progressive and efficient designs of screw working bodies in their designs. In addition, the research synthesises mechanisms with structures of screw working bodies using morphological analysis and selects several competitive designs. However, no designs with improved technical and economic characteristics have been identified.

In addition, work [30] presents the design of screw conveyors with hopper loading and screw conveyors with loading through nozzles. In addition, a classification of loaders for screw transport and technological mechanisms is presented. However, there are no analytical dependencies for determining the design parameters of screw loaders.

Work [31] presents the calculation of the structural and power parameters of screw loaders, but the proposed methodology does not fully provide opportunities to carry out engineering and technological calculations of the structural and energy parameters of screw loaders.

Thus, the research deals with the establishment of structures of screw conveyors using structural and schematic synthesis by using hierarchical groups and morphological analysis. The research analyses the influence of many factors on the processes of moving bulk cargo by flexible conveyors with screw working bodies and establishes the structural elements of these conveyors that determine the design features of these means of transport.

CONCLUSIONS

The designs of screw conveyors with hopper loading and screw conveyors with nozzle loading are presented. In addition, a classification of loaders for screw transport and technological mechanisms is presented. The mathematical dependencies for determining the geometric and design parameters of loaders with screw working bodies are presented.

Using the method of structural analysis, the synthesis of screw loaders and mixers with screw working bodies was performed, establishing designs with the best technical-economic characteristics and selecting competitive designs.

The research presents a system for coding and synthesis of structures of screw mechanisms, which allowed consistently conducting engineering and technological calculations to establish some relevant constraints and using computer software to develop and select competitive structures of screw working bodies that would ensure high-quality and productive implementation of technological processes.

It has been established that the choice of design solutions for screw implements will depend on the type of technological process and the magnitude and nature of the load on the screw implements. For this purpose, based on the necessity to ensure the strength of the screw working bodies in the design, it is necessary to limit the number of variants of mechanism designs and develop workable designs of the sections of flexible screw mechanisms of screw conveyors for the transport of bulk materials.

Engineering and technological calculations of the structural and energy parameters of the presented screw loader have been performed, which can be of practical use in the design of similar mechanism designs.

The prospect for these studies will be to determine the kinematic parameters of screw conveyors based on ensuring maximum conveyor performance, damage to bulk materials, the size of curved routes and the rheological properties of bulk materials.

REFERENCES

[1] Bulgakov, V., Nikolaenko, S., Holovach, I., Adamchuk, V., Kiurchev, S., Ivanovs, S., & Olt, J. (2020). Theory of grain mixture particle motion during aspiration separation. *Agronomy Research*, 18(1), 18-37.

[2] Loveikin, V.S., & Romasevych Yu.O. (2017). Dynamic optimization of a mine winder acceleration mode. *Naukovyi Visnyk Natsionalnoho Hirnychoho Universytetu*, 4, 81-87.

[3] Pylypaka, S.F., Klendii, M.B., & Klendii, O.M. (2017). Particle motion over the surface of a rotary vertical axis helicoid. *INMATEH – Agricultural Engineering*, 51(1), 15-28.

[4] Patent No. 67426A Ukraine, B65633/16. Screw conveyor. Klendiy M.B., Pavlova I.O., Gevko R.B., Tkachenko .G. No. 2003010046. Bull. No. 8. Retrieved from https://base.uipv.org/searchINV/search.php?action=viewdetails&IdClaim=75911.

[5] Liaposchenko, O., Pavlenko, I., & Nastenko, O. (2017). The model of crossed movement and gas-liquid flow interaction with captured liquid film in the inertial-filtering separation channels. *Separation and Purification Technology*, 173, 240-243.

[6] Hevko, B.M., Hevko, R.B., Klendii, O.M., Buriak, M.V., Dzyadykevych, Y.V., & Rozum, R.I. (2018). Improvement of machine safety devices. *Acta Polytechnica*, 58(1), 17-25.

[7] Pylypaka, S., Kremets, T., & Klendii, O. (2018). Particle motion over the surface of a cylinder, which performs translational oscillations in a vertical plane. *Engineering Journal*, 22(3), 83-92.

[8] Adamchuk, V., & Kuvachev, V. (2021). Results of experimental studies of a block-modular agricultural unit. *Herald of Agrarian Science*, 99(7), 49-58.

[9] Rohatynskyi, R.M. (1997). *Mechanical and technological basis of interaction of screw working bodies with raw materials of agricultural production* (Doctoral thesis, National University of Life and Environmental Sciences of Ukraine, Kyiv, Ukraine).
[10] Bulgakov, V., Holovach, I., Nadykto, V., Parakhin, O., Kaletnik, H., Shymko, L., & Olt, J. (2020). Motion stability estimation for modular traction vehicle-based combined unit. *Agronomy Research*, 18(4), 2340-2352. doi: 10.15159/ar.20.183.
[11] Bulgakov, V., Pascuzzi, S., Ivanovs, S., Kaletnik, G., & Yanovich, V. (2018). Angular oscillation model to predict the performance of a vibratory ball mill for the fine grinding of grain. *Biosystems Engineering*, 171, 155-164. doi: 10.1016/j.biosystemseng.2018.04.021.
[12] Kresan, T., Pylypaka, S., Ruzhylo, Z., Rogovskii, I., & Trokhaniak, O. (2020). External rolling of a polygon on a closed curvilinear profile. *Acta Polytechnica*, 61(1), 270-278. doi: 10.14311/AP.2020.60.0313.
[13] Hevko, B.M., Hevko, R.B., Klendii, O.M., Buriak, M.V., Dzyadykevych, Y.V., & Rozum, R.I. (2018). Improvement of machine safety devices. *Acta Polytechnica*, 58(1), 17-25. doi: 10.14311/AP.2018.58.0017.
[14] Hevko, R., Rohatynskyi, R., Hevko, M., Lyashuk, O., & Trokhaniak, O. (2020). Investigation of sectional operating elements for conveying agricultural materials. *Research in Agricultural Engineering*, 66(1),18-26. doi: 10.17221/25/2019-RAE.
[15] Hevko, R.B., Lyashuk, O.L., Dzyura, V.O., Dovbush T.A., Trokhaniak, O.M., & Liashko, A.P. (2021). Experimental studies of the process of loose material transportation by a pneumatic-screw conveyor. *INMATEH – Agricultural Engineering*, 63(1), 479-487.
[16] Tkachenko, I., Hevko, R., Gandziuk, M., Synii, S., & Trokhaniak, O. (2021). Substantiation of the parameters of a horizontal conveyer-cleaner of root crops. *Bulletin of the Transilvania University of Brasov*, 1, 213-222. doi: 10.31926/BUT.FWIAFE.2021.14.63.1.19.
[17] Hevko, R., Zalutskyi, S., Tkachenko, I., Lyashuk, O., & Trokhaniak, O. (2021). Design development and study of an elastic sectional screw operating tool. *Acta Polytechnica*, 61(5), 624-632. doi: 10.14311/AP.2021.61.0624.
[18] Kuvachov, V., Bulgakov, V., Adamchuk, V., Kaminskiy, V., Melnik, V., & Olt, J. (2021). Experimental research into new harrowing unit based on gantry agricultural implement. *Agronomy Research*, 19(1), 126-135. doi: 10.15159/ar.20.239.
[19] Bulgakov, V., Trokhaniak, O., Adamchuk, V., Olt, J., & Ivanovs, S. (2022). Experimental studies of flexible sectional screw conveyor torque value. In *Engineering for rural development: Contents of proceedings of the 21st international scientific conference* (pp. 472-477). Jelgava: Latvia University of Life Sciences and Technologies.
[20] Bulgakov, V., Olt, J., Ivanovs, S., Trokhaniak, O., Gadzalo, J., Adamchuk, V., Chernovol, M., Pascuzzi, S., Santoro, F., & Arak, M. (2022). Research of a contact stresses in swivel elements of flexible shaft in screw conveyor for transportation of agricultural materials. *Estonian Academic Agricultural Society*, 1, 1-7. doi: 10.15159/jas.22.12.
[21] Baryshev, A.I., Budishevsky, V.A., Sklyarov, N.A., Sulima, A.A., & Tkachuk, A.M. (2005). *Calculation and design of transport vehicles of continuous action*. Donetsk: Nord-Press.
[22] Gevko, B.M., Danylchenko, M.G., Rohatynskyi, R.M., Pylypets, M.I., & Matviychuk, A.V. (1993). *Mechanisms with screw devices*. Lviv: Svit.
[23] Rohatynskyi, R.M., Gevko, I.B., & Dyachun, A.E. (2014). *Scientific and applied foundations of the creation of screw transport and technological mechanisms*. Ternopil: Ivan Pulyuy Technical University.
[24] Gevko, I.B., Leshchuk, R.Ya., Gud, V.Z., Dmytriv, O.R., Dubynyak, T.S., Navrotska, T.D., & Kruglyk, O.A. (2019). *Flexible screw conveyors: design, manufacturing technology, experimental. Research*. Ternopil: PE V.A Palyanytsia.
[25] Gevko, I. (2000). Structure analysis and calculation of the loading capacity of nozzles of screw conveyors. *Collection of Scientific Papers of NAU*, 7, 160-163.
[26] Gevko, B.M., & Rogatynskyi, R.M. (1989). *Screw feed mechanisms of agricultural machines*. Lviv: Higher School.
[27] Kuznetsov, Yu.M., Lutsiv, I.V., & Dubynyak, S.A. (2007). *Theory of technical systems*. Kyiv: Ternopil.
[28] DSTU 2763-94 "Screw conveyors. Terms and definitions". (1996). Derzhspozhyvstandart Ukrainy.
[29] Rohatynskyi, R.M. (1997). *Mechanical and technological basis of interaction of screw working bodies with raw materials of agricultural production* (Doctoral thesis, National Agrarian University, Kyiv, Ukraine).
[30] Hevko, I. (2012). Structural synthesis of impulse safety couplings and screws by the method of morphological analysis. *Bulletin of TNTU*, 67(3), 121-134.
[31] Gevko, I.B., Tarasyuk, Yu.M., & Klendius, V.M. (2014). Justification of parameters of screw loaders. *Interuniversity Collection "Scientific Notes"*, 44, 57-63.

Микола Богданович Клендій
Кандидат технічних наук, доцент
Відокремлений підрозділ національного університету біоресурсів і природокористування України
«Бережанський агротехнічний інститут»
47501, вул. Академічна, 20, м. Бережани, Тернопільська область, Україна
https://orcid.org/0000-0001-8271-5381

Іван Володимирович Логуш
Кандидат технічних наук, доцент
Відокремлений підрозділ національного університету біоресурсів і природокористування України
«Бережанський агротехнічний інститут»
47501, вул. Академічна, 20, м. Бережани, Тернопільська область, Україна
https://orcid.org/0000-0001-5075-1054

Андрій Петрович Драган
Кандидат технічних наук
Відокремлений підрозділ національного університету біоресурсів і природокористування України
«Бережанський агротехнічний інститут»
47501, вул. Академічна, 20, м. Бережани, Тернопільська область, Україна
https://orcid.org/0000-0001-7195-1127

Ігор Іванович Чвартацький
Кандидат технічних наук, доцент
Відокремлений підрозділ національного університету біоресурсів і природокористування України
«Бережанський агротехнічний інститут»
47501, вул. Академічна, 20, м. Бережани, Тернопільська область, Україна
https://orcid.org/0000-0001-5689-4603

Андрій Володимирович Грабар
Аспірант
Відокремлений підрозділ національного університету біоресурсів і природокористування України
«Бережанський агротехнічний інститут»
47501, вул. Академічна, 20, м. Бережани, Тернопільська область, Україна
https://orcid.org/0000-0001-8208-6212

Обґрунтування та розрахунок конструктивно-силових параметрів гвинтових завантажувачів

Анотація. Існуючі конструкції гвинтових робочих органів транспортно-технологічних машин не завжди можуть забезпечити необхідну продуктивність та уникнення перевантаження, що веде до деформацій і пошкоджень деталей механізмів. Тому необхідно створювати нові ефективні гвинтові робочі органи, які б забезпечували виконання технологічного процесу. Метою роботи було обґрунтування і дослідження конструкції та методики розрахунку основних конструктивно-силових параметрів розробленого гвинтового завантажувача, проведення синтезу гвинтових завантажувачів з використанням методу морфологічного аналізу для того, щоб одержати конструкції механізмів з кращими технічними і економічними характеристиками. Для проведення досліджень використано методи теорії поверхонь, аналітичної та диференціальної геометрії, систем комп'ютерної графіки і математики. В результаті проведених теоретичних та експериментальних досліджень приведено конструкції гвинтових конвеєрів з бункерним завантаженням та гвинтових конвеєрів із завантаженням через насадки. Також приведена класифікація завантажувачів гвинтових транспортно-технологічних механізмів. Визначено залежності для розрахунку конструкцій завантажувачів гвинтових конвеєрів. Здійснено синтез завантажувачів та змішувачів методом морфологічного аналізу для одержання конструкцій механізмів з кращими технічними і економічними характеристиками та створено конкурентоздатні конструкції механізмів. Запропоновано систему кодування та синтезу елементів конструкцій і механізмів гвинтових робочих органів із покращеними технологічними властивостями та відібрано конкурентоздатні конструкції шнекових робочих органів, які якісно та продуктивно виконують технологічні процеси. Розроблено методику розрахунку основних конструктивно-силових параметрів гвинтового завантажувача, за допомогою якої можливо визначити параметри гвинтового завантажувача. Матеріали статті можуть бути використані при подальших дослідженнях гвинтових конвеєрів і зокрема гвинтових завантажувачів з визначення їх конструктивних, технологічних, енергетичних та силових параметрів

Ключові слова: шнековий конвеєр; насадка; транспортно-технологічний механізм; конструктивні елементи; структурний синтез; морфологічний аналіз; методика розрахунку

Machinery & Energetics
Vol. 13, No. 4. 2022

Journal homepage:
https://technicalscience.com.ua/en

UDC 621:615.015.45
DOI: 10.31548/machenergy.13(4).2022.60-71

Valerii Kryvonosov*
Full Doctor in Technical Sciences, Professor
National University of Life and Environmental Sciences of Ukraine
03041, 15 Heroiv Oborony Str., Kyiv, Ukraine
https://orcid.org/0000-0002-8219-021X

Nataliia Prudnikova
PhD in Technical Sciences
National University of Life and Environmental Sciences of Ukraine
03041, 15 Heroiv Oborony Str., Kyiv, Ukraine

Lilia Martyniuk
National University of Life and Environmental Sciences of Ukraine
03041, 15 Heroiv Oborony Str., Kyiv, Ukraine

Justification of the electrical scheme of biological tissue replacementunder the action of DC voltage

Abstract. The change in the impedance of biological tissue under the influence of voltage is used in the diagnosis and treatment of various diseases. Mathematical models describing physical and biological processes in biological objects are based on electrical substitution schemes. The subject of research of this work was the study of the change in the impedance of biological tissue in the transient process of ionization under the action of DC voltage. An analysis of the known substitution schemes was carried out, the shortcomings of their application were identified when the transient processes of ionization in the tissue under the action of direct current voltage were studied, and the substitution scheme with the introduction of additional resistance was substantiated, both analytically and experimentally. In the work, the bioimpedance method is applied when direct current voltage is applied to biological tissue, taking into account the law of commutation in transient ionization processes. An invasive measurement of the change in impedance with needle electrodes was carried out, and it was proved that the active component proportionally depends on the distance between the electrodes, while the capacitive component remains unchanged. It is shown that the ionization time constant is a criterion parameter and can be used in the diagnosis of the development of ischemic disease of muscle tissue, the change in the state of biological tissue when blood flow is stopped during the application of a tourniquet. It has been proven that the ionization time constant does not change with an unchanged ionic composition of the tissue and can be used in the analysis of the composition of the intercellular space. A simultaneous invasive measurement was performed in two identical places of different limbs, on one of which a hemostatic tourniquet was applied. The obtained results made it possible to conclude that a change in the constant time from 15% to 50% compared to two constant times allows for rapid diagnosis, within 2 minutes, of the state of biological tissue and can be used in the study of the development of diseases associated with ischemia. The results of the study can be used for rapid diagnosis of the state of a biological object and the creation of an inexpensive device for its use in surgery and research laboratories

Keywords: impedance; transient process; ionization process; cell resistance; capacitance; ionization time constant; diagnostics; ischemia

Article's History: Received: 08.07.2022; Revised: 12.10.2022; Accepted: 23.11.2022.

Suggested Citation:
Kryvonosov, V., Prudnikova, N., & Martyniuk, L. (2022). Justification of the electrical scheme of biological tissue replacement under the action of DC voltage. *Machinery & Energetics,* 13(4), 60-71.

*Corresponding author

INTRODUCTION

In diagnostic and medical practice, the bioimpedance method – a change in the complex resistance (impedance) of biological tissue under the action of voltage - has found wide application [1-3]. The effect of direct and alternating electric current on the electrical conductivity of biological tissue has been the subject of many scientific studies [4; 5].

The electrical resistance of biological tissue is one of the criteria for studying the processes of state change and detecting various diseases in a biological object [6; 7]. Resistance measurements are used to study limb ischaemia, diagnose the affected skin surface with haemangioma, and detect pathological changes in tissue in small volumes when diagnosing cancer, otorhinolaryngological, gynaecological, and other tumours [8-10].

The flow of direct current through living cells activates the movement of electrolyte ions and other charged particles. The mobility of these particles is different, so their redistribution occurs. Biological tissue for studying the effects of voltage is represented by an electrical substitution circuit. Depending on the object of study, different substitution circuits are used; simple ones consist of a capacitor and a resistor, complex ones of several resistors and capacitors. Depending on the objectives of the study, they are combined into different substitution schemes [4; 5; 11].

Both in scientific research and in the design of medical devices that use both direct and alternating currents, it is important to build a mathematical model that reliably describes the biophysical processes occurring in biological tissues.

The reliability of the mathematical model and the results obtained depends on the choice of the electrical scheme for replacing biological tissue.

The influence and application of direct current on the processes occurring in living organisms have been studied in [4; 12; 13]. Direct current is more often used in treatment as described in [7; 8; 13]. Current of variable frequency and amplitude is more commonly used in research. Papers [14; 15] investigated the effect of alternating current and alternating frequency from 10 to 44000 Hz on the change in biological tissue impedance using the frequencies of therapeutic intensities of drug penetration into cells. In these works [16-18], an electrical substitution circuit with a series connection of capacitance and active resistance was used to study the change in impedance under the action of alternating current. Using such a substitution scheme to study the effect of direct current on biological tissue would be incorrect. In steady-state mode, at zero voltage frequency, the capacitance is equal to infinity, and the current should be zero.

Papers [5; 8; 10] show the change in impedance under the influence of a variable frequency voltage. This paper also uses traditional substitution circuits with both series connection of the capacitive and active elements and parallel connection, and the expression of Ohm's law is given for these circuits.

In [3; 14], the use of the bioimpedance method was proved to study changes in the state of biological tissues and detect diseases. To build mathematical models that characterise changes in the properties of biological tissue, in [5; 6], various schemes applied to alternating current of different frequencies and amplitudes were analysed.

It should be noted that the above-mentioned scientific sources insufficiently investigated the impact of the choice of electrical circuit for biological tissue replacement on the study of the transient process of impedance change and the change in the ionisation time constant as an information and diagnostic criterion parameter in the diagnosis of various diseases. For example, the imperfection of the choice of electrical replacement circuits does not allow us to establish patterns of changes in electrical resistance and changes in tissue viability in partial and complete ischaemia. It should also be noted that equipment using direct current is less complex and cheaper.

The purpose of the study was to analyse existing electrical schemes for biological tissue replacement.

To achieve this goal, the following tasks were formulated: substantiation of a biological tissue replacement circuit with the introduction of an additional active resistance to study transient ionisation processes in biological tissue; development of a replacement circuit for a heterogeneous ionic composition of biological tissue from one to n types of ions; substantiation of changes in the time constant as a criterion for studying the dynamics of limb ischaemia and determining the time of ischaemia development when a tourniquet is applied.

MATERIALS AND METHODS

To achieve this goal, the bioimpedance method was used, which allows monitoring the change in the impedance of biological tissue in the transition period using invasive measurement of the electrical resistance of biological tissue under the influence of direct current voltage.

In the course of the research work, theoretical methods of approximation of experimental studies, laws of biophysics of cells and intercellular space of biological tissue were used to determine the change in biological impedance in the transient process under the influence of DC voltage.

The study was conducted at the Photonics Laboratory of Vinnytsia State Technical University. In Figure 1 shows a laboratory setup for measuring the electrical conductivity of biological tissue.

Materials: biological object (sexually mature guinea pigs – males weighing 500-600 g). Studies were performed under anaesthesia (composition: sodium thiopental 10 mg/ml – 3-4 ml). Anaesthesia was administered 30 minutes before the start of the study. Within 0.5 hours, premedication was performed with the following composition: dimedrol 1% ¬ 0.3 ml and analgin 50% ¬ 0.3 ml. When working with animals, the provisions of Article 26 of the Law of Ukraine No. 3447-VI of 16.10.2012 "On the Protection of Animals from Cruelty" [19], the "General Ethical Principles for Animal Experiments" approved at the First National Congress on Bioethics [20], the requirements of the European Convention for the Protection of Vertebrate Animals

Used for Research and Other Scientific Purposes [21], and the Declaration on the Humane Treatment of Animals [22] were followed.

Equipment: Figure 2 shows a block diagram of the equipment for measuring the conductivity of biological tissue.

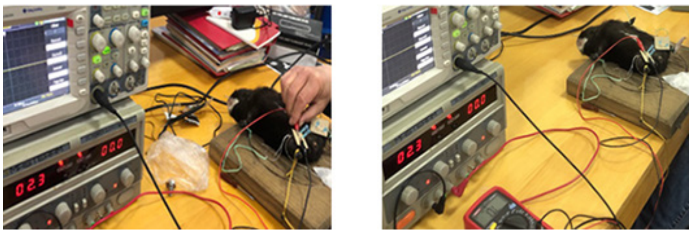

Figure 1. Laboratory setup for measuring the electrical conductivity of biological tissue

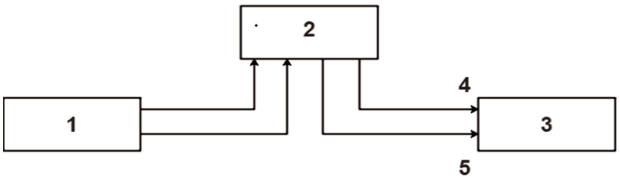

Figure 2. Block diagram of connection of equipment for measuring the conductivity of biological tissue, where indicated: 1 – DC voltage control unit; 2 – two-channel oscilloscope; 3 – biological object (guinea pig); 4 and 5 sensors for invasive conductivity measurement

DC power supply – voltage (0-50), current 10 A, voltage adjustment step 0.5 V, measurement error 1%. The oscilloscope is a Sony-Tektronix 314 two-channel portable storage oscilloscope with a bandwidth of 10 MHz. Medical needles (5 mm^3 syringe) with stepwise adjustment of the distances between them were used as sensors for invasive measurement. The adjustment step is 1 cm. The needles are insulated with varnish, except for the tips with an open part that is inserted into the tissue, which is 5 mm.

To build mathematical models and analyse the impact of extraneous factors on biological tissue, electrical substitution schemes are used for both tissue sections and individual organs [7]. The criterion for choosing an electrical substitution scheme was to match the physical process in the biological environment that it describes.

RESULTS AND DISCUSSION

It is known from studie [3; 8] that the applied DC voltage to biological tissue causes the redistribution of free ions and the appearance of an electromotive force (EMF). Figure 3 shows a physical model of the electrical conductivity of biological tissue: the ionisation current directed against the current caused by the applied voltage depends on the number and types of ions.

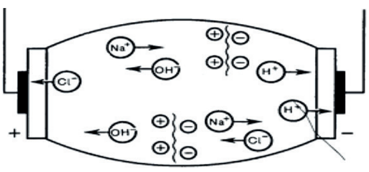

Figure 3. A physical model of the electrical conductivity of biological tissue

The heterogeneous structure of a biological object or tissue part, with its structural and physical features, constitutes the resistive characteristic of the object under study when exposed to an electric current. The structure of biological objects determines the total impedance (electrical resistance or electrical conductivity), which can vary depending on the current state of the object and the influence of an external factor, such as voltage, electromagnetic fields, etc.

A constant voltage applied to a biological object during the transient period causes electric currents, one of which is the current caused by the polarisation properties of the tissue. The total electrical resistance of a biological tissue is defined as:

$$R = \rho \frac{L}{S}, \tag{1}$$

$$R_c = \frac{1}{\omega C}. \tag{2}$$

Where indicated:
R – active component of tissue impedance; R_c – the capacitive component of tissue impedance; ρ – the specific component of biological tissue; L – the length of the current path; S – cross-section for current flow; C – the capacitance; ω – current frequency.

The total resistance in a current circuit is the impedance Z, which is defined by formula (3):

$$Z = \sqrt{R^2 + R_c{}^2}. \tag{3}$$

Electrical substitution circuits are constructed depending on the connection of active and capacitive resistances, which correspond to their mathematical model, which should reliably describe biophysical processes in biological tissue. Traditional circuits are used to study the effect of voltage of different currents. Figure 4 shows the traditional electrical circuits for replacing biological tissue used in the above works.

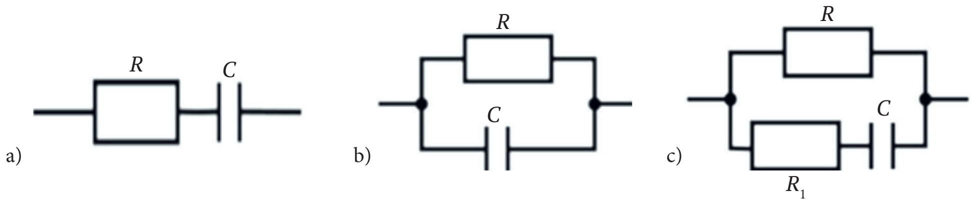

Figure 4. Traditional electrical circuits for biological tissue replacement, where R – active resistance in the intercellular space, R_1 – active resistance of tissue cells, C – capacitive component of the cell

Scheme A (Fig. 4a) is the simplest fabric replacement scheme. The input impedance – Z_{inp1} is given by formula (3). This scheme is not practically used in DC studies because, in the steady-state mode of the input current, I_{inp} tends to 0, since the impedance Z_{inp1}→∞. This, when using this substitution scheme, gives significant deviations and errors of experimental measurements from theoretically calculated ones.

$$Z_{inp2} = \frac{R \cdot R_c}{R+R_c} = \frac{R\frac{1}{\omega C}}{R+\frac{1}{\omega C}}. \tag{4}$$

Analysing expression (4), we see that at the initial time t=0, $R_c = \frac{1}{\omega C} \to \infty$,the input current I_{inp} tends to infinity I_{inp},→∞, since the active component of the impedance R is shunted. The use of this substitution scheme has significant deviations and errors from experimental measurements when studying the transient process of impedance change.

For the substitution scheme (Fig. 4c), the input impedance, Z_{inp3}, in the transient process has the form:

$$Z_{inp3} = \frac{R \cdot \sqrt{R_1^2 + (\frac{1}{\omega C})^2}}{R + \sqrt{R_1^2 + (\frac{1}{\omega C})^2}}. \tag{5}$$

Replacement scheme (Fig. 4c), is a common model for AC voltage studies, but when studying the transient process under the action of DC voltage at the initial switch-on (time point equal to zero t=0), given that the active component of the tissue cell impedance is less than the active component of the cell impedance R<R_1, the input current I_{inp} will be limited by the active component of the impedance $R_{inp3} = \frac{RR_1}{R+R_1}$, since R_{inp3}<R<R_1. The input current I_{inp} should exceed the steady-state value by several times, which is not observed in practice. In both schemes (Fig. 4b) and (Fig. 4c), at the initial moment of current flow, it causes the release of heat that can harm the tissue (local overheating [23]), which is not observed in practice. The use of a substitution scheme (Fig. 4c) also causes deviations and errors in experimental measurements from theoretically calculated ones.

To create a mathematical model that allows analysing transient ionisation processes under the action of DC voltage in tissues, the authors used the substitution scheme of Figure 5. Study of transient ionisation processes in tissues under the influence of DC voltage with different blood flow and different amounts of ions in the same volume, a tourniquet was applied to one paw of a guinea pig. The substitution scheme of Figure 5b corresponds to physicochemical processes with a reduced amount of ions, the simulation of ischemia is the scheme of Figure 5a, this scheme corresponds to the study of healthy biological tissue.

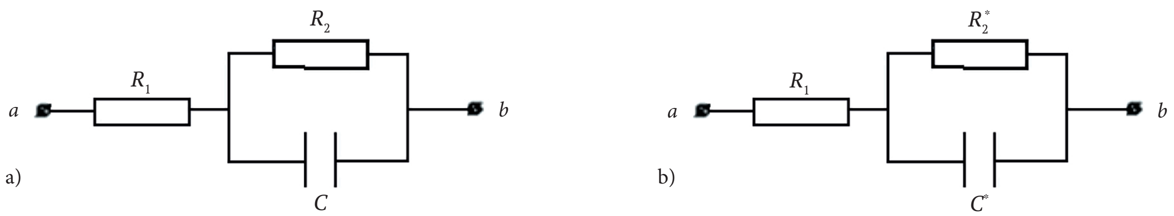

Figure 5. Electrical schemes of biological tissue replacement: a) without a tourniquet; b) with a tourniquet applied

In Figures 5a and 5b, R_1 is the active component of the impedance in the intercellular space, R_2 and R_2^* are the active components of the impedance of tissue cells without and with a tourniquet, C is the capacitive component of the impedance of tissue cells without a tourniquet, which characterises the process of ionisation in healthy biological tissue, and C^* is the capacitive component of the impedance with a tourniquet. At the initial switching on (time point t=0) (scheme of Fig. 5b), taking into account the switching law [24], is replaced by the equivalent scheme of Figure 6.

Figure 6 shows an equivalent replacement circuit to Figure 5a.

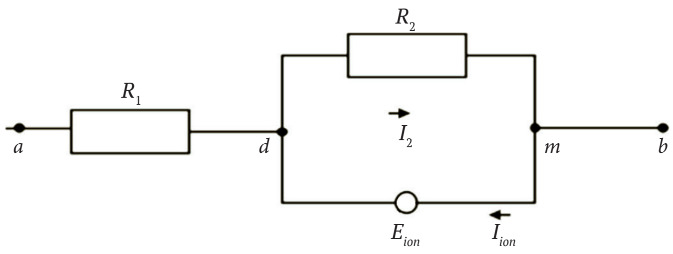

Figure 6. Electrical substitution scheme that takes into account the ionisation process

Note: E_{ion} is an electromotive force caused by the ionisation process, caused by the movement of free charged ions under the action of the source electric field. a, d, m, b are potential points. The voltage applied to the biological tissue is $U_{ab}=\varphi_a-\varphi_b$. φ_a and φ_b are the potentials at points a and b. The directional vector E_{ion} is opposite to the vector U_{ab}, I_2 is the current flowing in the area with the active impedance component R_2, I_{ion} is the current flowing in the area with the capacitance

According to the first Kirchhoff rule for the nodal connection at point d, Figure 6, the current balance is as follows:

$$I_{inp}+I_2-I_{ion}=0. \qquad (6)$$

The voltage balance, according to Kirchhoff's second rule, looks like this:

$$U_{ab}=\Delta U_1+\Delta U_2. \qquad (7)$$

Where ΔU_1, ΔU_2 – voltage drop on the active impedance components R_1 i R_2.

Equation (2), which characterises the change in E_{ion}, taking into account the boundary conditions, is written in the form:

$$\frac{dE_{ion}}{dt}+\left(\frac{1}{R_2 \cdot C}\right)\cdot E_0, \qquad (8)$$

where E_0 – is the value of the electromotive force of ionisation in steady state and is equal to $\Delta U_2=U_{dm}$.

$E_0=I_2 \cdot R_2=I_1 \cdot R_2$, worthy of the replacement scheme (Fig. 6), for the moment of time t=0, $I_2=I_1$.

The solution with respect to E_{ion} is known [24] and has the form:

$$E_{ion}=E_0\left(1-e^{-\frac{t}{\tau_{4.1}}}\right), \qquad (9)$$

where $\tau_{4.1}$ – is the time constant of the ionisation process for the biological object under consideration and is equal to $\tau_{4.1}=C \cdot R_2$.

Let us write equation (2) in the form:

$$U_{ab}=\Delta U_1+E_0\left(1-e^{-\frac{t}{\tau_{4.1}}}\right). \qquad (10)$$

According to equations (1), (4), (5), the input current is determined by the expression:

$$I_1=\frac{U_{ab}}{R_1+R_2\left(1-e^{-\frac{t}{\tau_{4.1}}}\right)}=\frac{U_{ab}}{Z_{inp4}}, \qquad (11)$$

where Z_{inp4} – is the input impedance of the biological tissue and is defined as:

$$Z_{inp4}=R_1+R_2\left(1-e^{-\frac{t}{\tau_{4.1}}}\right). \qquad (12)$$

It was verified the correctness of the choice of the electrical replacement circuit that describes the physical processes in the tissue and the obtained dependencies (10), (11), and (12) by transforming the diagram of Figure 6 for each boundary condition.

The first boundary condition is time t= 0, and, according to the law of switching in transients [25], E_{ion}=0, and $I_{ion}=I_1$.

The substitution scheme for this boundary condition t=0 (the initial moment of the transient) is shown in Figure 7.

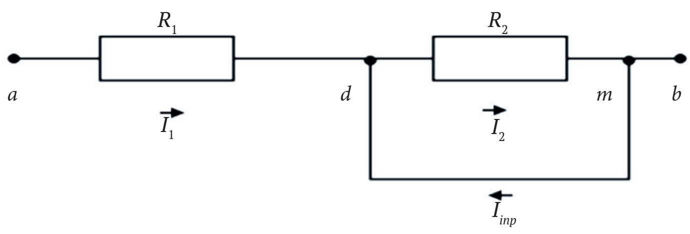

Figure 7. Scheme of biological tissue replacement for the first boundary condition

Note: I_2 is the current flowing in the active resistance R_2, I_2=0 since it is shunted, $I_1=I_{inp}$ is the input current for the first boundary condition

Thus, expression (12) is a mathematical model of the impedance change for the substitution Figure 5a). The input current is determined by expression:

$$I_1=I_{inp}=\frac{U_{ab}}{R_1} \qquad (13)$$

and has a maximum value and is limited by R_1 – the active component of the impedance in the intercellular space. The second boundary condition at time $t\to\infty$ is the steady state, with, according to the law of switching in transients [25], I_{ion}=0, $E_{ion}=\Delta U_2=U_{dm}$.

Figure 8 shows the substitution scheme for the second boundary condition.

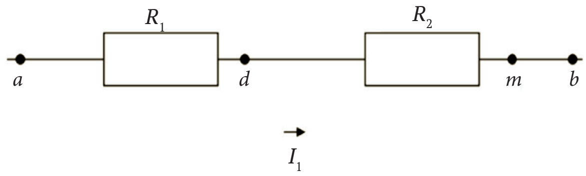

Figure 8. Scheme of biological tissue replacement for the second boundary condition, where I_1=I_{inp}

The input current is defined by the expression:

$$I_1 = I_{inp} = \frac{U_{ab}}{R_1 + R_2}. \quad (14)$$

Using the same calculation algorithm as for the replacement circuit in Figure 5a, it was obtained mathematical models of impedance change over time for the electrical replacement circuits shown in Figures 4a, 4b, 4c.

For the replacement circuit shown in Figure 4a, the mathematical model has the form:

$$Z_{inp1} = Re^{-\frac{t}{\tau_{11}}}, \quad (15)$$

where *R* is the total component of the active impedance resistance, which consists of the active impedances of cellular and intercellular connections.

τ_{11} – is the time constant determined by the formula τ_{11}=*CR*.

The performance of the mathematical model of expression (15) is checked for the boundary conditions:

The moment of time is zero *t*=0, Z_{inp1}=*R*.

The moment of time is $t \to \infty$, Z_{inp1}=0.

The mathematical model meets the requirements of the boundary conditions.

Due to such regularities of impedance changes, this replacement scheme is not used in practice.

For the substitution scheme shown in Figure 4b, the mathematical model has the form:

$$Z_{inp2} = R(1 - e^{-\frac{t}{\tau_{2.1}}}), \quad (16)$$

where *R* is a component of the total active impedance resistance, which consists of the active impedances of cellular and intercellular connections.

$\tau_{2.1}$ – time constant – determined by the formula τ_{21}=*C.R*.

The performance of the mathematical model of expression (16) is checked for the boundary conditions:

the moment of time is zero *t*=0, $Z_{inp.1}$=0,

the moment of time is equal to $t \to \infty$, Z_{inp1}=*R*.

The mathematical model meets the requirements of the boundary conditions.

To obtain the mathematical model, the substitution scheme shown in Figure 4c, it is advisable to use the electrical conductivity – $G_{inp3} = \frac{1}{Z_{inp3}}$.

For the substitution scheme shown in Figure 4c, the mathematical model is as follows:

$$G_{inp3} = \frac{1}{R} + \frac{1}{R_1} e^{-\frac{t}{\tau_{3.1}}}, \quad (17)$$

where $\tau_{3.1}$ – is the time constant determined by the formula $\tau_{3.2}$=CR_1. *R* and R_1 – correspond to the marks of the active resistance diagram of the substitution circuit Figure 4c.

The mathematical model was tested for boundary conditions:

the moment of time is zero *t*=0,

$$G = \frac{1}{R} + \frac{1}{R_1}, \; Z_{inp3} = \frac{R \cdot R_1}{R + R_1};$$

the moment of time is equal to $t \to \infty$, Z_{inp3}=*R*.

The mathematical model meets the requirements of the boundary conditions.

To analyse the correspondence of the experimentally obtained results of the impedance change over time with the results obtained using mathematical models, formulas (12), (16), (17), and the substitution schemes shown in Figures 5a, 4a, 4b, 4c, we constructed graphs of the dependence *R*=*f*(*t*), which are shown in Figure 9.

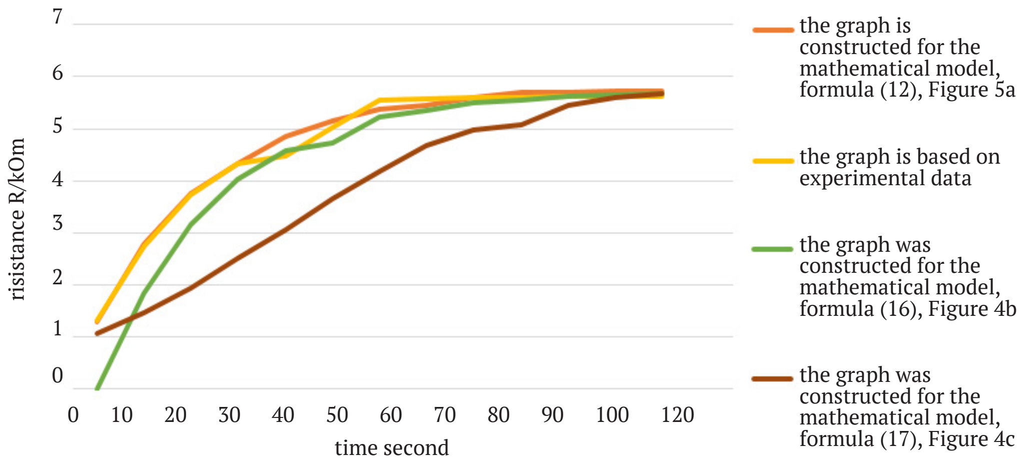

Figure 9. The graphs of the dependence R=f(t) for substitution schemes

To analyse the effect of the number of ions on changes in the conductivity of biological tissue, the scheme under consideration is shown in Figure 5b. The tourniquet applied to the guinea pig's paw stops blood flow in the tissue and prevents the flow of free ions. Such a study is important for determining the dynamics of ischaemia in the limbs and determining the time of the tissue's limiting state when a tourniquet is applied during domestic, industrial and military injuries

As is known from [8; 12], the main component of the biological tissue environment is blood, which is a solution of electrolytes. For example, blood plasma contains 0.32% NaCa, where the concentration of Na+ ions is 142 mmol/l, and K+ – 5 mmol/l. Current is a directed movement of positive and negative ions, which is defined for an electrolyte solution according to [4] as follows:

$$j_+=q_+\cdot n_+\cdot v_+;\ j_-=q_-\cdot n_-\cdot v_-, \tag{18}$$

where q_+ is the positive charge of the carrier, q_- is the negative charge of the carrier n_+, n_- are the number of positively and negatively charged ions, v_+, v_- are the concentration of positively and negatively charged ions, respectively.

The total current will be equal to: The total current will be equal:

$$G=j_++j_-=q_+\cdot n_+\cdot v_++q_-\cdot n_-\cdot v_-. \tag{19}$$

Expression (18) indicates that the electrical conductivity of biological tissue is proportional to n_+, n_- – the number of positively and negatively charged ions and v_+, v_- – the concentration of positively and negatively charged ions, respectively.

The rate of orderly movement of ions is directly proportional to Eion, which is caused by the movement of free charged ions under the influence of the source electric field and is defined:

$$V=g\cdot E_{ion}, \tag{20}$$

where g – coefficient of proportionality of media mobility.

The specific electrical conductivity δ for an electrolyte is written in the form:

$$\delta=\frac{1}{Z}=b_+\cdot n_+\cdot v_++b_-\cdot n_-\cdot v_-+b\cdot n\cdot v. \tag{21}$$

The input impedance of the biological tissue for the scheme of Figure 5c with a limited number of ions, having carried out similar calculations as for the scheme of Figure 5a, is determined by the expression:

$$Z^*_{inp4}=R_1+R_2\left(1-e^{-\frac{t}{\tau^*_{4.1}}}\right), \tag{22}$$

where $\tau^*_{4.1}$ – is the time constant of the ionisation process for a biological object with a reduced number of ions and is equal to $\tau^*_{4.1}=CR_2$.

The analysis of expressions (20), (21), (22) shows that the ionisation process time constant $\tau^*_{4.1}=C\cdot R_2$ directly depends on the number of charged ions, their concentration in the biological tissue, the level of intensity E_{ion}, the composition of salts in the biological tissue and is a constant value characterising the course of this process.

Biological tissue is complex and heterogeneous in composition and environment. Tissue contains not only sodium and potassium, but also other ions. The introduction of new elements (active resistances and unities) into the substitution scheme will allow us to study biological tissue with any ion composition. Figure 10 shows a substitution scheme for a biological tissue with a heterogeneous composition of n ions.

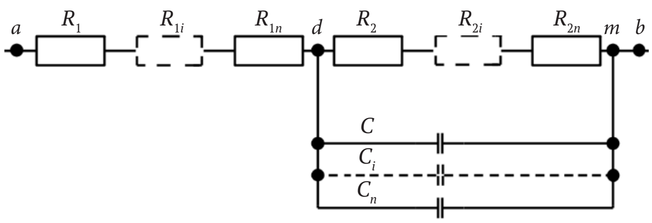

Figure 10. Scheme of replacement of biological tissue containing n-ions
Note: R_1, R_{1i}, R_{1n} – active components of impedance in the intercellular space, R_2, R_{2i}, R_{2n} – active resistance of tissue cells in a complex medium, C, C_i, C_n – capacitive component of impedance of tissue cells in a complex medium

Using the device, Figure 2, for invasive impedance measurement, data on changes in tissue impedance over time for different distances between needle electrodes were obtained, which are presented in Table 1.

Table 1. Results of studying the change in impedance over time depending on the distance between the needle electrodes

sec	0 kOm	10 kOm	20 kOm	30 kOm	40 kOm	50 kOm	60 kOm	70 kOm	80 kOm	90 kOm	100 kOm	110 kOm	120 kOm
L=1 cm	1.30	2.78	3.76	4.32	4.85	5.17	5.37	5.46	5.6	5.7	5.71	5.72	5.73
L=3 cm	1.65	3.16	4.10	4.65	5.16	5.42	5.67	5.86	5.99	6.13	6.34	6.34	6.42
L=5 cm	1.90	3.49	4.33	4.92	5.25	5.60	5.93	6.13	6.25	6.45	6.58	6.65	6.65

In Figure 11 shows the graphs of impedance changes in the transient period depending on the distance L between the needle electrodes, which were obtained experimentally. The studied biological object was not damaged after the completion of the research.

To investigate the use of the ionisation time constant as a diagnostic criterion, impedance changes were measured simultaneously invasively on two limbs in identical locations. A tourniquet was applied to one limb. Table 2 shows the results of the study.

In Figure 12 shows a graph of tissue impedance changes as a function of time. The tourniquet was applied to one paw, and the blood circulation was stopped for 30 minutes.

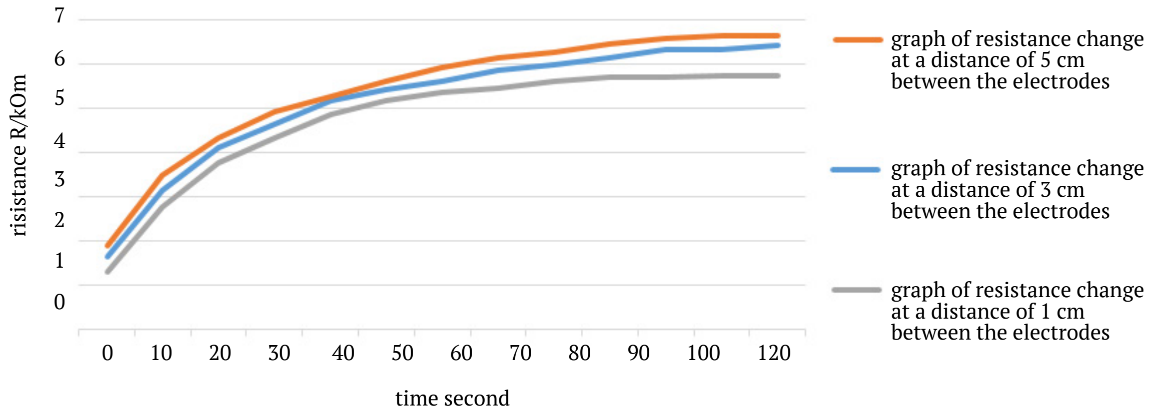

Figure 11. Dependence of the change in impedance $R=f(t)$, depending on the distance between the electrodes L=1 cm, L=3 cm and L=5 cm

Table 2. Impedance change measurement data over time

Time, sec	0	10	20	30	40	50	60	70	80	90	100	110	120
Limb without tourniquet	0.43	1.26	1.95	2.42	2.78	3.17	3.38	3.59	3.76	3.98	4.12	4.27	4.4
Limb from a tourniquet	1.1	2.89	3.82	4.53	5.12	5.65	6.06	6.50	6.79	7.17	7.46	7.69	7.98

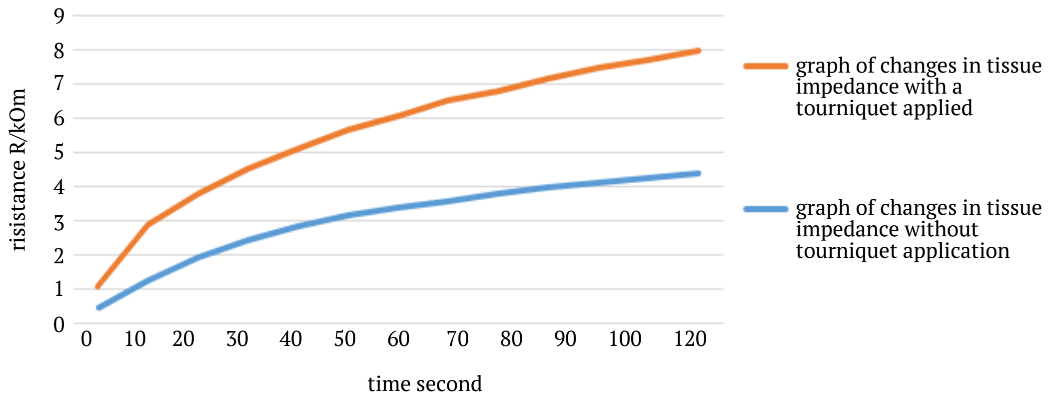

Figure 12. Graph of changes in tissue resistance depending on time, the tourniquet is applied to one paw for 30 minutes

Thus, this paper considers the issue of obtaining patterns of changes in the impedance of biological tissue under the influence of DC voltage in the transient process as an information parameter for the rapid diagnosis of limb muscle ischaemia. The authors proposed the introduction of an additional active resistance into the known electrical substitution circuit, which is traditionally used in AC voltage studies.

DISCUSSION

In well-known works, the issue of the influence of voltage of variable amplitudes and frequencies on biological tissue and the application of the obtained results for the diagnosis of a disease and its treatment is thoroughly studied. In [3; 9], the substitution scheme shown in Figure 4b. In [2; 6; 10], the substitution scheme shown in Figure 4c.

To substantiate the introduction of an additional active resistance in the proposed electrical substitution circuit, mathematical models for known substitution circuits were built and the change in $R=f(t)$ was analysed. Analysis of the results of the correspondence of the physiological process for the substitution schemes, Figure 4b and Figure 4c, and their corresponding mathematical models, expressions (15), (16), and (17), with the substitution scheme proposed by the authors, Figure 5, and the mathematical model, expression (12), for the transient mode under the action of a DC voltage, was carried out by comparing the compliance coefficient - q, which is determined by Eq:

$$q = \left(1 - \frac{S_{ex}}{S_{inp\ i}}\right) \cdot 100\%, \quad (23)$$

where S_{ex} – is the result of integration of the experimentally obtained function $Z=f(t)$, which is defined by the expression; $S_{ex}=\int_0^{100} Z_{inp\ i}dt$; $S_{inp\ i}$ – the result of integration of the function $Z=f(t)$ of each mathematical model. $S_{inp\ i}=\int_0^{100} Z_{inp\ i}dt$.

The numerical values used in the integration were obtained as a result of experiments, so the ionisation time constant is τ=25 seconds, the active components are R_1=1,3 kOm, R_2=4.43 kOm. The calculation results are shown in Table 3.

Table 3. The results of calculating the compliance ratio

	The proposed replacement scheme is shown in Figure 5	The substitution scheme is shown in Figure 4b, used in [5; 8; 10]	The substitution scheme is shown in Figure 4c, used in [3; 6; 14]
The value of the matching coefficient.	2.8%	13.8%	18.7%

The proposed electrical substitution scheme and its mathematical model have a convergence with experimental data of up to 3%, depending on the traditional substitution schemes, which have a convergence of 13% and higher.

Thus, the introduction of an additional active resistance in the electrical circuits of biological tissue replacement, under the action of a DC voltage, allows to study the transient ionisation process and increase the reliability of the results obtained in determining the impedance components with a reliability of ±3%. The field measurements of the impedance change during the transient process allowed us to confirm that the ionisation time constant is equal to $\tau = \frac{1}{4}T_{ion}$ with a probability (P=0.95), where T_{ion} is the transient time. This allows us to more reliably determine the capacitive component of the tissue under study. The capacitive component for the proposed substitution scheme is $C = \frac{25}{4{,}43} = 5{,}64 \cdot 10^{-3}$ F, for the traditional substitution schemes $C = \frac{25}{5{,}73} = 4{,}16 \cdot 10^{-3}$F, and the difference is 35.5%.

An analysis of expressions (12), (15) and (16) and the graphs in Figure 9, shows that traditional substitution circuits should be used for studies under the action of voltage of variable frequencies and amplitudes, as well as in steady-state modes under the action of DC voltage. To study the transient process, it is necessary to use an adjusted electrical substitution scheme.

In the reviewed and analysed results of well-known works [5; 8; 10] and [3; 6; 14], the invasive method of measuring the impedance of biological tissue is not considered. The analysis of the obtained data of the impedance components by the invasive method, shown in the graph (dependence $R=f(t)$ for different distances between electrodes in Figure 10), shows that the active component of the impedance, both intercellular and cellular, varies according to a linear law depending on the distance between the electrodes, which corresponds to the pattern according to formula (1). The capacitive component, formula (2), which leads to the transient process caused by ionisation, does not change. The sensitivity of the needle sensor increases by (8-9)% when the distance between the electrodes is reduced by every ΔL=1 cm. To study the change in impedance in an invasive way, it is sufficient to have a distance of -1 cm between the needle electrodes, which makes the sensor compact and less traumatic.

The theoretically obtained dependence $R=f(t)$ according to expression (12) for the proposed replacement circuit shown in Figure 5 gives the right to assert that at the initial time (t=0), the resistance of biological tissue is not zero, which is confirmed by experimental data. The additional resistance of the replacement circuit corresponds to the active resistance of the intercellular space, which limits the initial input current, so the active resistance at the initial time (t=0) is within 1-2.0 kΩ.

The authors first proposed a method for diagnosing changes in the properties of biological tissue in case of blood flow disorders using a direct current voltage in the transient ionisation process. Papers [6; 16; 17; 27; 28] consider methods of using impedance changes to diagnose and determine the composition of biological tissue with subsequent treatment of deviations. Paper [26] presents a method for diagnosing skin myeloma. All of these methods use AC voltage and frequency, which requires sophisticated equipment and a certain amount of time for research. The article proposes a method of rapid diagnosis - the diagnostic period takes from 100s to 120s, which does not require sophisticated equipment.

The proposed method is based on the comparison of two simultaneously obtained integrated functions q of healthy and diseased tissue and the analysis of the relativity coefficient -q, which is determined by the formula $q = \left(1 - \frac{S_{ex}}{S^{*}_{ex}}\right) \cdot 100\%\cdot$

Where S_{ex} – is the result of integrating the function $Z=f(t)$ without a tourniquet; S^{*}_{ex} – is the result of integrating the function $Z=f(t)$ with a tourniquet applied.

If the relativity coefficient is q=0±0.05%, this indicates unchanged properties of biological tissues in both limbs.

If the relativity coefficient varies – q=0.05% to 1, it indicates changes in the properties of biological tissues in both limbs.

At a value of q=0.5 and below, it indicates the presence of irreversible processes of ischaemia in muscle tissue.

The data presented in Table 2 and the graphs shown in Figure 12 show that the comparison of two integral ionisation functions in biological tissue without a tourniquet and in tissue with a tourniquet is a criterion parameter for diagnosing the development of ischaemia.

CONCLUSIONS

Traditional electrical substitution circuits and their corresponding mathematical models should be used to study changes in biological tissue under the influence of alternating frequency voltage or in steady-state mode under the influence of direct current voltage. When using these substitution schemes to study the transient process under DC voltage, the error of the results obtained is 13% and higher. To study ionisation transients under DC voltage, it is necessary to use a corrected electrical substitution circuit with an additional active resistance. The introduction of an additional active resistance made it possible to obtain a convergence of the experimentally obtained measurements with the analytically obtained results up to ±3%, which indicates that the developed mathematical model is suitable for describing the transient process occurring in biological tissue under the action of a DC voltage.

It is analytically confirmed that the ionisation time constant can be determined with confidence (P=0.95) from the experimental data as $\tau = \frac{1}{4}T_{ion}$, where T_{ion} is the time of the transient process.

The mathematical model of the corrected electrical substitution scheme allowed us to obtain numerical values of the capacitive components of the impedance. The reliability of the determined capacitive component of the impedance compared to traditional substitution circuits and their corresponding mathematical models increased by 35%, which made it possible to determine and control the composition of biological tissue. Based on the results obtained, an electrical substitution circuit was developed for the complex composition of the biological environment.

Based on the results of the transient process study, a method for detecting changes in the properties of biological tissue in case of circulatory disorders was developed. The time of the transient process is 100s-120s, which allows for rapid diagnosis of ischemia of the patient's limb muscle tissue.

The method is based on the comparison of two simultaneously obtained integrated functions of healthy and diseased tissue and the analysis of the relativity coefficient -q, which is determined by the formula $q = \left(1 - \frac{S_{ex}}{S_{ex}^{*}}\right) \cdot 100\%$, where S_{ex} is the result of integrating the function Z=$f(t)$ without a tourniquet, S_{ex}^{*} is the result of integrating the function Z=$f(t)$ with a tourniquet. If the relativity coefficient is q=0±0.05%, this indicates that the properties of biological tissues in the two limbs are unchanged. If the relativity coefficient varies from 0.05% to 1, it indicates changes in the properties of biological tissues in both limbs. At the value of q=0.5 and below, it indicates the presence of irreversible processes of ischaemia development in muscle tissue. Thus, it was established that when simultaneously measuring the change in impedance in two identical limb areas, the ionisation time constant is a criterion parameter in the study of ischaemia development.

The obtained results of experimental and analytical studies have shown that, depending on the set tasks and goals of studying changes in biological tissues, electrical substitution schemes adequately describe the physiological processes of a biological object when corrected.

The development of rapid diagnostic methods based on data obtained in the transient processes of biological tissue ionisation requires further research together with the results of changes in tissue properties obtained by biopsy.

REFERENCES

[1] Jiang, Zh., Yao, J., Wang, L., Wu, H., Huang, J., Zhao, T., & Takei, M. (2019). Development of a portable electrochemical impedance spectroscopy system for Bio-detection. *IEEE Sensors Journal*, 19(15), 5979-5987. doi: 10.1109/JSEN.2019.2911718A.

[2] Gupta, A., Sharma, A., Batra, P., & Kapoor, R. (2013). *Bioelectrical impedance: A future healthcare technology*. Noida: AMITY University.

[3] Koutsouras, D.A., Lingstedt, L.V., Lieberth, K., Reinholz, J., Mailänder, V., Blom, P.W.M., & Gkoupidenis, P. (2019). Probing the impedance of a biological tissue with PEDOT:PSS-Coated metal electrodes: Effect of electrode size on sensing efficiency. *Advanced Healthcare Materials*, 8(23). doi: 10.1002/adhm.201901215.

[4] Illarionov, V., Solovev, M., Yuldashev, Z., Khapaev, R., & Nimaev, V. (2019). Three-frequency bioimpedance method of evaluating extracellular and intracellular fluid volumes, fat and muscle mass parameters on groups of patients with untypical body structure. *2019 International Multi-Conference on Engineering, Computer and Information Sciences*, 2019, 0344-0346. doi: 10.1109/SIBIRCON48586.2019.8958288.

[5] Naranjo-Hernández, D., Reina-Tosina, J., & Min, M. (2019). Fundamentals, recent advances, and future challenges in bioimpedance devices for healthcare applications. *Journal of Sensors*, 2019, article number 9210258. doi: 10.1155/2019/9210258.

[6] Mansoorifar, A., Koklu, A., Ma, Sh., Raj, G.V., & Beskok, A. (2018). Electrical impedance measurements of biological cells in response to external stimuli. *Analytical Chemistry*, 90(7), 4320-4327. doi: 10.1021/acs.analchem.7b05392.

[7] Tereshchenko, S.M., Tsapenko, V., & Chuhrayev N. (2017). Study of the effect of direct and alternating current on biological objects, *Bulletin of Kyiv Polytechnic Institute. Series Instrument Making*, 53(1), 87-94.

[8] Oh, S.H., Lee, B.I., Woo, E.J., Lee, S.Y., Kim, T.S., Kwon, O., & Seo, J.K. (2005). Electrical conductivity images of biological tissue phantoms in MREIT. *Physiological Measurement*, 26(2), 279-288. doi: 10.1088/0967-3334/26/2/026

[9] Tereshchenko, N.F., Tsapenko, V.V., & Chuhraev, N.V. (2017). Research of electrical conductivity of biological animals. *Bulletin of NTUU "KPI". Instrumentation Series*. 53(1), 87-94.

[10] Yao, J., Wang, L., Liu, K., Wu, H., Jingshi, H., & Li, J. (2019). Evaluation of electrical characteristics of biological tissue with electrical impedance spectroscopy. *Electrophoresis*, 41(16-17), 1425-1432. doi: 10.1002/elps.201900420.

[11] Bera, T.K. (2018). Bioelectrical Impedance and the frequency dependent current conduction through biological tissues: A short review. *IOP Conf. Series: Materials Science and Engineering*, 331, article number 012005. doi: 10.1088/1757-899X/331/1/012005.

[12] Antonyuk, V.S., Bondarenko, M.O., Vashchenko, V.A., Kanashevich, G.V., Tymchyk, G.S., & Yatsenko, I.V. (2012). *Biophysics and biomechanics*. Kyiv: NTUU "KPI".

[13] Didukh, V.D., Rudyak, Yu.A., & Bagrii-Zaiats, O.A. (2021). *Biological physics with physical methods of analysis*. Ternopil: Publishing House "Textbooks and Manuals".

[14] Freeborn, T.J., & Critcher, S. (2021). Cole-impedance model representations of right-side segmental arm, leg, and full-body bioimpedances of healthy adults: Comparison of fractional-order. *Fractal and Fractional*, 5(1), article number 13. doi: 10.3390/fractalfract5010013.

[15] Prasad, A., & Roy, M. (2020). Bioimpedance analysis of vascular tissue and fluid flow in human and plant body: A review. *Biosystems Engineering*, 197, 170-187.

[16] Bera, T.K. (2014). Bioelectrical impedance methods for noninvasive health monitoring: A review. *Journal of Medical Engineering*, 2014, article number 381251. doi: 10.1155/2014/381251.

[17] Roy, A., Mallick, A., Das, S., & Aich, A. (2020). An experimental method of bioimpedance measurement and analysis for discriminating tissues of fruit or vegetable. *AIMS Biophysics*, 7(1), 41-53. doi: 10.3934/biophy.2020004.

[18] Bera, T.K., Jampana, N., & Lubineau, G. (2016). A LabVIEW-based electrical bioimpedance spectroscopic data interpreter (LEBISDI) for biological tissue impedance analysis and equivalent circuit modeling. *Journal of Electrical Bioimpedance*, 7(1), 35-54. doi: 10.5617/jeb.2978.

[19] Law of Ukraine No. 3447-VI "On the Protection of Animals from Cruelty". (2012, October). Retrieved from https://zakon.rada.gov.ua/laws/show/3447-15#Text.

[20] Reznikov, O.G. (2003). General ethical principles of experiments on animals. The first national congress on bioethics. *Endocrinology*, 8(1), 142–145.

[21] European convention for the protection of vertebrate animals used for experimental and other scientific purposes. (1986). Retrieved from https://rm.coe.int/168007a67b.

[22] Universal Declaration on Animal Welfare. (2007). Retrieved from https://www.worldanimalprotection.ca/sites/default/files/media/ca_-_en_files/case_for_a_udaw_tcm22-8305.pdf.

[23] Kryvonosov, V. (2017). Diagnostics of the state of insulation of an asynchronous motor and a supply cable under conditions of local compensation. *Energy. International Scientific and Technical Magazine*, 60(6), 536-543.

[24] Kryvonosov, V., & Vasilenko, S. (2015). Influence of a dusty environment on the service life of the stator windings of asynchronous motors. *Energy. International Scientific and Technical Magazine*, 58(6), 35-40.

[25] Boyko, V.S., Boyko, V.V., Vydolob, Yu.F., Kurylo, I., Shekhovtsov, V., & Shidlovska, N. (2004). *Theoretical foundations of electrical engineering* (Vol. 1). Kyiv: IVC "Polytechnic Publishing House".

[26] Tereshchenko, M.F., Martynenko, V.I., & Yakovenko, I.O. (2020). Patent of Ukraine No. 144016 "Method of complex bioimpedancemetry". Retrieved from https://iprop-ua.com/inv/sfzjfjbl/.

[27] Bobyr, S. (2021). Theoretical Aspects of Hydrogen Diffusion in Metals. *Scientific Herald of Uzhhorod University. Series "Physics"*, (50), 31-38.

[28] Bence, N., Lengyel, A. & Tarics, Z. (2022). A simple model for describing the minimum differential cross-section of elastic proton scattering on protons at high energies. *Scientific Herald of Uzhhorod University. Series "Physics"*, (51), 30-38.

Валерій Єгорович Кривоносов
Доктор технічних наук, професор
Національний університет біоресурсів і природокористування України
03041, вул. Героїв Оборони, 15, м. Київ, Україна
https://orcid.org/0000-0002-8219-021X
Наталія Дмитрівна Пруднікова
Кандидат технічних наук
Національний університет біоресурсів і природокористування України
03041, вул. Героїв Оборони, 15, м. Київ, Україна
Лілія Володимирівна Мартинюк
Національний університет біоресурсів і природокористування України
03041, вул. Героїв Оборони, 15, м. Київ, Україна

Обґрунтування електричної схеми заміщення біологічної тканини при дії напруги постійного струму

Анотація. Зміна імпедансу біологічної тканини під дією напруги використовується в діагностиці та лікуванні різних захворювань. Математичні моделі, що описують фізико-біологічні процеси в біологічних об'єктах, засновані на електричних схемах заміщення. Метою цієї роботи було дослідження зміни імпедансу біологічної тканини в перехідному процесі іонізації під дією напруги постійного струму. В роботі застосовано біоімпендантний метод при впливі на біологічну тканину напруги постійного струму з урахуванням закону комутації у перехідних процесах іонізації. Було проведено аналіз відомих схем заміщення виявлені недоліки їх застосування при вивчені перехідних процесів іонізації в тканині при дії напруги постійного струму та обґрунтовано, як аналітично так і експериментально, схему заміщення із запровадженням додаткового опору. Було здійснено інвазійний вимір зміни імпедансу голчастими електродами, доведено, що активна складова пропорційно залежить від відстані меж електродами, а ємкісна складова залишається незмінною. Показано, що постійна часу іонізації є крітеріальним параметром та може використовуватись в діагностиці розвитку ішемічної хвороби м'язової тканини, зміна стану біологічної тканини при зупинці кровотоку під час накладання кровоспинного джгута. Доведено, що постійна часу іонізації не змінюється при незмінному іонному складу тканини і може використовуватися при аналізу складу міжклітинного простору. Було проведено одночасне інвазійне вимірювання у двох ідентичних місцях різних кінцівок, на однієї було накладено кровоспинний джгут. Отримані результати дозволили зробити висновки, що зміна постійної часу від 15 % до 50 % у порівнянні двох постійних часу дозволяє робити експрес діагностики, протягом 2 хвилин, стану біологічної тканини і може використовуватись при вивченні розвитку хвороби пов'язаних з ішемією. Результати дослідження можуть використовуватися при експрес діагностиці стану біологічного об'єкту та створенні не дорогого приладу для його застосування в хірургії та дослідних лабораторіях при вивчені розвитку ішемії

Ключові слова: імпеданс; перехідний процес; процес іонізації; опір клітини; ємність; постійна часу іонізації; діагностика; ішемія

Machinery & Energetics
Vol. 13, No. 4. 2022

Journal homepage:
https://technicalscience.com.ua/en

UDC 621.87
DOI: 10.31548/machenergy.13(4).2022.72-80

Yuriy Romasevych
Full Doctor in Technical Sciences
National University of Life and Environmental Sciences of Ukraine
03041, 15 Heroiv Oborony Str., Kyiv, Ukraine
https://orcid.org/0000-0001-5069-5929

Viacheslav Loveikin
Full Doctor in Technical Sciences
National University of Life and Environmental Sciences of Ukraine
03041, 15 Heroiv Oborony Str., Kyiv, Ukraine
https://orcid.org/0000-0003-4259-3900

Valery Makarets*
Postgraduate Student
National University of Life and Environmental Sciences of Ukraine
03041, 15 Heroiv Oborony Str., Kyiv, Ukraine
https://orcid.org/0000-0002-9116-0784

PID-controller tuning algorithm development for a "crane-load" dynamical system

Abstract. One of the main problems in the operation of cranes is the oscillation of the load on a flexible suspension. One of the ways to eliminate load oscillations on a flexible suspension is to use a proportional-integral-differential controller that generates a control signal for the crane movement. However, for it to function properly, it must be properly tuned. Standard approaches to tuning a PID controller, which is common in the practice of engineering calculations, do not allow solving this problem, and that is why it can be considered as a scientific and applied one. The research aims to develop an algorithm for tuning a proportional-integral-differential controller. For this purpose, a research issue was defined, which includes a mathematical model of the dynamic system, constraints on the overload capacity of the crane drive and the control function, conditions for achieving the steady-state speed of the crane and eliminating pendulum oscillations of the load on a flexible suspension. Using the modified particle swarm method, ME-D-PSO, the coefficients of the proportional-integral-differential controller were determined for a wide range of values of the load mass and the length of the flexible suspension. Based on the obtained values of the coefficients, an algorithm is presented that allows calculating the values of the coefficients for any values of the load mass and the length of the suspension. The dynamics of the movement of the crane-load system are analyzed for the smallest and largest selected parameters and for the case obtained by applying the developed algorithm. Practical application of the developed algorithm will allow obtaining optimal values of the proportional-integral-differential controller, which in turn eliminates oscillations of the load on a flexible suspension during crane operation, which in turn increases the safety of crane operation, structural durability, and increases the crane's capacity

Keywords: mathematical model; constraints; load pendulum oscillations; particle swarm method; capacity

Article's History: Received: 03.06.2022; Revised: 30.09.2022; Accepted: 23.11.2022.

Suggested Citation:
Romasevych, Yu., Loveikin, V., & Makarets, V. (2022). PID-controller tuning algorithm development for a "crane-load" dynamical system. *Machinery & Energetics,* 13(4), 72-80

*Corresponding author

INTRODUCTION

It is difficult to overestimate the importance of cranes in modern manufacturing, agriculture, or logistics. To improve the quality of crane operation, it is necessary to ensure the high capacity of hoisting machines. One of the modern approaches to solving this problem is the use of PID controllers (proportional-integral-differential controllers) to control the movement of crane mechanisms. This allows optimizing crane operation by reducing dynamic loads in the crane's metal structure and drive, ensuring energy efficiency, and reducing wear and tear on crane components.

Many scientists worked on developing methods for tuning PID controllers. For example, in [1], the author proposed an algorithm for tuning the proportional, integral, and differential coefficients of a PID controller using fuzzy logic methods based on logical and linguistic models. The structure of an automatic control system based on a fuzzy PID controller was developed, the main components of which are a fuzzy PID controller and the transfer function of the plant.

The authors of [2] proposed an autotuning method that consists in estimating the key points of transients in a relay identification experiment and then applying the proposed analytical dependencies to find the optimal set of PID controller tuning parameters.

In [3], the authors proposed a method for reducing load oscillations on a flexible suspension using proportional-differential (PD) and PID controllers. The PD controller affects the dynamics of crane movement, and the PID controller affects the movement of the load. The criteria of the integral of the absolute and quadratic error were used to tune the PID controller. The particle swarm method (PSO) was used to find the optimal coefficients of the controllers.

In [4], the authors gains the PSO method to tune the PID-PD controller. The time criterion function was used for control. The main task of the criterion used is to track the time spent on lifting and lowering the load and re-regulation. The PID controller is used for positioning the overshoot crane, and the PD controller is used to control the oscillations of the load.

In [5], the authors developed a method for reducing load fluctuations using a PID controller, which was tuned using a oscillations PSO algorithm and a simulation annealing algorithm (SA).

The authors of [6] proposed the Ziegler-Nichols method to tune the PID controller. The PID controller controls the position of a crane that transports load with maximal speed.

In [7], the authors proposed a method of automatic PID controller tuning using the method of differential evolution to determine the optimal values of the controller gains that satisfy the stability criterion of Kharitonov polynomials.

In [8], the authors proposed a method for tuning a PID controller using fuzzy logic, genetic algorithms, and the bee algorithm. The research proposes replacing the PID controller with a fuzzy logic controller. PID controllers tuned using genetic and bee algorithms are used to control linear horizontal motion.

In [9], the authors propose an intelligent hybrid structure used for the online tuning of a PID controller. It is based on two adaptive neural networks, both with built-in Chebyshev and orthogonal polynomials. The first neural network with an endocrine factor is used to approximate control signals that are introduced in the form of stimuli from the environment. These, in turn, are used to adapt the second neural network, whose main task is to generate control signals.

The authors of [10] proposed an intelligent crane control system with communication delays that can learn from past mistakes and use genetic algorithms to adjust the PID controller. The new parameters of the PID controller are memorized and if a similar delay occurs in the future, the parameters are read from the memory.

In the analyzed sources, the authors concentrate on solving a narrow range of problems of moving a crane with a load with the elimination of load oscillations. However, they did not consider the factors of the duration of elimination of pendulum oscillations of the load, the constraints imposed on the crane drive mechanisms, the variability of the parameters of the dynamic system, etc. In this work, all these factors are addressed.

MATERIALS AND METHODS

To conduct the research, a two-axis dynamic model was used, as shown in Figure 1. The model (Fig. 1) has been tested for research tasks and for controlling pendulum oscillations of a load on a flexible suspension [11-13].

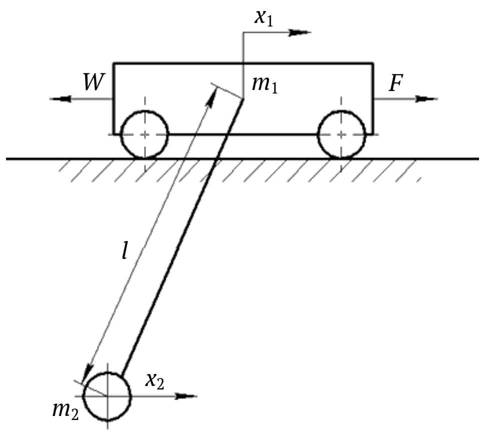

Figure 1. A dynamic model of the "crane-load" movement system
Source: compiled by the authors

The dynamic model shown in Figure 1, is described by the mathematical model (1):

$$\begin{cases} F - W = m_1\ddot{x}_1 + m_2\ddot{x}_2; \\ x_1 = x_2 + \frac{l}{g}\ddot{x}_2, \end{cases} \quad (1)$$

where x_1 and x_2 – generalized coordinates of the combined masses of the crane and the load respectively; m_1

and m_2 – total mass of the crane and load respectively; F – total driving or braking force of the crane drive; W – the force of static resistance to crane movement (W=(m_1+m_2) g·0,01); l – length of flexible load suspension; g – free-fall acceleration.

Differentiating the second equation of system (1), the following is true:

$$\dot{x}_1 = \dot{x}_2 + \frac{l}{g}\dddot{x}_2. \tag{2}$$

Differentiating the resulting expression (2), the following is true:

$$\ddot{x}_1 = \ddot{x}_2 + \frac{l}{g}\overset{IV}{x}_2. \tag{3}$$

Substituting (3) into the first equation of system (1), the result is as follows:

$$\begin{aligned} F - W = m_1\left(\ddot{x}_2 + \frac{l}{g}\overset{IV}{x}_2\right) + m_2\ddot{x}_2 = m_1\ddot{x}_2 + \\ +m_1\frac{l}{g}\overset{IV}{x}_2 + m_2\ddot{x}_2 = (m_1 + m_2)\ddot{x}_2 + m_1\frac{l}{g}\overset{IV}{x}_2. \end{aligned} \tag{4}$$

Simplify equation (4):

$$F - W = (m_1 + m_2)\ddot{x}_2 + m_1\frac{l}{g}\overset{IV}{x}_2. \tag{5}$$

Dividing the result by m_1, the output is:

$$\frac{F-W}{m_1}\frac{g}{l} = \frac{m_1+m_2}{m_1}\frac{g}{l}\ddot{x}_2 + \overset{IV}{x}_2. \tag{6}$$

Let introduce some denotions:

$$\frac{\text{F-W}}{m_1} = u, \frac{m_1+m_2}{m_1}\frac{g}{l} = \Omega^2, \frac{g}{l} = \Omega_0^2,\ \dot{x}_2 = v_2, \tag{7}$$

where u – crane acceleration, v_2 – load velocity on flexible suspension; Ω and Ω_0 – "crane-load" system for the movable and mathematical pendulum.

The following is true:

$$u\Omega_0^2 = \dot{v}_2\Omega^2 + \dddot{v}_2. \tag{8}$$

The 3rd-order equation (8) is represented as three first-order equations (9):

$$\begin{cases} \dot{v}_2 = a_2; \\ \dot{a}_2 = b_2; \\ b_{\dot{2}} = u\Omega_0^2 - a_2\Omega^2. \end{cases} \tag{9}$$

where a_2 – load acceleration; b_2 – load jerk (rate of acceleration change).

The constraints associated with the overload capacity of the crane movement drive can be represented as follows:

$$u_{min} \leqslant u \leqslant u_{max}, \tag{10}$$

where u_{min} and u_{max} – maximum and minimum possible values of crane acceleration.

To ensure the elimination of oscillations of the load on a flexible suspension and the crane's reaching a steady-state speed, a PID controller will be used [14-16]. It's generally accepted mathematical model is as follows:

$$\begin{cases} u_0 = K_P e + K_I \int_0^t e dt + K_D \frac{de}{dt}; \\ e = V - v_2, \end{cases} \tag{11}$$

where e – load velocity regulation error; K_P, K_I, and K_D – gains of the proportional, integral, and differential components of the PID controller; V – constant movement speed of the crane and load on a flexible suspension; u_0 – control function (signal from the PID output). Given the constraints imposed by (10), the following is obtained:

$$u = \begin{cases} u_0, \text{if } u_{min} \le u \le u_{max}; \\ u_{max}, \text{if } u_0 \ge u_{max}; \\ u_{min}, \text{if } u_0 \le u_{min}. \end{cases} \tag{12}$$

Thus, it is necessary to find the values K_P, K_I, and K_D, that would ensure the meeting of the control problem, namely, the output of the trolley to a steady-state speed at which the acceleration and load jerk will be equal to zero. As such, it is possible to note:

$$\begin{cases} \lim\limits_{t\to\infty} v_2 = V; \\ \lim\limits_{t\to\infty} a_2 = 0; \\ \lim\limits_{t\to\infty} b_2 = 0. \end{cases} \tag{13}$$

However, for practical purposes, the expression t→∞ does not meet the conditions of crane operation. Therefore, the expressions (13) are replaced by the following:

$$\begin{cases} v_2(T) = V \pm \Delta v; \\ a_2(T) = 0 \pm \Delta a; \\ b_2(T) = 0 \pm \Delta b, \end{cases} \tag{14}$$

where Δv, Δa, Δb – permissible deviations of the speed, acceleration, and load jerk from the set values (13) at a given time T; T – duration of the controlled crane movement mode.

For variables m_2 and l coefficients K_P, K_I and K_D of the PID controller will be different. Therefore, the problem of tuning the PID controller for different combinations of m_2 and l was solved many times. In each such problem, conditions (14) were set. The solution to each problem was obtained using the ME-D-PSO particle swarm method [17]. A swarm of 30 particles was used for the solution and 200 calculation iterations were performed. In each problem, the values of m_2 and l were varied within certain limits that correspond to the conditions of crane operation practice: the mass of the load was varied from 500 kg to 20,000 kg in increments of 500 kg; the length of the flexible load suspension was varied from 2 to 12 meters in increments of 1 meter. From the data obtained as a result of the calculation, a data array is created that includes 451 sets of gains K_R, K_I, and K_D of the PID controller.

RESULTS AND DISCUSSION

In the operation of cranes, such ratios are not common. Therefore, the PID controller needs to be set in such a way as to obtain results regardless of the load mass and the length of the flexible suspension.

For example, the case of applying this methodology to the parameters m_2=18700 kg ang l=11.5 m was considered.

The algorithm diagram for finding the PID controller coefficients is shown in Figure 2.

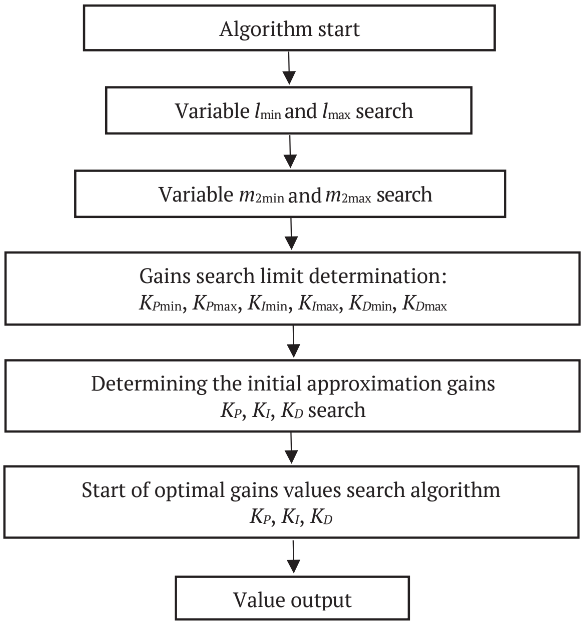

Figure 2. Diagram of searching for PID controller gains

Source: compiled by the authors

First, the tabulated values of the length of the flexible suspension and the mass of the load are found, for which the following inequalities are valid:

$$l_{min} \leqslant l_r \leqslant l_{max};\ m_{2min} \leqslant m_{2r} \leqslant m_{2max}, \tag{15}$$

where m_{2r} and l_r – the actual mass of the load and the length of the flexible suspension (certain values for the crane movement cycle with a load on a flexible suspension); l_{min} and l_{max} – the minimum and maximum tabulated values of the length of the flexible suspension for which the inequalities are valid (15); m_{2min} and m_{2max} – the minimum and maximum tabulated values of the cargo weight for which the inequalities are valid (15).

Next, the coefficients K_P, K_I, K_D are determined for four parameter combinations: l_{min}, m_{2min}; l_{min}, m_{2max}; l_{max}, m_{2min}; l_{max}, m_{2max} (Table 1).

Table 1. Values of the gains K_P, K_I, K_D for all possible combinations l_{min}, m_{2min}; l_{min}, m_{2max}; l_{max}, m_{2min}; l_{max}, m_{2max}

Coefficients Parameters	K_P	K_I	K_D
l_{min}, m_{2min}	K_{P1} = 4.023	K_{I1} = 6.491	K_{D1} = 19.756
l_{min}, m_{2max}	K_{P2} = 3.854	K_{I2} = 6.305	K_{D2} = 19.114
l_{max}, m_{2min}	K_{P3} = 2.962	K_{I3} = 4.541	K_{D3} = 14.899
l_{max}, m_{2max}	K_{P4} = 3.815	K_{I4} = 5.918	K_{D4} = 19.365

Source: compiled by the authors

Next, using the created array of gains K_P, K_I, K_D define the boundaries of their search. Using the array, the already calculated gains for the crane parameters are selected, which are one step less and one step more than the desired parameters.

For the example of calculation under consideration, using Table 1, the following search boundaries are obtained: K_{Pmin}=K_{P3}, K_{Pmax}=K_{P1}, K_{Imin}=K_{I3}, K_{Imax}=K_{I1}, K_{Dmin}=K_{D3}, K_{Dmax}=K_{D1}. For the option considered in this case: l_{min}=11 m, l_{max}=12 m, m_{2min}=18500 kg, m_{2max}=19000 kg.

The next step is to calculate initial gains values for K_P, K_I, K_D (first iteration) from which the search for values for the "crane-load" system parameter variant will begin m_2=m_{2r}, l=l_r. These initial values of the gains are determined as an arithmetic average for all 4 options (Table 1). For example, for the proportional component of the K_R, the following is true:

$$K_{P.0} = \frac{K_{P1}+K_{P2}+K_{P3}+K_{P4}}{4}, \tag{16}$$

where $K_{P.0}$ – initial gains value K_P, from which the search for value K_P is started. Initial values for gains $K_{I.0}$ and $K_{D.0}$ are determined similarly.

The following algorithm is used to find the values of the gains K_P, K_I, K_D for set values m_2 and l, based on the modified particle swarm method ME-D-PSO [10]. In this case, the optimization criterion is the following expression obtained based on conditions (14):

$$\underset{K_P,K_I,K_D}{argmin}(V - v_2(T))^2 + (a_2(T))^2 + (b_2(T))^2. \quad (17)$$

The algorithm presented in the flowchart (Figure 2) allows to quickly obtain the values of the coefficients K_P, K_I, K_D.

To analyze the dynamics of motion control of the dynamic system, three options were chosen: at the lowest values of the load mass and the length of the flexible suspension (l=2 m, m_2=500 kg) – the first option; at the highest values (l=11,5 m, m_2=18700 kg) – the second option and for (l=12 m, m_2=20000 kg) – third variant. The values of the gains used in the calculation of these parameters are shown in Table 2.

Table 2. Gains value K_P, K_I, K_D for three variants used to analyze the efficiency of the algorithm

Coefficients Parameters	K_P	K_I	K_D
l = 2 m, m_2 = 500 kg	2. 027	5. 706	12. 449
l = 11,5 m, m_2 =18700 kg	3. 348	5. 250	16. 707
l = 12 m, m_2 = 20000 kg	2. 553	3. 924	12. 883

Source: compiled by the authors based on research

Figure 3 shows the phase profile of load oscillations during crane acceleration to the steady-state speed V. As can be seen from Figure 3a, the maximum load deflection is 0.26 m, and in Figures 3b and 3c, it is 0.98 m, which is explained by the longer length of the flexible suspension. In addition, the shapes of the phase trajectories are also different, as can be seen in Figure 4. They are caused by the form of change in the driving force: for the first case, it changes smoothly, not reaching the minimum limit (minimum allowable control).

Figure 4 shows plots of changes in the driving and braking forces of the crane drive.

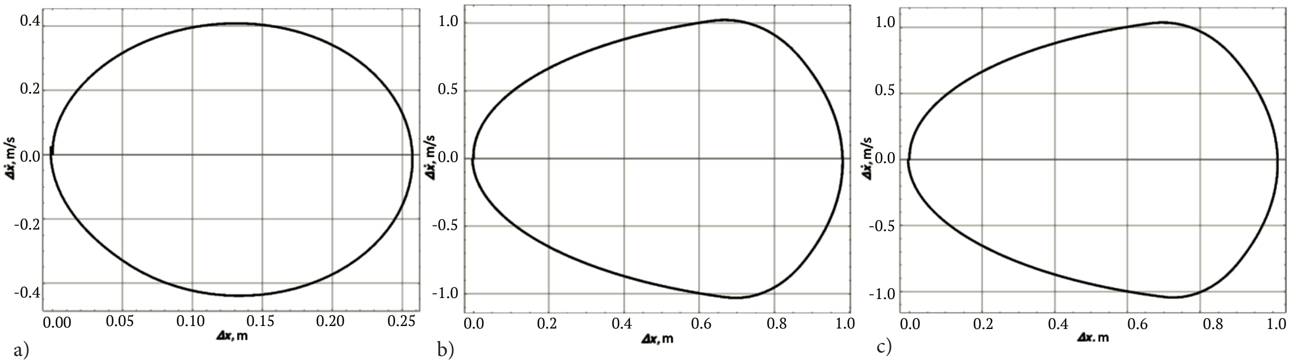

Figure 3. The phase profile of load pendulum oscillations during crane acceleration:
a) l=2 m, m_2=500 kg, b) l=11.5 m, m_2=18700 kg c) l=12 m, m_2=20000 kg

Source: compiled by the authors

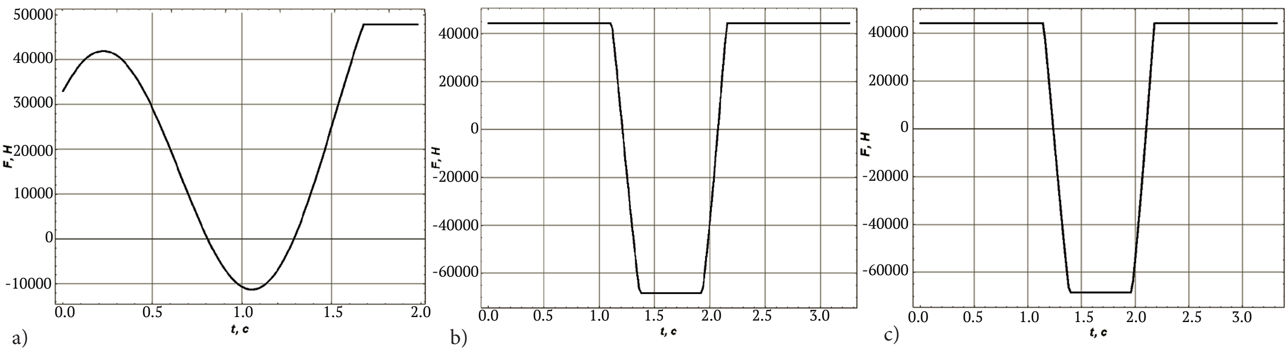

Figure 4. Plots of changes in crane drive force:
a) l=2 m, m_2=500 kg, b) l=11.5 m, m_2=18700 kg c) l=12 m, m_2=20000 kg

Source: compiled by the authors

As can be seen from Figure 4, the duration of the movement of the dynamic system for the first variant is 2 s, and for the second 3.5 s. This is since with an increase in the length of the flexible suspension, the period of oscillation of the load increases, so more time is needed to eliminate oscillations in the second case.

Figure 4 demonstrates the force in both cases having a familiar character. The decrease in force for the first case

(Figure 4a) is smooth and starts at 0.4 s. The force reaches its minimum value (-11000 N) at 1.1 s. Figure 4c shows that the change in force occurs abruptly from 1.4 s to 2 s. The force reaches its minimum value (-68000 N) from 1.3 s to 1.9 s. Figure 4b is similar to Figure 4c, but in the case of Figure 4c, the change in force occurs from 1.2 s to 1.8 s. The minimum value of the force, as in the case of Figure 4c (-68000 N).

Here are also plots of changes in crane speed (Figure 5).

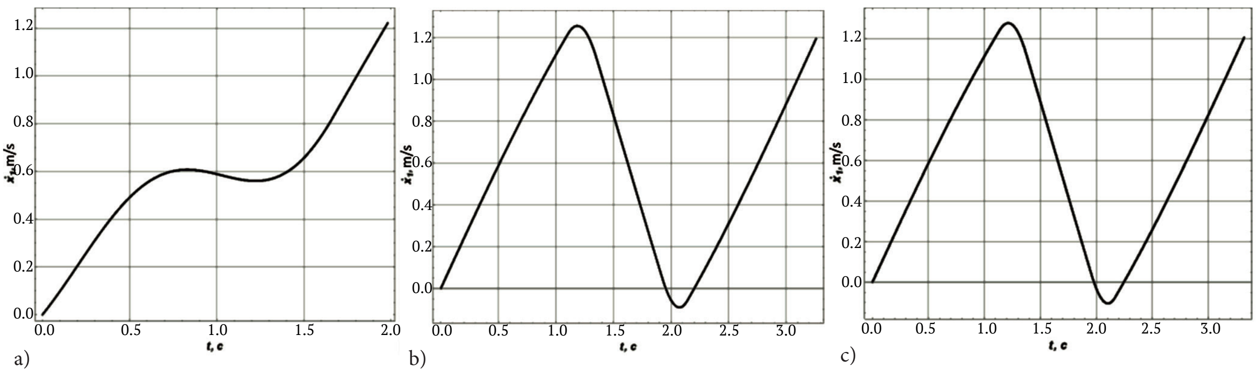

Figure 5. Plots of crane speed changes: a) l=2 m, m_2=500 kg, b) l=11.5 m, m_2=18700 kg c) l=12 m, m_2=20000 kg
Source: compiled by the authors

For the second variant (Fig. 5c), the maximum velocity of 1.22 m/s is reached at 1.2 s, after reaching the peak, the velocity decreases from 1.23 s to 3.4 s. Moreover, Figure 5c shows that for a short period, the velocity becomes negative, which is a negative factor that should be avoided. Figure 5a shows a slight (from 0.6 m/s to 0.55 m/s) decrease in velocity in the period from 0.6 s to 1.4 s, the maximum velocity, in this case, reaches 1.21 m/s, which corresponds to the numerical value of V used in the calculations. As can be seen from Figures 5c and b, they are very similar to each other, the difference between them is that in Figure 5b the velocity value becomes negative for a shorter period from 1.9 s to 2.3 s, and the maximum velocity of 1.21 m/s is reached at 1.2 s. The graphs of the crane drive power change are shown in Figure 6. The graph shown in Figure 6a shows that the minimum power value is 8000 W, i.e., for a certain period, the crane drive motor will operate in generator mode. The maximum power value is 58000 W, which is achieved at 1.98 s. The plot in Figure 6c shows that the minimum power value is much higher (-75000 W), it is reached at 1.4 s, and the maximum value is the same as for the first option and is reached at 1.25 s. The graph in Figure 6b shows that the maximum power value is 58 kW, reached at 1.1 s, and the minimum value is -70 kW, reached at 1.35s.

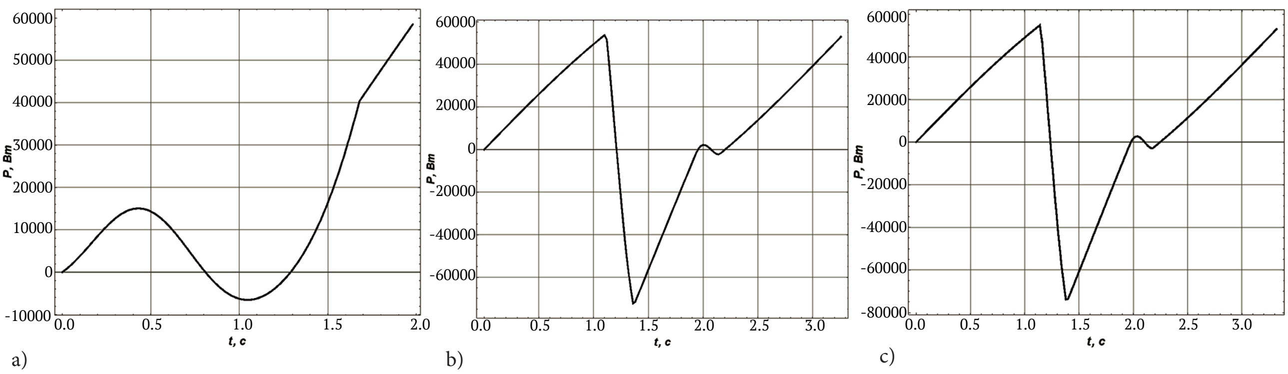

Figure 6. Crane drive power plot: a) l=2 m, m_2=500 kg, b) l=11.5 m, m_2=18700 kg c) l=12 m, m_2=20000 kg
Source: compiled by the authors

Thus, to implement the obtained control laws, regenerative braking should be provided in the drive of the crane movement mechanism. By comparing the methods and results of this research with well-known studies, in particular [3; 4], a commonality of using modifications of the PSO method [18-21] can be noted. Thus, it can be considered an effective tool for solving similar problems. These works also use mathematical models that consider pendulum effects (oscillations of a load on a flexible suspension). However, this research considers the overload capacity of the drive of the crane movement mechanism, which corresponds to the consideration of a crane as an electromechanical system. Consequently, the statement part of the problem is wider than those presented in [3; 4].

The calculation of the controller parameters in [3; 4] was performed for a limited set of system parameters (length of the flexible suspension, the mass of the load, etc.). However, in this research, an algorithm for finding the optimal PID controller gains for a wide range of system parameters that correspond to those encountered in crane operation practice was obtained. This is undoubtedly an advantage of this research over studies [3; 4]. Some authors [9; 10] used artificial neural networks to tune PID controllers, the obvious disadvantage of which is the need to process a large amount of data, which significantly slows down the process of tuning the PID controller and increases the requirements for computing. In the case of [10], the tuning process requires a constant connection to the Internet. The use of such tuning methods increases the flexibility of the parameters during tuning but reduces the autonomy. In studies [6; 7], the authors proposed methods for autotuning PID controllers; the models used in the works are based on an analytical model derived from the transient characteristics of the control object. In calculations, analytical models require the use of several assumptions, for example, the nonlinearity of the object is not considered, and differentiation errors are not considered. The calculations do not address system constraints, which leads to an error in system identification and a decrease in the quality of optimization. The research partially considers the features of this system. In [2], the author used the fuzzy logic method to tune the PID controller, which is based on several sets and variables that are formed by a base (set) of rules formed by a human expert. The rules used may be contradictory or incomplete. The fuzzy logic method used in this research is effective only for a narrow range of system parameters (drive power of the crane movement mechanism, load mass, and length of the flexible suspension). This does not involve changing the microcontroller and other means (sensors, controlled drives, etc.), so in terms of software and hardware, such approaches can be equally effective for different crane parameters. In this research, the author did not consider changes in the parameters (load mass, suspension length, etc.) of the dynamic system. In [8], the authors use several different methods to tune PID controllers to realize optimal control (genetic algorithm, bee algorithm, which belongs to the class of swarm intelligence methods, and fuzzy logic method). The genetic algorithm was used to tune the PID controllers responsible for the crane movement. The linear movement of the crane is provided by PID controllers configured using the bee and genetic algorithms, and the positioning of the load is provided by PID controllers configured using fuzzy logic. Using other parameters requires recalculation of the controller settings each time. This places stringent requirements on the computing capabilities of the crane motion control system, which, of course, makes it more expensive than similar systems. The algorithm developed by the authors and presented in this article makes it possible to find the optimal values of the PID controller settings using insignificant computing resources.

CONCLUSIONS

The problem of tuning the gains of a PID controller that contrals the movement of the crane-load system is formulated. Using the ME-D-PSO method, solutions to the problem were obtained for sets of changes in system parameters: load mass – from 500 kg to 20,000 kg in increments of 500 kg; length of flexible load suspension from 2 to 12 meters in increments of 1 meter.

An algorithm for calculating the values of the coefficients of the PID controller is developed. The first step of the algorithm is to determine the upper and lower limits of the parameters m_2 and l for which the PID-controller gains K_P, K_I, K_D are searched. Next, an initial approximation of the gains values is determined, and the values of the gains are determined using the modified particle swarm method ME-D-PSO.

The dynamics of movement of the crane-load system are analyzed for two variants of the load mass and the length of the flexible load suspension (l=2 m, m_2=500 kg; l=12 m, m_2=20000 kg and l=11.5 m, m_2=18700 kg). As can be seen from the results of the study, the second and third options are similar. The duration of the movement at the minimum parameters is 2 s, and at the maximum – 3.5 s, which is caused by a longer period of pendulum oscillations of the load. The maximum amplitude of load deflection for the first variant is 0.26 m, and for the second and third – 0.98 m. The maximum power for all the considered options is the same – 58 kW. In all the cases considered, the pendulum oscillations of the load are eliminated during the crane acceleration.

Further research in this area should address other constraints on the kinematic, energy, and dynamic characteristics of the system's motion, as well as other criteria for tuning the PID controller (RMS value of the driving force, the amplitude of pendulum oscillations, etc.).

REFERENCES

[1] Gerasimov, M.V. (2020). The algorithm for adjusting the coefficients of the PID controller using fuzzy logic methods. *Methods and Examples of Quality Control* , 2(45), 102-108. doi: 10.31471/1993-9981-2020-2(45)-102-108.

[2] Stepanets, O.V., & Mariyash, Yu.I. (2018). Automatic adjustment of the PID controller to the minimum integral time-weighted modular criterion of work quality. *Informatics, Computer Technology and Automation*, 29(68))(1), 23-28.

[3] Jaafar, H.I., Mohamed, Z., Mohd Subha, N.A., Husain, A.R., Ismail, F.S., Ramli, L., Tokhi, M.O., & Shamsudin, M.A. (2018). Efficient control of a nonlinear doublependulum overhead crane with sensorless payload motion using an improved PSO-tuned PID controller. *Journal of Vibration and Control*, 25(4), 907-921. doi: 10.1177/1077546318804319.

[4] Nur Iffah, M.A., Nafrizuan, M.Y., Ho, J.F., & Wan Azhar, W.Y. (2019). Optimization of the PID-PD parameters of the overhead crane control system by using PSO algorithm. *MATEC Web of Conferences*, 255, article number 04001. doi: 10.1051/matecconf/201925504001.

[5] Li, H., Hui, Y.-B., Wang, Q., Wang, H.-X., & Wang, L.-J. (2022). Design of anti-swing PID controller for bridge crane based on PSO and SA algorithm. *Electronics*, 11(19), article number 3143. doi: 10.3390/electronics11193143.
[6] Mohd Tumari, M.Z., Shabudin, L., Daud, M.R., Zawawi, M.A., & Mohd Tumari, M.Z. (2013). Experimental investigation on active sway control of a gantry crane system using PID controller. In *2nd International Conference on Electrical, Control and Computer Engineering*, (pp. 295-299). Pahang, Malaysia.
[7] Solihin, M.I., Wen, M.Ch., Heltha, F., & Lye, L.Ch. (2014). Robust PID controller tuning for 2d gantry crane using Kharitonov's theorem and differential evolution optimizer. *Advanced Materials Research*, 903, 267-272. doi: 10.4028/www.scientific.net/amr.903.267.
[8] Esleman, E.A., Önal, G., & Kalyoncu, M. (2021). Optimal PID and fuzzy logic based position controller design of an overhead crane using the Bees Algorithm. *SN Applied Sciences*, 3, article number 811. doi: 10.1007/s42452-021-04793-0.
[9] Milovanović, M.B., Antić, D.S., Milojković, M.T., Nikolić, S.S., Perić, S.L., & Spasić, M.D. (2016). Adaptive PID control based on orthogonal endocrine neural networks. *Neural Networks*, 84, 80-90. doi: 10.1016/j.neunet.2016.08.012.
[10] Hanchevici, A.B., & Dumitrache, I. (2012). Intelligent PID control for linear SISO system with random communication delay by using online genetic algorithms. *FAC Proceedings Volumes*, 45(7), 140-145. doi: 10.3182/20120523-3-CZ-3015.00029.
[11] Grigorov, O.V. (1995). *Improvement of operating characteristics of crane mechanisms*. Kharkiv: Kharkiv State Polytechnic University
[12] Loveykin, V.S., & Romasevich, Yu.O. (2016). *Dynamics and optimization of movement modes of bridge cranes*. Kyiv: Comprint.
[13] Gerasymyak, R.P., & Leshchev, V.A. (2008). *Analysis and synthesis of crane electromechanical systems*. Odessa: SMIL.
[14] Borase, R.P., Maghade, D.K., Sondkar, S.Y., & Pawar, S.N. (2021). A review of PID control, tuning methods and applications. *International Journal of Dynamics and Control*, 9, 818-827.
[15] Wang, L. (2020). *PID control system design and automatic tuning using MATLAB/Simulink*. doi: 10.1002/9781119469414.
[16] Ulusoy, S., Nigdeli, S.M., & Bekdaş, G. (2021). Novel metaheuristic-based tuning of PID controllers for seismic structures and verification of robustness. *Journal of Building Engineering*, 33, article number 101647. doi: 10.1016/j.automatica.2020.109185.
[17] Romasevych, Y., Loveikin, V., & Makarets, V. (2020). Optimal constrained tuning of PI-controllers via a new PSO-based technique. *International Journal of Swarm Intelligence Research*, 11(4), 87-105.
[18] Poli, R., Kennedy, J., & Blackwell, T. (2007). Particle swarm optimization. *Swarm Intelligence*, 1, 33-57. doi: 10.1007/s11721-007-0002-0.
[19] Clerc, M. (2010). *Particle swarm optimization*. Hoboken: Wiley. doi: 10.1002/9780470612163.
[20] Qinghai, B. (2010). Analysis of particle swarm optimization algorithm. *Computer and Information Science*, 1, 33-57.
[21] Chovnyuk, Y., Diachenko, L., Ivanov, Y., Dichek, N., & Orel, O. (2022). Optimisation of dynamic loads of rope systems of lifting mechanisms of bridge cranes during cargo handling. *Scientific Herald of Uzhhorod University. Series "Physics"*, (51), 59-73.

Юрій Олександрович Ромасевич
Доктор технічних наук
Національний університет біоресурсів і природокористування України
03041, вул. Героїв Оборони, 15, м. Київ, Україна
https://orcid.org/0000-0001-5069-5929
Вячеслав Сергійович Ловейкін
Доктор технічних наук
Національний університет біоресурсів і природокористування України
03041, вул. Героїв Оборони, 15, м. Київ, Україна
https://orcid.org/0000-0003-4259-3900
Валерій Володимирович Макарець
Аспірант
Національний університет біоресурсів і природокористування України
03041, вул. Героїв Оборони, 15, м. Київ, Україна
https://orcid.org/0000-0002-9116-0784

Розробка алгоритму налаштування ПІД-регулятора руху системи «кран-вантаж»

Анотація. Однією із основних проблем при роботі вантажопідйомних кранів є коливання вантажу на гнучкому підвісі. Одним із способів усунення коливань вантажу на гнучкому підвісі є застосування пропорційно-інтегрально-диференціального регулятора, що виконує формування керуючого сигналу руху крана. Однак, для виконання цієї задачі він повинен бути відповідним чином налаштованим. Стандартні підходи до налаштування ПІД-регулятора, які поширені у практиці інженерних розрахунків, не дозволяють вирішити цю задачу, і саме тому її можна розглядати як науково-прикладну. Основною метою роботи була розробка алгоритму налаштування пропорційно-інтегрально-диференціального регулятора. Для цього виконано постановку задачі, яка включає: математичну модель динамічної системи, обмеження на перевантажувальну здатність приводу крану та функцію регулювання, умови досягнення усталеної швидкості руху крана та усунення маятникових коливань вантажу на гнучкому підвісі. Користуючись модифікованим методом рою часток ME-D-PSO визначено коефіцієнти пропорційно-інтегрально-диференціального регулятора для широкого діапазону значень маси вантажу та довжини гнучкого підвісу. На основі отриманих значень коефіцієнтів представлено алгоритм, який дозволяє розраховувати значення коефіцієнтів для будь-яких значень маси вантажу та довжини підвісу. Проведено аналіз динаміки руху системи «кран-вантаж» для найменших і найбільших обраних параметрів та для випадку, який отриманий на основі застосування розробленого алгоритму. Практичне застосування розробленого алгоритму дозволить отримати оптимальні значення пропорційно-інтегрально-диференціального регулятора, що в свою чергу усуває коливання вантажу на гнучкому підвісі при роботі крану, що в свою чергу підвищує безпеку експлуатації кранів, довговічність конструкції, збільшує продуктивність роботи крана

Ключові слова: математична модель; обмеження; маятникові коливання вантажу; метод рою часточок; продуктивність

Machinery & Energetics
Vol. 13, No. 4. 2022

Journal homepage:
https://technicalscience.com.ua/en

UDC 514.18
DOI: 10.31548/machenergy.13(4).2022.81-88

Serhii Pylypaka
Full Doctor in Technical Sciences, Professor
National University of Life and Environmental Sciences of Ukraine
03041, 15 Heroiv Oborony Str., Kyiv, Ukraine
https://orcid.org/0000-0002-1496-4615

Tetiana Kresan
PhD in Technical Sciences, Associate Professor
National University of Life and Environmental Sciences of Ukraine
03041, 15 Heroiv Oborony Str., Kyiv, Ukraine
https://orcid.org/0000-0002-8280-9502

Vyacheslav Hropost*
Postgraduate Student
National University of Life and Environmental Sciences of Ukraine
03041, 15 Heroiv Oborony Str., Kyiv, Ukraine
https://orcid.org/0000-0001-9363-3955

Vitalii Babka
PhD in Technical Sciences, Associate Professor
National University of Life and Environmental Sciences of Ukraine
03041, 15 Heroiv Oborony Str., Kyiv, Ukraine
https://orcid.org/0000-0003-4971-4285

Iryna Hryshchenko
PhD in Technical Sciences, Associate Professor
National University of Life and Environmental Sciences of Ukraine
03041, 15 Heroiv Oborony Str., Kyiv, Ukraine
https://orcid.org/0000-0002-1000-9805

Calculation of the bending parameters of a flat workpiece into a twist of a helicoid torso

Abstract. Helical surfaces are deployable and non-deployable. The first is the surface of a helical conoid widely used in technology, known as the screw. The second one is the surface of an unfolding helicoid or torso-helicoid. In both cases, the surface is formed from a blank - a sweep in the form of a flat ring. If in the first case the sweep can be calculated approximately, since the exact one does not exist due to the properties of non-expanded surfaces, then in the second case it is calculated exactly. However, this does not mean that it is just as possible to form a ready-made product from it - a twist of a helicoid torso. In contrast to non-expanded surfaces, during the manufacture of which the workpiece is subjected to complex stretching and compression deformations, an expanded surface can be obtained by bending with minimal plastic deformations, the magnitude of which depends on the thickness of the sheet. Bending occurs along rectilinear generators, which are theoretically located on the workpiece. In the process of bending, the location of these generators should not change. In the theory of differential geometry, such a process can be described

Article's History: Received: 16.06.2022; Revised: 04.10.2022; Accepted: 23.11.2022.

Suggested Citation:
Pylypaka, S., Kresan, T., Hropost, V., Babka, V., & Hryshchenko, I. (2022). Calculation of the bending parameters of a flat workpiece into a twist of a helicoid torso. *Machinery & Energetics,* 13(4), 81-88.

*Corresponding author

analytically and is called continuous bending. With regard to the manufacture of the twist of the torso-helicoid, this means a gradual increase in the step to the desired value. The work contains parametric equations that describe this method of bending. At the same time, not only stretching of the workpiece along the axis of the coil occurs, but also its twisting around the axis. A comparison of these two movements was made and it was found that the relationship between them is not linear. The work gives a formula describing this dependence. According to it, when the workpiece is uniformly stretched along the axis, the angle of its twist around the axis increases according to a dependence close to quadratic. In the work, examples of the use of the torso-helicoid are given, the surface is visualized, and graphs are constructed. Confirmation of the reliability of the obtained results is the first found quadratic form of the torso-helicoid, which does not change when the surface is bent

Keywords: surface area; conveyor screw; continuous divination; parametric equation; traction; torsional twisting

INTRODUCTION

The production of these surfaces differs significantly from one another. When forming a flat workpiece into the surface of a helical conoid, significant plastic deformations occur, stretching the inner part of the surface adjacent to the shaft and compressing the outer part. During the formation of the helicoid torso, bending occurs along straight lines, and the plastic deformations are minimal and caused by the thickness of the sheet material of a workpiece. If for an unexpanded surface a conditional sweep can only be constructed approximately, then for an expanded surface it is constructed exactly. To form a spreadable surface from a flat workpiece by bending it, it is necessary to know the dynamics of the process.

The scientific novelty is that an analytical description of the continuous bending of the helicoid torso has been obtained, which allows making recommendations for its practical manufacture.

Screw surfaces are widely used in the tasks of transportation of technological material. They can be stationary in gravity descents [1; 2]. In paper [3], it is carried out on a stationary surface under the action of the force of the particle's own weight, which is used in gravity descents. The productivity of helical surfaces for transporting technological material depending on the size of the pitch of the turn is considered in the paper [7]. They are very common in agricultural production [8-10]. In paper [11], the surface (torso-helicoid) is mobile. Papers [3; 11] show the use of a helicoid torso for transporting particles of technological material, while this transportation can be of different nature. Therefore, a significant part of the papers is devoted to improving the designs of screw devices and the technology of manufacturing spiral turns [12-14]. It rotates around its own axis and thereby sets the particle in motion. The technical and economic justification of their production is described in paper [15].

The research purpose was an analytical description of the process of continuous bending of a flat ring in the form of a sweep of a twist of a helicoid torso into a finished product.

MATERIALS AND METHODS

To achieve the research purpose, the methods of differential geometry, which relate to the internal theory of surfaces, were used. According to the theory of the internal geometry of the length of the lines on the surface, the angles between them do not change when the surface is bent.

A flat blank in the form of a ring with a cutout can be bent in different ways. If the straight lines along which the bending occurs are located radially, i.e., towards the center of the ring, then with gradual bending along them the ring will turn into a truncated cone (Fig. 1).

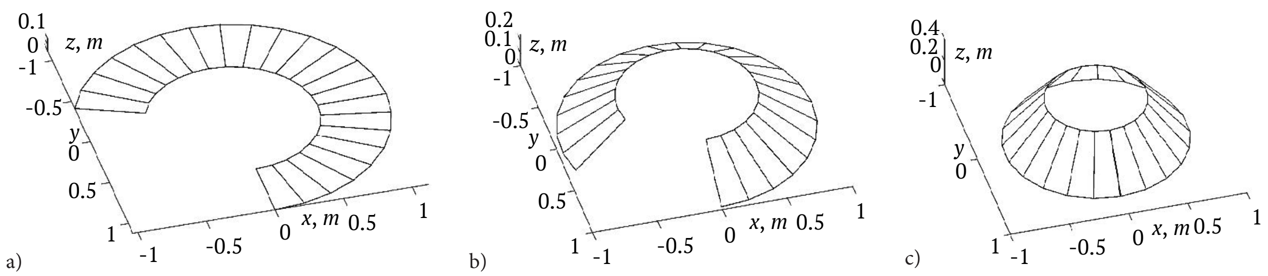

Figure 1. Graphic illustrations of the gradual bending of a flat ring into a truncated cone: a) flat ring with a cutout; b) intermediate stage during bending; c) truncated cone

In fact, bending is reduced to twisting the ring around a vertical axis passing through its center until the moment when the extreme limiting lines converge. Twisting can be continued further. Then the surface of the cone will overlap, and the angle of inclination of its rectilinear generators to the base will increase. However, a flat ring can be bent in another way, when the straight lines of the bend are located at a certain angle to the radial direction (Fig. 2a).

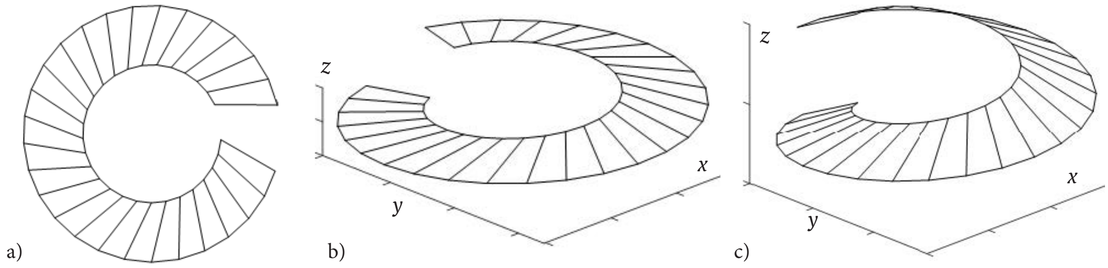

Figure 2. Graphical illustrations of the gradual bending of a flat ring into an expanding helicoid: a) flat ring with a cutout; b) intermediate stage during bending; c) twist of a helicoid torso

When a flat ring is uniformly bent along such lines, it is not only twisted around the vertical axis, but also stretched along it (Fig. 2b, 2c). Figure 4 shows the frontal (Fig. 3a) and horizontal (Fig. 3b) projections of one turn of a helicoid torso. The limiting circles of the ring turned into helical lines located on cylinders of radius r and R. The value H, by which the ring was stretched, is the pitch of a helicoid torso.

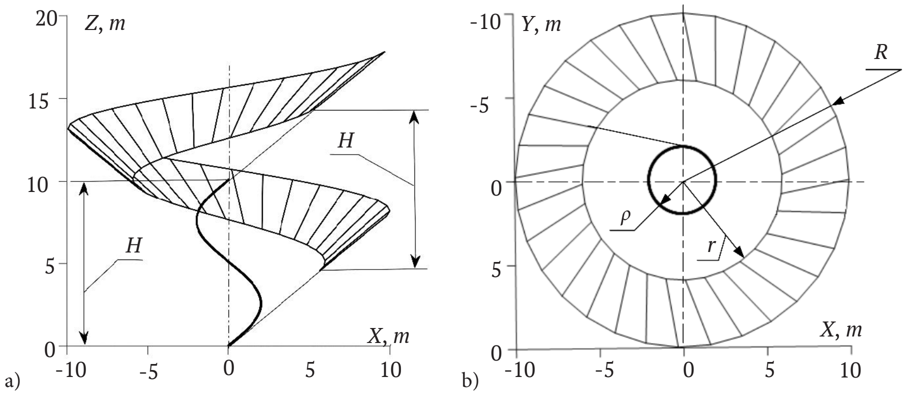

Figure 3. Twist of an unfolding helicoid, which turned into a flat ring: a) frontal projection; b) horizontal projection

In addition to the dimensions r, R and H, there is another dimension ρ, which depends on the direction of the straight lines, along which bending occurs. This is the size of the radius of a cylinder, on which the helical line of pitch H is located. If you extend the bend lines, then they will all be tangent to this helical line, which is called the turning edge. During the reverse deformation of the twist of a helicoid torso into a flat ring, the edge of the return is also deformed – its pitch decreases and turns into an arc of a circle on a developed view.

It is known from differential geometry that the length of the turning edge and its curvature do not change when the unfolded surface is bent [16; 17], although the shape of the turning edge itself changes and it becomes a flat curve on a developed view. In our case, when the turning edge is deformed by stretching, the arc of the circle will turn into a spiral line with an increase in its pitch H_i. Since the length of the deformed helical line does not change, it is clear that the radius ρ_i will also decrease during such deformation. It was controlled the bending of a helicoid torso through the deformation of its turning edge (helix line) in the described way. The parametric equations of a helical line as a function of the length s of its arc have the following form:

$$Rx = \rho \cos\frac{s}{\sqrt{\rho^2+h^2}};\ y = \rho \sin\frac{s}{\sqrt{\rho^2+h^2}};\ z = \frac{hs}{\sqrt{\rho^2+h^2}}, \tag{1}$$

where h is the helical parameter that is related to the pitch H by the dependence H=$2\pi h$, ρ is the radius of the cylinder, on which the helical line is located.

The curvature of the helical line is constant and depends on two parameters: ρ and h. After deformation, the helical line will remain helical, but with other parameters ρ_i and h_i. On the basis of the well-known expression of the curvature of a helical line [17], we equate it with each other before and after deformation:

$$\frac{\rho}{\sqrt{\rho^2+h^2}} = \frac{\rho_i}{\sqrt{\rho_i^2+h_i^2}}. \tag{2}$$

Equality (2) can be solved with respect to ρ_i or h_i. Let's solve it with respect to h_i, since in this case the solution will be simpler:

$$h_i = \sqrt{\frac{\rho_i}{\rho}(\rho^2 + h^2 - \rho\rho_i)}\,. \tag{3}$$

Let's substitute into equation (1) the new notation ρ_i (new value of the radius) instead of ρ and expression (3), i.e., the new value of the screw parameter, instead of h_i, and we will obtain the following parametric equations:

$$x_i = \rho_i \cos\sqrt{\frac{\rho}{\rho_i(\rho^2+h^2)}}s;\quad y_i = \rho_i \sin\sqrt{\frac{\rho}{\rho_i(\rho^2+h^2)}}s;$$
$$z_i = \sqrt{1-\frac{\rho\rho_i}{\rho^2+h^2}}s. \tag{4}$$

The resulting parametric equations (4) describe a set of helical lines of the same curvature. Their parameters (pitch and radius) depend on the value of the constant ρ_i. When $\rho_i=\rho$, equation (4) turns into equation (1), i.e., describes the original helical line. In the partial case, the spiral line turns into a flat circle. This happens when $h_i=0$. Let's equate expression (3) to zero and solve it with respect to ρ_i:

$$\rho_i = \frac{\rho^2+h^2}{\rho}. \tag{5}$$

The value of the radius ρ_i is the maximum possible, otherwise the radical expression in the last equation (4) will take on a negative value. When reducing ρ_i from the maximum value (5) to ρ, the line (4) will transform by increasing the pitch from the circle to the original helical line. With a further decrease in ρ_i, the pitch of the spiral line will increase, but when $\rho_i=0$, the line according to equations (4) cannot be obtained, since the root expressions in the first two equations (4) become undefined. This is explained by the fact that at $\rho_i=0$, the spiral line should turn into a vertical straight line, which is impossible under the condition of a given constant curvature, since the curvature of the straight line is zero.

The helical line (4) is a guide for the formation of a helicoid torso. Its surface is formed by a set of rectilinear generators tangent to the helical line. The directional vector of these generators is the expression of the first derivatives of equations (4). Since the helical line (4) is given by the equations as a function of the length s of its arc, the derivatives will represent the projections of the unit direction vector. The parametric equations of the surface will be written as a set of tangent lines to the helical line (4), the direction of which is specified by a unit vector:

$$X_i = \rho_i \cos\sqrt{\frac{\rho}{\rho_i\sqrt{(\rho^2+h^2)}}}s - u\rho_i\sqrt{\frac{\rho}{\rho_i\sqrt{(\rho^2+h^2)}}}\sin\sqrt{\frac{\rho}{\rho_i\sqrt{(\rho^2+h^2)}}}s;$$
$$Y_i = \rho_i \sin\sqrt{\frac{\rho}{\rho_i\sqrt{(\rho^2+h^2)}}}s + u\rho_i\sqrt{\frac{\rho}{\rho_i\sqrt{(\rho^2+h^2)}}}\cos\sqrt{\frac{\rho}{\rho_i\sqrt{(\rho^2+h^2)}}}s;$$
$$Z_i = \sqrt{1-\frac{\rho\rho_i}{\rho^2+h^2}}s + u\sqrt{1-\frac{\rho\rho_i}{\rho^2+h^2}}, \tag{6}$$

where u is the second variable of the surface – the length of the rectilinear generator, the count of which starts from the point of contact with the helical line.

The coefficients of the first quadratic form of the torso-helicoid (6) have the following form:

$$G = \left(\frac{\partial X_i}{\partial s}\right)^2 + \left(\frac{\partial Y_i}{\partial s}\right)^2 + \left(\frac{\partial Z_i}{\partial s}\right)^2 = \frac{h^4+\rho^4+\rho^2(2h^2+\rho^2)}{(h^2+\rho^2)^2};$$
$$F = \frac{\partial X_i}{\partial s}\cdot\frac{\partial X_i}{\partial u} + \frac{\partial Y_i}{\partial s}\cdot\frac{\partial Y_i}{\partial u} + \frac{\partial Z_i}{\partial s}\cdot\frac{\partial Z_i}{\partial u} = 1;$$
$$E = \left(\frac{\partial X_i}{\partial u}\right)^2 + \left(\frac{\partial Y_i}{\partial u}\right)^2 + \left(\frac{\partial Z_i}{\partial u}\right)^2 = 1. \tag{7}$$

Thus, the quadratic form will be written as follows:

$$dS^2 = Gds^2 + 2dsdu + Edu^2 = = \frac{h^4+\rho^4+\rho^2(2h^2+\rho^2)}{(h^2+\rho^2)^2} + 2dsdu + du^2. \tag{8}$$

The quadratic form (7) does not include the parameter ρ_i. Its value affects the shape of the surface (6), but does not affect the quadratic form itself. This indicates that equation (6) is the equation of continuous bending of a helicoid torso by a uniform decrease of its pitch from the initial value to zero when the helicoid torso turns into a sweep and vice versa – from the sweep to the finished surface. When $\rho_i=\rho$, equation (6) describes the initial surface of the helicoid torso, and when ρ_i is equal to the value given in (5) – its sweep. In order to construct the required surface section, it is necessary to know the limits of change of parameters s and u. One turn of the surface corresponds to a 360° rotation of the turning edge point (1). Let's equate the expression that determines the current value of the angle to 360°, and solve it with respect to s:

$$\frac{s}{\sqrt{\rho^2+h^2}} = 2\pi \text{ from which } s = 2\pi\sqrt{\rho^2+h^2}. \tag{9}$$

Therefore, the parameter s (independent variable) should vary between zero and the value (9). The second independent variable u is the distance of a point on the rectilinear generator from the turning edge. Therefore, it should vary from ur, which corresponds to the internal limiting spiral line of radius r (Fig. 3b) to uR, which corresponds to the external limiting spiral line of radius R. These spiral lines on the horizontal projection are projected by circles of radius r and R. Let us find the distance L from the axis helicoid torso to an arbitrary point of the initial surface according to the well-known formula:

$$L = \sqrt{X_i^2 + Y_i^2} = \rho\sqrt{\rho_i\left(\rho_i + \frac{\rho u^2}{\rho^2+h^2}\right)}. \tag{10}$$

Let us set the initial surface at $\rho_i=\rho$, then substitute this value into (10) and solve with respect to u:

$$u = \frac{1}{\rho}\sqrt{(L^2-\rho^2)(\rho^2+h^2)}. \tag{11}$$

If we substitute the values of ρ and h into formula (11), and the value of the radius r instead of L, we will get the value of ur. Accordingly, by replacing L with R, we find the value of uR. The difference between these uR-ur values is the length of the rectilinear generators within the flat ring, along which it is bent, so they are unchanged in the bending process. Let's substitute (11) into (10), and after simplifications we get:

$$L_i = \sqrt{\rho_i\left(\frac{L^2}{\rho^2} + \rho_i - \rho\right)}. \tag{12}$$

Formula (12) makes it possible to monitor the change of the radii ρ, r and R in the process of bending the surface depending on the value of ρ_i. For example, when $\rho_i=\rho$ (initial surface) we have: $L_i=L$. This means that when substituting the radii ρ, r and R instead of L, we get the same values. To obtain the values of ρ_o, r_o, and R_o on the sweep (i.e., L_o), we must substitute the corresponding value of ρ_o from (5) into formula (12). After substitution, we get:

$$L_0 = \frac{1}{\rho}\sqrt{(L^2+h^2)(\rho^2+h^2)}. \tag{13}$$

The obtained values of the design parameters are sufficient for the construction of the sweep.

RESULTS AND DISCUSSION

Helical linear surfaces can be of two types – deployable and non-deployable. An example can be a reinforced auger of a grain harvester, which comprises two helical surfaces. Figure 4a shows a fragment of the auger, and Figure 4b shows a fragment of a twist constructed with the help of a computer based on the equations of these surfaces. The active turn, marked with the number 1, is unexpanded and represents the surface of a helical conoid. Turn 2 serves to strengthen the main one and is an expanding surface – a helicoid torso.

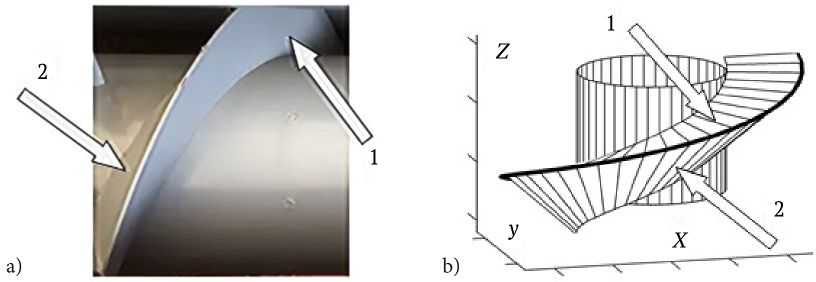

Figure 4. Graphic illustrations of the structure of the auger of a grain harvester: a) fragment of the auger of a natural product; b) fragment of the auger, the surfaces of which are built with the help of computer software

Let's consider an example. Let's bend a helicoid torso with the given dimensions H=10 (h=1.6), ρ=2, r=6, R=10. Let's find the extent, to which the independent variables s and u. From expression (8), we find that s=16.09. Therefore, s=0…16.09. The alternate substitution of r and R instead of L in formula (10) gives the limits of the distance change u=7.2…12.5. According to formula (5), we find the maximum possible value of ρ_i, which corresponds to the sweep of the twist of a helicoid torso: ρ_i=3.28. Therefore, ρ_i can have values within ρ_i=2…3.28. When ρ_i=2, we have the initial surface, the projections of which are shown in Figure 4. It was gradually increased the value of ρ_i. In Figure 5, projections of the surface at different values of the constant ρ_i are constructed according to equations (6). It should be noted that in equations (6), we change only ρ_i, while other parameters, including the limits of change of independent variables s and u, remain preliminary. When substituting L=r=6 and L=R=10 in (13) alternately, we find the values of the radii of the bounding circles on the sweep: r_o=7,95 i R_o=12.97, as well as ρ_o=3.28, i.e., the initial values of the corresponding radii r, R, and ρ increased from 6, 10, and 2 to 8, 13, and 3.3, respectively. It should be noted that the obtained results are broader in comparison with those known, for example, in paper [9]. In this paper, the original surface and its sweep without intermediate positions during bending are given.

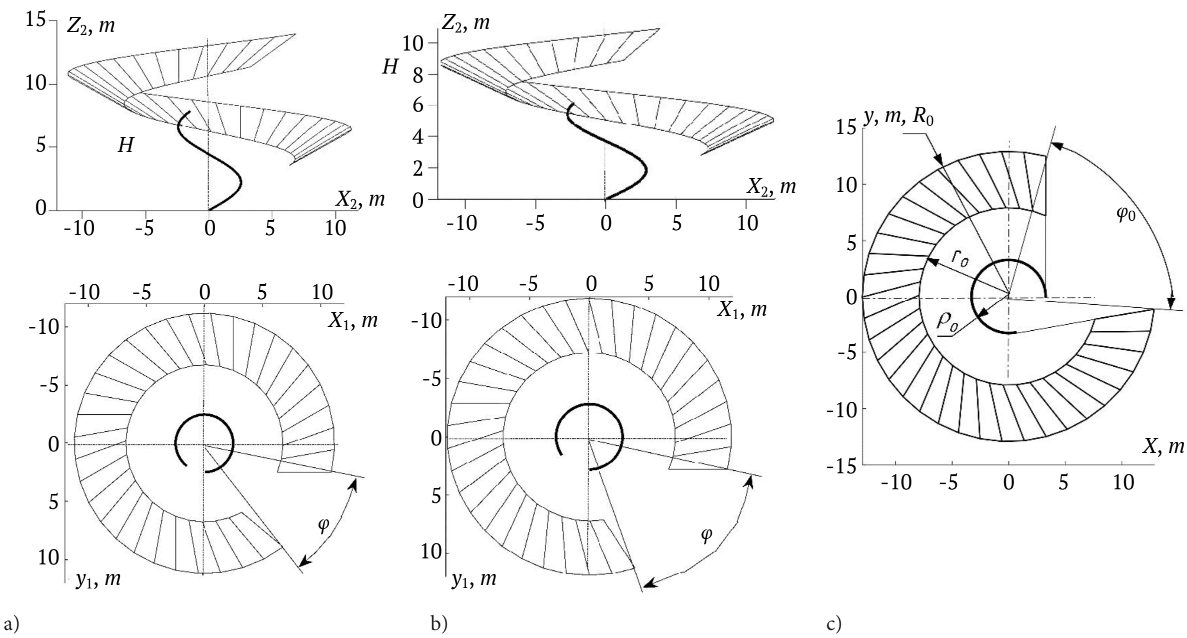

Figure 5. Helicoid torso projections constructed according to equations (6) at different values of ρ_i
a) ρ_i=2.5; b) ρ_i=2.8; c) ρ_i=3.28 (sweep)

Analyzing the projections of the helicoid torsos as a result of bending the original one (Fig. 3), its intermediate positions during bending (Fig. 5a and Fig. 5b) and ending with the sweep (Fig. 5c), it is possible to draw certain conclusions, namely: when reducing the pitch of the coil, the angle φ appears, which was not present on the original surface and which acquired the maximum value on the sweep. In addition, the radii ρ, r, and R increase, which also reach the maximum values of ρ_o, r_o, and R_o on the sweep. The dimensions ρ_o, r_o and R_o determine the contours of the sweep of the coil, and ρ_o makes is possible to determine the direction of the straight lines, along which the bending occurs.

Let's find an expression for the angle φ. When the arc length s changes from zero to the value (8), equation (1) describes one turn of the helical line, i.e., the angle α in this case will be equal to 2π. The same will be the case for the helical line (4) under the condition that ρ_i=ρ. In other cases, when $\rho_i \neq \rho$ the angle α will be smaller than 2π, i.e., the angle will appear as the difference 2π-α_i. Taking into account this and the value of s from (8), we can write the following:

$$\phi_i = 2\pi - s\sqrt{\frac{\rho}{\rho_i(\rho^2+h^2)}} = 2\pi\left(1-\sqrt{\frac{\rho}{\rho_i}}\right). \quad (14)$$

When ρ_i=ρ, i.e., in the initial surface, the angle φ=0. By increasing ρ_i, we will obtain certain values of the angle φ_i. At the maximum possible value of ρ_i according to (5), we will get the angle φ_o on the sweep. Let's substitute ρ_i from (5) into (14) and get:

$$\phi_0 = 2\pi\left(1-\frac{\rho}{\sqrt{\rho^2+h^2}}\right). \quad (15)$$

For the given h=1.6, ρ=2, using formula (15), we find that φ_o=79°. The found values of ρ_o, r_o, R_o and φ_o are sufficient to construct a flat ring – the sweep of one turn of a helicoid torso – and determine the direction of the straight lines, along which bending occurs. Therefore, when a flat ring is bent into the surface of a helicoid torso, deformation occurs with its simultaneous stretching along the axis and twisting around the axis. Let's find an analytical relationship between these two movements.

Pitch H_i can be found if we multiply the helical parameter h_i (3) by the angle α_i. It can also be found as the z_i coordinate in equations (4) at the value of s from (8). In both cases, we get the following:

$$H_i = 2\pi\sqrt{\rho^2+h^2-\rho\rho_i}. \quad (16)$$

When stretching the ring, it must simultaneously twist around the axis from the angle $2\pi-\varphi_o$ (Fig. 5c) to the angle 2π (Fig. 4b). Within these limits, the angle α_i changes, the expression of which according to (14) is written as follows:

$$\alpha_i = 2\pi\sqrt{\frac{\rho}{\rho_i}}. \quad (17)$$

Excluding ρ_i from expressions (16) and (17), we find the dependencies α_i=$\alpha_i(H_i)$ or H_i=$H_i(\alpha_i)$:

$$\alpha_i = \frac{4\rho\pi^2}{\sqrt{4\pi^2(\rho^2+h^2)-H_i^2}}.\ H_i = \frac{2\pi}{\alpha_i}\sqrt{\alpha_i^2(\rho^2+h^2)-4\pi^2\rho^2}. \quad (18)$$

Figure 6a plots the dependence of α_i=$\alpha_i(H_i)$ on the set parameters of the loop. Pitch H_i changes from zero to the final value H=10. At the same time, the angle α_i changes from the initial value of 281° to the final value of 360°. The difference between these values gives the angle φ_o, i.e., in fact, it is a graph of the dependence φ=$\varphi(H_i)$. It shows that with uniform stretching of a workpiece, its twisting occurs unevenly: at first the angle grows slowly, and then its growth accelerates according to a dependence close to quadratic. The workpiece could be stretched further with simultaneous twisting. At the same time, the angle of rise of the helical line (turning edge), which is the angle of inclination of the rectilinear generators to the horizontal plane, increases.

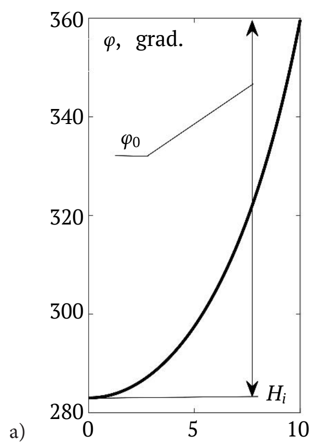

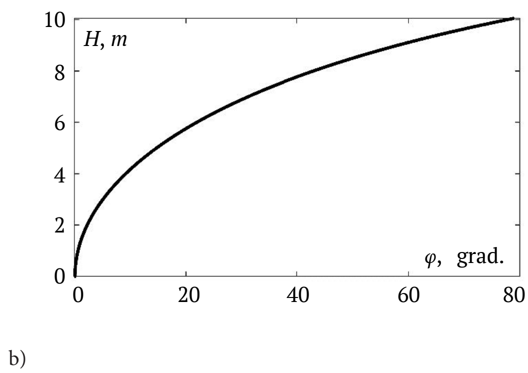

Figure 6. Graphs characterizing the relationship between the two movements when bending a workpiece into a helicoid torso turn: a) dependence of the angle of rotation φ with a linear increase in the pitch H; b) dependence of the pitch H with a linear increase in the angle of rotation φ

Figure 6b shows the graph of the dependence H=$H(\varphi)$, which gives an idea of the regularity of the change of the pitch H during uniform twisting of the workpiece. With a linear increase in the angle φ, the stretching of the workpiece does not occur uniformly: at the initial stage, the step increases rapidly and later this growth slows down.

CONCLUSIONS

When forming a coil of a helicoid torso from a flat workpiece, which is its sweep, it is necessary to correctly bend it. The theoretical description of the process of continuous bending makes it possible to identify the required ratio of two movements during the production of a coil by the bending method. In the process of forming the coil, it is necessary to ensure its stretching along the axis with simultaneous twisting around the axis, and the ratio of these two movements is non-linear. This requires special equipment to obtain the finished product. A theoretical result was obtained, which indicates a non-linear dependence between these movements. Prospects for further research consist in the development of technological equipment for the implementation of the described method of bending a flat sweep into a finished product.

REFERENCES

[1] Volina, T.M. (2021). Screw descent, analytical description of which includes the equation of particle movement on an inclined plane. *Applied Geometry and Engineering Graphics*, 100, 89-98.

[2] Kresan, T.A. (2020). Screw descent, analytical description of which includes the equation of particle movement on an inclined plane. *Machinery & Energetics. Journal of Rural Production Research*, 11(2), 49-57.

[3] Volina, T. M. (2020). Research of particle movement on rough surface formed by screw movement of sinusoid under action of own weight. *Machinery & Energetics. Journal of Rural Production Research*, 11(3), 187-194.

[4] Pankiv, V.R., & Tokarchuk, O.A. (2017). Investigation of constructive geometrical and filling coefficients of combined grinding screw conveyor. *INMATEH–Agricultural Engineering*, 51(1), 59-68.

[5] Gevko, I.B., Leschuk, R.Ya., Gud, V.Z., Dmytriv, O.R., Dubynyak, T.S., & Navrotska, T.D. (2019). *Flexible screw conveyors: Design, manufacturing technology, experimental research*. Ternopil: Individual Entrepreneur V.A. Palianytsia.

[6] Dubynyak, T.S. (2018). *Justification of structures and parameters of protective mechanisms of flexible screw conveyors* (Candidates thesis, Ternopil National Technical University named after Ivan Pulyu, Ternopil, Ukraine).

[7] Grudovy, R.S. (2017). Examination of productivity of the spiral conveyer with equiincreased turn thread during. *Visnyk ZHNAEU*, 1(2), 139-147.

[8] Kulykivskyi, V. L. (2018). Influence of screw conveyors on the grain quality indicators of cereals. *Scientific Journal “Engineering of Nature Management”*, 2, 108-114.

[9] Klendiy, M.B., & Dragan, A.P. (2021), Substantiation of the design of the working body of the screw section of the combined tillage tool. *Perspective Technologies and Devices*, 18, 66-73.

[10] Vanin, V.V., Hrubych, M.V., & Yurchuk, V.P. (2017). Geometric modeling of switching surfaces of the changed step for the design of voltage copies. *Visnyk Kherson National Technical University*, 3(62), 256-259.

[11] Kresan, T.A. (2021). Movement of soil particles on surface of developable helicoid with horizontal axis of rotation with given angle of attack. *Machinery & Energetics. Journal of Rural Production Research*, 12(2), 67-75.

[12] Gevko, B.M., Slobodian, L.M., Marunych, O.P., & Hupka, V.V. (2018). Design features of screw loaders of machines. *Technical Service of Agro-Industrial, Forestry and Transport Complexes*, 12, 125-129.

[13] Hevko, I.B., Hud, V.Z., & Kruglik, O.A. (2018). Synthesis of the spiral crews coiling methods. *Perspective Technologies and Devices*, 12, 39-47.

[14] Lyashuk, O.L., Dyachun, A.E., Klendiy, V.M., Teslia, V.O., Navrotska, T.D., & Radik, M.D. (2018). Study of the dynamics of the process of calibration of the turn of a conical screw workpiece per step. *Technical Service of Agro-Industrial, Forestry and Transport Complexes*, 12, 39-47.

[15] Lyashuk, O.L., Dyachun, A.E., Tretyakov, O.L., Navrotska, T.D., & Kruglyk, O.A. (2019). Technical and economic justification of the process of manufacturing screw working bodies. *Bulletin of the Petro Vasylenko Kharkiv National Technical University of Agriculture*, 198, 244-251.

[16] Milinsky, V.I. (1934). *Differential geometry*. leningrad: KUBUCH.

[17] Vygodsky, M.Ya. (1949). *Differential geometr*y. moscow: GITTL.

Сергій Федорович Пилипака
Доктор технічних наук, професор
Національний університет біоресурсів і природокористування України
03041, вул. Героїв Оборони, 15, м. Київ, Україна
https://orcid.org/0000-0002-1496-4615

Тетяна Анатоліївна Кресан
Кандидат технічних наук, доцент
Національний університет біоресурсів і природокористування України
03041, вул. Героїв Оборони, 15, м. Київ, Україна
https://orcid.org/0000-0002-8280-9502

Вячеслав Іванович Хропост
Аспірант
Національний університет біоресурсів і природокористування України
03041, вул. Героїв Оборони, 15, м. Київ, Україна
https://orcid.org/0000-0001-9363-3955

Віталій Миколайович Бабка
Кандидат технічних наук, доцент
Національний університет біоресурсів і природокористування України
03041, вул. Героїв Оборони, 15, м. Київ, Україна
https://orcid.org/0000-0003-4971-4285

Ірина Юріївна Грищенко
Кандидат технічних наук, доцент
Національний університет біоресурсів і природокористування України
03041, вул. Героїв Оборони, 15, м. Київ, Україна
https://orcid.org/0000-0002-1000-9805

Розрахунок параметрів згинання плоскої заготовки у виток торса-гелікоїда

Анотація. Гвинтові поверхні є розгортні і нерозгортні. До перших відноситься широко використовувана в техніці поверхня гвинтового коноїда відома під назвою шнек. До других – поверхня розгортного гелікоїда або торса-гелікоїда. В обох випадках поверхню формують із заготовки – розгортки у вигляді плоского кільця. Якщо в першому випадку розгортка може бути розрахована наближено, оскільки точної не існує в силу властивостей нерозгортних поверхонь, то в другому випадку вона розраховується точно. Однак це не означає, що так само точно можна сформувати із неї готовий виріб – виток торса-гелікоїда. Більш детальне вивчення цієї проблематики зумовлює актуальність досліджень.Метою дослідження є опис процесу неперервного згинання плоского кільця у вигляді розгортки витка торса-гелікоїда у готовий виріб. Для цього була задіяна теорія і методи диференціальної геометрії. В роботі складено параметричні рівняння, які описують такий спосіб згинання. При цьому відбувається не тільки розтягування заготовки вздовж осі витка, а і його скручування навколо осі. Здійснено порівняння цих двох рухів і з'ясовано, що залежність між ними не є лінійною. В роботі наведено формулу, що описує цю залежність. Основним результатом є отримання цієї залежності, яка служить основою для практичної реалізації формування витка торса-гелікоїда із плоскої заготовки способом згинання. В роботі наведено приклади застосування торса-гелікоїда, зроблено візуалізацію поверхні, побудовано графіки. Підтвердженням достовірності отриманих результатів є знайдена перша квадратична форма торса-гелікоїда, яка не змінюється при згинанні поверхні. Матеріал статті буде корисним спеціалістам, що займаються холодним гнуттям плоских листових заготовок

Ключові слова: поверхня; шнек; неперервне згинання; параметричні рівняння; розтягування; скручування

ТЕХНІКА ТА ЕНЕРГЕТИКА

Науковий журнал

Том 13, № 4. 2022

Заснований у 2010 р. Виходить чотири рази на рік

Оригінал-макет видання виготовлено у відділі науково-технічної інформації
Національного університету біоресурсів і природокористування України

Відповідальний редактор:
Г. Івченко

Редагування англомовних текстів:
С. Воровський, К. Касьянов

Комп'ютерна верстка:
О. Глінченко

Підписано до друку 23 листопада 2022 р. Формат 60*84/8
Умов. друк. арк. 10,4
Наклад 50 прим.

Адреса видавництва:
Національний університет біоресурсів і природокористування України
вул. Героїв Оборони, 15, м. Київ, 03041, Україна
E-mail: info@technicalscience.com.ua
www: https://technicalscience.com.ua/uk

MACHINERY & ENERGETICS

Scientific Journal

Volume 13, No. 4. 2022

Founded in 2010. Published four times per year

The original layout of the publication is made in the Department of Scientific and Technical Information of National University of Life and Environmental Sciences of Ukraine

Managing editor:
H. Ivchenko

Editing English-language texts:
S. Vorovsky, K. Kasianov

Desktop publishing:
O. Glinchenko

Signed for print of November 23, 2022. Format 60*84/8
Conventional printed pages 10.4
Circulation 50 copies

Editors Office Address:
National University of Life and Environmental Sciences of Ukraine
03041, 15 Heroiv Oborony, Kyiv, Ukraine
E-mail: info@technicalscience.com.ua
www: https://technicalscience.com.ua/en